2015

# Passive and linear hybrid vibration energy harvesting transducer

Sara Zolfaghar Tehrani
*University of Wollongong*

UNIVERSITY OF WOLLONGONG

**Department of Electrical, Computer and**
**Telecommunications Engineering**

# PASSIVE AND LINEAR HYBRID VIBRATION ENERGY HARVESTING TRANSDUCER

**SARA ZOLFAGHAR TEHRANI**

**This thesis is presented as part of the requirement for the**
**Award of the Degree Of**
**Master of Engineering by Research of the**
**University of Wollongong**

**August 2015**

# ABSTRACT

This research first attempts to identify the effective parameters in the EMEH and PEH system. These systems with a transducer used in applications as a sensor or an actuator. On the other hand, there is an output interface with electrical circuit and function of converting and regulating AC signal to the DC operational output energy for the load.

The proposed design in chapter five is the result of the study about the effect of input parameters such as input frequency and acceleration to the output voltage and power regarding physical structure of transducers.

Having a successful model for effective physical design with considering a mixture of electromagnetic induction and piezoelectric effect mechanisms base on input motion bring the necessity of chapter two, three and four focusing on the developed designs and models with similar purposes to objectives of this thesis.

The analysis of PEH and EMEH devices with different approaches are modelled analytically or numerically to define the relation between effective parameters depending on the purpose and usage of the system. Modelling with either lumped or distributed parameters numerically consuming software such as MATLAB, ANSYS and COMSOL to use automatically the defined equations (use for complicated and nonlinear systems) via Finite Element Analysis (FEA).

Modelling is an effective way to estimate the output changes based on manipulation of the input parameters. There is usually some constitutive motion equations in the electromagnetic and piezoelectric system since the source of energy for harvesting enough charge is from mechanical vibration source.

Based on the research in EMEH transducers the effective architecture for maximum output from EMEH transducer is the use of more than one magnet while the magnet is in line with the coil. For the PEH system, the materials for inactive and active layer equally important and their positions and size respected to each other and related to the electrodes change the properties of the transducer. The research in Chapter two and four clearly express the effectiveness of bimorph layers with 31-mode configuration. The model which is indicated in chapter four can extend for the uni-morph piezoelectric layer and also considering the model for a 33-mode electrode with one or two piezoelectric layers.

The model for the electromagnetic system first depends on the magnetic field strength (fixed or alternative) in the coil and/or around the coil with considering the distance and position of coil -magnet with magnetization inside the magnet from N pole to S pole. Also, the effect of motion in coil or magnet from input mechanical vibration that effect on the area of coil or magnet which also effects the magnetic field and the amount of generated flux.

The input motion usually is a harmonic movement that could model by sine or cosine wave with mechanical and electrical damping and frequency. In this thesis, we are interested to find resonance frequency of the new engineering composite from piezoelectric materials category for the purpose of optimizing and implementing the device as a hybrid resonance device to generate maximum output with an optimal load. Although, the limitations of simulation and enough information about constitutive parameters of the piezoelectric layer in the datasheet of cantilever plate generates a lot of difficulty in modelling and recognizing of effective parameters to evaluate the design.

# ACKNOWLEDGEMENTS

First and foremost, I would like to thank my supervisor Dr. Peter Vial and my co-supervisor Dr. Prashan Premaratne for their valuable guidance and advice regarding my project. Both their willingness to motivate me contributed tremendously to better skills and increased knowledge. I also would like to thank my sister Sanaz Zolfaghar Tehrani for support and given instruction related to my research.

Besides, I would like to thank the authority of Wollongong University (UOW) for providing me with a good research environment and chance to discover valuable information and create devices for my research.

Finally, an honourable mention goes to my parents and friends for their understandings and supports on me in completing this project. Without help from the particular individuals mentioned above, I would face many more difficulties while understanding this study.

Sara Zolfaghar Tehrani

# TABLE OF CONTENTS

ABSTRACT ..... i
ACKNOWLEDGEMENTS ..... iii
TABLE OF CONTENTS ..... iv
LIST OF FIGURES ..... vii
LIST OF TABLES ..... x
NOMENCLATURE ..... xi
ABBREVIATION ..... xiii
CHAPTER ONE ..... 1
INTRODUCTION ..... 1
1.1 Overview ..... 1
1.2 Motivation ..... 2
1.3 Problem statement ..... 3
1.4 Objectives ..... 4
1.5 Thesis Structure ..... 4
CHAPTER TWO ..... 6
LITERATURE REVIEW ..... 6
2.1 Synopsis ..... 6
2.2 Introduction ..... 6
2.3 Physical Design Structure ..... 10
2.3.1 Electromagnetic Energy Harvester (EMEH) ..... 10
2.3.2 Piezoelectric Energy harvesting (PEH) ..... 16
2.4 Modelling and Testing ..... 24
2.4.1 Transducer ..... 25
2.4.2 Power Converter interface and Load ..... 35
2.5 State of the Art and Potential Applications ..... 38
2.5.1 PEH-shoe insert ..... 38
2.5.2 PEH/EMEH-condition monitoring ..... 39
2.5.3 PEH/EMEH-in-ear device ..... 39
2.5.4 EMEH-remote car key ..... 40
2.6 Summary ..... 40
CHAPTER THREE ..... 42

DESIGN OF AN ELECTROMAGNETIC ENERGY HARVESTING SYSTEM ....42
3.1 Synopsis....42
3.2 Vibration based EMEH ....42
3.2.1 Design and modelling ....42
3.2.2 Testing and Simulation ....44
3.3 Summary ....49
CHAPTER FOUR....50
DESIGN OF A PIEZOELECTRIC ENERGY HARVESTING SYSTEM ....50
4.1 Synopsis....50
4.2 Vibration based PEH ....50
4.2.1 Design and modelling ....50
4.2.2 Testing and Simulation ....56
4.2.2.1 Changes in Piezoelectric Materials of the PEH Transducer....56
4.2.2.2 Physical Size effect in the (Lead Nickel Niobate) PEH Transducer ....59
4.2.2.3 Evaluation of PEH System ....60
4.3 Summary ....61
CHAPTER FIVE....62
DESIGN OF A HYBRID MECHANISMS OF PIEZOELECTRIC AND ELECTROMAGNETIC ENERGY HARVESTING SYSTEM ....62
5.1 Synopsis....62
5.2 Hybrid Transducer Design and Modelling ....63
5.3 Resonance Frequency....61
5.4 The COMSOL Software....65
5.5 Physics used for Electromagnetic and Piezoelectric Energy Harvester ....68
5.6 Meshing....67
5.7 Material Properties ....69
5.8 Simulation Result ....70
5.8.1 Stationary Analysis ....69
5.8.2 Parametric Sweep Analysis....71
5.9 Experimental Laboratory Work....73
CHAPTER SIX ....79
CONCLUSION AND RECOMMENDATIONS....79
6.1 Conclusion and Recommendations ....79

References: ..... 81
Appendix A ..... 86
A.1 EMEH SYSTEM ..... 86
A.2 PEH SYSTEM ..... 87
Appendix B ..... 90
Appendix C ..... 106

# LIST OF FIGURES


FIGURE 2.1: THE HYBRID PEH AND EMEH SYSTEM WITH A, B, C DIFFERENT POSITIONING OF MAGNET TO COIL [16] ..... 9

FIGURE2.2: CANTILEVER STRUCTURE OF EMEH SYSTEM ..... 13

FIGURE2. 3: CYLINDRICAL STRUCTURE OF EMEH SYSTEM ..... 15

FIGURE2. 4: DISC STRUCTURE OF EMEH SYSTEM ..... 16

FIGURE 2.5: THE COUPLING MODE BETWEEN PIEZOELECTRIC LAYER AND ELECTRODES A) THE $d31$ MODE WITH ELECTRODES DISTANCE OF $L1$ B) THE $d33$ MODE WITH ELECTRODES DISTANCE OF $L3$ [33] ..... 18

FIGURE2.6: THE PIEZOELECTRIC LAYER CONFIGURATIONS A) BI-MORPH IN SERIES ELECTRICAL CONNECTION [37] B) BI-MORPH IN PARALLEL ELECTRICAL CONNECTION [37] C) UNI-MORPH [36] ..... 19

FIGURE 2.7: A) THE MECHANICAL BAND PASS FILTER B) THE FREQUENCY BAND AND PEAK POWER FREQUENCY [43] ..... 22

FIGURE2.8: EFFECT OF DIFFERENT SUBSTRATE MATERIALS ON THE OUTPUT POWER FOR THE DESIGN IN [44] ..... 24

FIGURE 2.9: THE EQUIVALENT CIRCUITS OF VIBRATION PEH SYSTEM WITH SDOF AND RESISTIVE LOAD $(RL)$ [47, 51-53] ..... 27

FIGURE2.10: THE COMPLETE EQUIVALENT CIRCUITS WITH A)OPEN CIRCUIT B)SHORT CIRCUIT OF VIBRATION PEH SYSTEM WITH SDOF AND RESISTIVE LOAD $(RL)$ [51]. ..... 28

FIGURE2.11: THE SUMMERY OF 33-MODE VIBRATION PEH SYSTEM ANALYTICAL MODELLING IN [1]. ..... 29

FIGURE2.12: THE MODELLING OF VIBRATION PEH SYSTEM IN [59] A) EQUIVALENT CIRCUIT B) EQUIVALENT EQUATIONS C) MASS-SPRING-DAMPER SCHEMATIC ..... 30

FIGURE 2.13: THE VIBRATION EMEH WITH MECHANICAL FREQUENCY UP-CONVERSION METHOD DESIGN IN [22, 23] ..... 31

FIGURE2.14: THE MODELLED EMEH PRESENTED IN [24] WITH A) EQUIVALENT CIRCUIT ELEMENTS B)MASS-SPRING-DAMPER SCHEMATIC C) THE DESIGN. ..... 32

FIGURE2.15: THE CYLINDER TUBE, HELICAL SPRING STRUCTURE AND UP CONVERSION, NON-RESONANCE VIBRATION EMEH A) MASS- SPRING-DAMPER SCHEMATIC B)THE DESIGN C) THE NUMERICAL ANALYSIS. ..... 33

FIGURE2.16: SCHEMATIC OF THE MODELLING PARAMETERS DEFINITIONS ..... 34

FIGURE 2.17: HYDRO ELECTROMAGNETIC ENERGY HARVESTER. EXPERIMENTAL SET UP ON THE LEFT AND ENERGY HARVESTER MODULE ON THE RIGHT [67]. ..... 40

FIGURE 2.18: SCHEMATIC OF PARTS IN VIBRATION ENERGY HARVESTING SYSTEM USING PIEZOELECTRIC AND ELECTROMAGNETIC MECHANISMS. ..... 41

FIGURE2.19: FLOWCHART OF DESIGN PROCESS IN VIBRATION ENERGY HARVESTING SYSTEM. ..... 41

FIGURE 3.1: SCHEMATIC OF TESTED MODEL FOR EMEH A) MASS-SPRING-DAMPER EQUIVALENT B) THE DESIGN PARAMETERS WITH MAGNET DIMENSIONS $(Lx, Ly, Lz)$. ..... 43

FIGURE 3. 2: THE SIMULINK BLOCK DIAGRAM OF MASS DISPLACEMENT Z (T) IN VIBRATION BASED EMEH. ..... 45
FIGURE 3. 3: UPWARD $z = Z1$ SIGNAL UNDER VIBRATION FREQUENCY OF 2HZ ..... 45
FIGURE 3. 4: DOWNWARD $z = -Z2$ SIGNAL UNDER VIBRATION FREQUENCY 2HZ. ..... 46
FIGURE 3. 5: SIMULATED AC VOLTAGE SIGNAL $f = 2\ Hz$ ..... 46
FIGURE 3. 6: SIMULATED AC VOLTAGE SIGNAL $f = 7\ Hz.$ ..... 46
FIGURE 3. 7: SIMULATED AC VOLTAGE SIGNAL $f = 56\ Hz.$ ..... 47
FIGURE 3.8: THE CHANGES OF $Vpeak$ TO THE LENGTH OF CANTILEVER (L) ..... 48
FIGURE 3.9: THE CHANGES OF $Vpeak$ TO THE RESONANCE FREQUENCY $(fn).$ ..... 48
FIGURE 4.1: SCHEMATIC STRUCTURE DESIGN OF A 31-MODE, BIMORPH VIBRATION PEH SYSTEM ..... 51
FIGURE 4.2: THE LUMPED PARAMETERS FOR MODELLING PEH SYSTEM A) MASS-SPRING-DAMPER MODEL B) EQUIVALENT CIRCUIT ELEMENTS (I) WITH RESISTIVE LOAD $(RL)$ (II) THERE IS A FULL BRIDGE DIODE RECTIFIER WITH STATES OF EITHER $D1, D3$ CONDUCTING IN POSITIVE CYCLE OR $D2, D4$ CONDUCTING IN NEGATIVE CYCLE. THERE IS A STATE WHERE ALL FOUR DIODES ARE NOT CONDUCTING. ..... 52
FIGURE 4.3: THE SIMULINK CIRCUIT FOR RESISTIVE LOAD. ..... 56
FIGURE 4.3: THE GRAPH OF OUTPUT PARAMETERS TO THE VARIOUS LOAD VALUE $(RL)$ FOR DIFFERENT MATERIALS A) OUTPUT POWER $(Pout = VoutIout)$ ACROSS $(RL)$ B) OUTPUT VOLTAGE $(Vout)$ IN OUTPUT PART OF CIRCUIT. ..... 58
FIGURE 4.4: THE GRAPH OF VARIOUS LOAD REISTANCE TO OUTPUT POWER WITH RESPECT TO SIZE MODIFICATION OF THE PEH SYSTEM. ..... 60
FIGURE 5.1: THE ELECTRICAL CIRCUIT TO MEASURE THE RESONANCE FREQUENCY A) THE SCHEMATIC B) THE EXPERIMENT SET UP ..... 64
FIGURE 5.2: THE VARIATION OF IMPEDANCE (OHM) TO FREQUENCY (HZ) A) REF. [75] B) BY SIMULATION. 64
FIGURE 5.3: THE INPUT AND OUTPUT SIGNAL FROM OSCILLOSCOPE AND THE RESONANCE RESULT A) INPUT VOLTAGE B) OUTPUT VOLTAGE C) INPUT SINE WAVE FREQUENCY D) THE PARALLEL RESONANCE FREQUENCY AT 890 KHZ. ..... 66
FIGURE 5.3 3-D COMSOL DESIGN OF HYBRID PIEZOELECTRIC AND ELECTROMAGNETIC ENERGY HARVESTING ..... 68
FIGURE 5.4: THE MESHING OF HYBRID PIEZOELECTRIC AND ELECTROMAGNETIC ENERGY HARVESTING SYSTEM ..... 69
FIGURE 5.5: SIMULATION CAPTURE OF CANTILEVER'S DISPLACEMENT AT SINE WAVE APPLIED FORCE WITH MAXIMUM DISPLACEMENT OF $1.52 \times 10 - 3$ MM AT THE FREE END ..... 71
FIGURE 5.6: SIMULATION CAPTURE OF GENERAL ELECTRICAL POTENTIAL WITH THE SIN WAVE APPLIED FORCE IN PIEZOELECTRIC FILM WITH MAXIMUM VALUE OF $4.5 \times 10 - 1$(V) ..... 72
FIGURE 5.7: THE 3D SIMULATION OF MAGNETIC FLUX DENSITY DISTRIBUTION IN HYBRID SYSTEM WITH MAXIMUM MAGNETIC FLUX DENSITY OF 8.36 T IN THE COIL ..... 72
FIGURE 5.8: SIMULATION OF PIEZOELECTRIC SYSTEM, GRAPH OF OUTPUT AC VOLTAGE IN THE RANGE OF FREQUENCY FROM 50 HZ TO 1 KHZ. ..... 73

FIGURE 5.9: SIMULATION OF PIEZOELECTRIC SYSTEM, GRAPH OF OUTPUT AC CURRENT IN THE RANGE OF F=50 HZ TO F=1 KHZ AND THROUGH $RL = 1\ k\Omega$ ..... 74
FIGURE 5.10: SIMULATION OF ELECTROMAGNETIC COIL SYSTEM, GRAPH OF OUTPUT AC VOLTAGE FOR FREQUENCY OF 10 KHZ. ..... 74
FIGURE 5.11: SIMULATION OF ELECTROMAGNETIC COIL SYSTEM, GRAPH OF OUTPUT AC VOLTAGE FOR FREQUENCY OF 890 KHZ. ..... 75
FIGURE 5.12 EXPERIMENTAL SET UP ..... 76
FIGURE 5.13 EXPERIMENTAL GRAPH OF FREQUENCY VERSUS PIEZOELECTRIC AND COIL AC VOLTAGE..... 76
FIGURE 5.14 EXPERIMENTAL GRAPH FOR PIEZOELECTRIC AC VOLTAGE TO THE CURRENT..... 77
FIGURE 5.15 EXPERIMENTAL GRAPH OF COIL VOLTAGE TO CURRENT..... 77

# LIST OF TABLES

TABLE2. 1: THE CLASSIFICATION OF COIL AND MAGNET COUPLING IN EMEH [14] ..... 7
TABLE 3.1: THE CANTILEVER, COIL AND MAGNET PARAMETERS IN SIMULATION ..... 47
TABLE3.2: OUTLINE OF MODEL ..... 49
TABLE 4.1: THE LUMPED PARAMETERS MODEL OF A 31-MODE, BIMORPH PEH SYSTEM ... 54
TABLE 4.2: FOUR DIFFERENT PIEZOELECTRIC MATERIALS COEFFICIENTS [32]. ..... 57
TABLE 4.3: THE PHYSICAL CANTILEVER AND MASS SIZE PARAMETERS OF DESIGN. ..... 59
TABLE 4.4: THE RESONANCE FREQUENCY CHANGES BY FOUR DIFFERENT MATERIALS (A, B, C, AND D) AND CHANGING OF TRANSDUCER SIZE (DECREASE, ORIGINAL, INCREASE) 61
TABLE 5.1: SPECIFICATIONS FOR DEVICE DESIGN AND MATERIALS ..... 70

# NOMENCLATURE

| | |
|---|---|
| g | Acceleration of gravity |
| $I_{ds}$ | Drain to source current |
| σ | Mechanical stress |
| $g_{ij}$ | Voltage constant |
| $d_{ij}$ | Piezoelectric strain constant |
| Q | Quality factor |
| B | Magnetic field |
| $B_c$ | Magnetic field of coil |
| $A_c$ | Coil surface area |
| N | Number of turns |
| m | Mass |
| c | Viscous damping coefficient |
| $c_m$ | Mechanical damping coefficient |
| $c_e$ | Electrical damping coefficient |
| k | Spring constant |
| L | Length of cantilever |
| $l_e$ | Length of electrode |
| $l_p$ | Length of piezoelectric layer |
| $t_p$ | Thickness of piezoelectric layer |
| $l_m$ | Length of mass |
| $t_m$ | Thickness of mass |
| $f_n$ | Natural frequency |
| T | Vectors of induced mechanical and electrical stress |
| E | Vectors of electric field |
| $s^E$ | Elasticity |
| $\varepsilon^T$ | Dielectric constant |
| D | Electrical displacement |
| S | Mechanical strain |
| $Y_p$ | Young modulus of piezoelectric |

| | |
|---|---|
| $Y_{sh}$ | Young modulus of shim |
| $C_p$ | Piezoelectric capacitor |
| $F_{in}$ | Input excitation force |
| $F_m$ | Mass force |
| I | Effective moment of inertia |
| M | Moment |
| $t_{sh}$ | Thickness of shim layer |
| a | Constant |
| $C_{st}$ | Storage capacitor |
| $\rho$ | Density |
| $f_r$ | Parallel resonance frequency |
| $f_a$ | Series resonance frequency |

# ABBREVIATION

| | |
|---|---|
| EMEH | electromagnetic energy harvester |
| PEH | piezoelectric energy harvester |
| VEHS | vibration energy harvesting system |
| EHS | energy harvesting system |
| MEMS | micro electromechanical system |
| NEMS | nano electromechanical system |
| SDOF | single degree of freedom |
| MDOF | multiple degree of freedom |
| EMF | electromotive force |
| PDMS | polydimethylsiloxane |
| SHM | structural health monitoring |
| MEMS | microelectromechanical systems |
| RMS | root mean square |
| FEA | finite element analysis |
| IDT | interdigital transducer |
| PVDF | poly vinylidene fluoride |
| Q-factor | quality factor |
| PMOS | p-type metal-oxide-semiconductor |
| NMOS | n-type metal-oxide-semiconductor |
| CMOS | complementary metal-oxide semiconductor |
| PDE | partial differential equation |
| ODE | ordinary differential equation |
| FEA | finite-element analysis |
| GCC | gate cross coupled |
| PMPG | piezoelectric micro power generator |
| FWBR | full wave bridge rectifier |
| FWSR | full-wave synchronous rectifier |
| BSR | boot strap rectifier |
| GCCR | gate cross coupled rectifier |
| SECE | synchronous electric charge extraction |
| SSHI | synchronous switch harvesting inductor |

| | |
|---|---|
| CMOS | complementary metal oxide silicon |
| MOSFET | the metal–oxide–semiconductor field-effect transistor |
| PMW | pulse width modulation |
| KVL | Kirchhoff’s voltage law |
| KCL | Kirchhoff’s current law |

# CHAPTER ONE

# INTRODUCTION

## 1.1 Overview

The most common ambient sources for energy harvesting are solar energy, electromagnetic field, gravitational field, temperature difference, pressure fluctuation, fluid flow, human movements, mechanical vibration and seismic vibrations. Among those energy sources, the solar energy is one of the most effective power sources with the highest output power density, although it has a usage limitation for outdoors and areas with light [1]. On the other hand, vibrational energy is an abundant non-exhaustive source, which obtains energy from a machine's vibration, human movement or another form of motions [2]. The ambient vibration from environment mostly goes unused. However, there are several methods to obtain electrical energy from these sources [3]. This kind of vibration energy has a considerable potential in Microsystems because of relatively high power density production, being easily accessible, having a simple manufacturing process, being reliable in a harsh environment, having an infinite lifetime and a necessary physical link to the outside [1]. Micro-power generation could be an ideal candidate for tiny wireless sensors, which need small self-supportive power needs for sensing and transferring signals [6].

An energy harvesting system needs proper energy conversion principles and efficient circuitry for the energy management. In the application of energy harvesting process, the electrical power is generated by conversion of environmental waste energy into a clean and renewable energy source that could be usable power for various applications. Applications of energy harvesting systems depending on the functionality and the performance of energy harvesters could evaluate [4, 5]. Besides, a transducer and a principle for energy conversion could be chosen for the system [4, 5]. Transducers are important for energy harvesting. In this case, there have been three different types of transducers to scavenge energy. They include electrostatic, electromagnetic and piezoelectric [1]. Furthermore, Transducers are sensors with sensing elements and physical properties. Moreover, they can convert information from one form to another

(harvesting electricity is from the process of conversion of energy) and make an interface between the processes controlled and controlling elements. Consequently, they are detecting input from the physical environment to the output signal and convert the signal to the human readable display.

The first type, Electrostatic energy harvesting systems, utilise several capacitors that have overlap areas and their capacitance changes by altering the area with applying ambient vibration to the structure. The second type is piezoelectric devices that scavenge energy utilising the piezoelectric effect of piezoelectric materials that have the capacity to convert mechanical strain into electrical energy. Thirdly and lastly, the inductive energy harvesters employ electromagnetic field in the coil to generate electrical energy from environmental vibration of the electromagnetic structure.

## 1.2 Motivation

There are several reasons for choosing vibration energy harvesting systems (VEHS) as my thesis topic that are as follows.

First, ambient energy harvesting system (EHS) has some benefits over the other battery based power generators. As mentioned in [6], they are including self-powering, last long operation without maintenance, safe without chemical disposal, no charging needed, cost-effective and flexible.

Electronic devices previously gain their power from batteries whereas batteries lifespan, and device's functionality bounded by the power consumption in the electronics [4]. Hence, developing fully self-powered circuitry is an objective consideration in the practical Vibration energy harvesting system (VEHS) [5].

Second, the amount of power which is available from the ambient source is practical for small electronics with improving output capacity.

Last, the system has potential in the market (wireless sensors, actuators) with a variety of types. In fact, the applications expand in several industries like biology science for biosensors especially the wearable one. Moreover, mechanical and civil engineering in building structure and rail tracks for health monitoring (condition monitoring). The researchers including Tsai, Kymissis, Elvin, James, Chao debated about applications with different types of VEHS [7-11].

For example, in [8] a heartbeat sensing device with stretch ability and electromechanical sensitivity from controlled multilayer PDMS, which are polymers and skin-like piezoelectric rubber films presented. The polymers are piezoelectric rubber films with suitable cellular structure and potential for sensing and powering for the specific application. Besides, A PEH system developed which uses ambient lost energy from walking to generate enough power for a radio transmitter [5-7]. In fact, it is a shoe- mounted piezoelectric generator to transmit identification code while the bearer walks and serves for a personal positioning system for military or police units as well as for personal navigator [5-7]. Additionally, there was a proposal to design embedded piezoelectric patches in the structure to measure the mechanical strain [8]. Also, James et al. in 2004 proposed a low power accelerometer as a sensor and a vibration based EMEH used to monitor condition applications such as structural health monitoring (SHM) as described in [10].

## 1.3 Problem statement

Vibration Energy Harvesting Systems (VEHS) has several problems and limitations. These include [6]:

(i) Bandwidth and linearity: narrow bandwidth implies constrained resonance frequency and limits applications. The range of frequencies which reduces the number of efficient nonlinear dynamics to increase the efficiency.

(ii) The capacity in MEMS/NEMS (Micro/Nanoelectromechanical system) technology: the limitations in MEMS/NEMS include the factors a) small mass and maximum displacement; b) miniaturisation issue for micro-magnets and piezo beams; and c) abound for power density in microscale systems especially for electrostatic systems.

(iii) Output results: the difficulty is with generating enough power in 10 mW to 100mW for milliwatts electronics and low output voltage for the EMEH device.

The electromagnetic and piezoelectric EHS each of them separately as transducers has specifications that limited their capacity.

Piezoelectric transducers generate desirable output voltages (2-10V) and well adopted in miniaturisation and compact technology [6]. However, this piezoelectric thin

film in the system has low electromechanical coupling coefficients that require large mechanical load in optimal electrical generation power point [5, 6]. On the other hand, electromagnetic transducers have a very low output voltage (0.1V). Also, they operate in the low-frequency range in medium size EHS with relatively low impedance at maximum power generation point. But, their microscale integration is expensive because of complex manufacturing of micro-magnets and the necessity for large mass displacement [6].

## 1.4 Objectives

In view of the above-mentioned needs, we embark on this study to determine and calculate higher output power and voltage with frequency band study for better efficiency for piezoelectric and/or electromagnetic energy harvesting system. To be more precise, the objective of this work was to:

1. Study the fundamental frequency vibrations to natural vibration of the beam.
2. Develop the understanding of the detailed[1] mechanical, electrical and electromechanical interaction of piezoelectric and electromagnetic energy harvesting.
3. Design a suitable model that can properly include the dynamics of both the mechanical and the electrical components with energy harvesting circuits with minimum error in comparison to physical experiments, and high accuracy on the harvesting power and efficiency.
4. The testing design of a hybrid electromagnetic and piezoelectric energy harvesting system with higher output results and more efficient in comparison to the stand-alone piezoelectric or electromagnetic energy harvester.

## 1.5 Thesis Structure

Chapter 1 defines the objectives of this work that include the effect of different piezoelectric materials on vibration beam, the specifics of mechanical and electrical

[1] mentioned in chapter two pgs.: 10-40

components of PEH and EMEH. There are also design and test a hybrid system to compare to the result of standalone PEH and EMEH. Furthermore, the main motivation of this study is to improve the energy harvesting systems by looking at different applications of PEH and EMEH.

In chapter 2 the literature is reviewed on the development of vibration based energy harvesting systems. It presents a comprehensive survey of existing models and design of electromagnetic energy harvester (EMEH) and piezoelectric energy harvester (PEH). The effective parameters for each system investigated. In the end, different application of each system is evaluated.

Chapter 3 presents the proposed evaluation on one of the best existing transducer's design with up converted input mechanical frequency. The modelling of the EMEH system based on Faraday's induction law and motion equation for cantilever beam evaluated. The system's performance is evaluated by implementing the changes to the cantilever length and resonance frequency with respect to the peak of output voltage.

Chapter 4 gives the existing lumped analytical model to describe one of the best piezoelectric energy harvesting system. The function of mechanical motion parameters and electrical domain of piezoelectric (electromechanical) harvester including the interface circuit is given in mode of circuit elements. The proposed evaluation in MATLAB for presented design and model tested for different system size and piezoelectric materials.

Chapter 5, an experimental testing of the proposed hybrid mechanisms of vibration based electromagnetic and piezoelectric energy harvester system is implemented. The results of experiment set up are compared to the results from MATLAB simulation and COMSOL modelling software.

Chapter 6 a conclusion and recommendation for future researches are given.

# CHAPTER TWO

# LITERATURE REVIEW

## 2.1 Synopsis

In this chapter, the concepts and literature of energy harvesting technology utilising mechanical vibration source, the electromagnetic and piezoelectric energy harvesting systems are examined. In Section 2.3, physical design structure of the existing EMEH and PEH systems are presented and they compared according to their effective features. The designs of EMEH are affected by coil-magnet physical positions and quantity of magnets. The design of PEH device depends on piezoelectric layer parameters and its relation to electrodes and inactive layers. In Sections 2.4, the analytical modelling with distributed or lumped parameters for the transducer, power converter and load in PEH and EMEH systems depending on physical design are reviewed. At the end, in Section 2.5, the existing applications for both PEH and EMEH system in different technologies presented.

## 2.2 Introduction

EMEH systems are inductive generators with an electromagnetic energy source and generate electrical energy from the conversion of mechanical energy of ambient vibration. The typical electricity generation is described by Faraday's induction law when magnetic force interacts with a coil (spiral or helix) as a conductor. There are different EMEH types of generators. They are classified based on the relative coupling of coil and magnet with respect to each other and the mechanical excitation. For example, the system could use a magnet moving with a spring or cantilever in simple harmonic motion [12, 13]. There are two modes, fixed coil and moving magnets in the same or opposite pole orientation [12]. Alternatively there could be a moving coil with a fixed magnets configuration. Further, coil and magnet are physically in line or perpendicular to each other with the congruent or orthogonal centre axis to oscillation direction with back iron or without back iron [14] as shown in Table 2.1.

Table 2.1: The classification of coil and magnet coupling in EMEH [14].

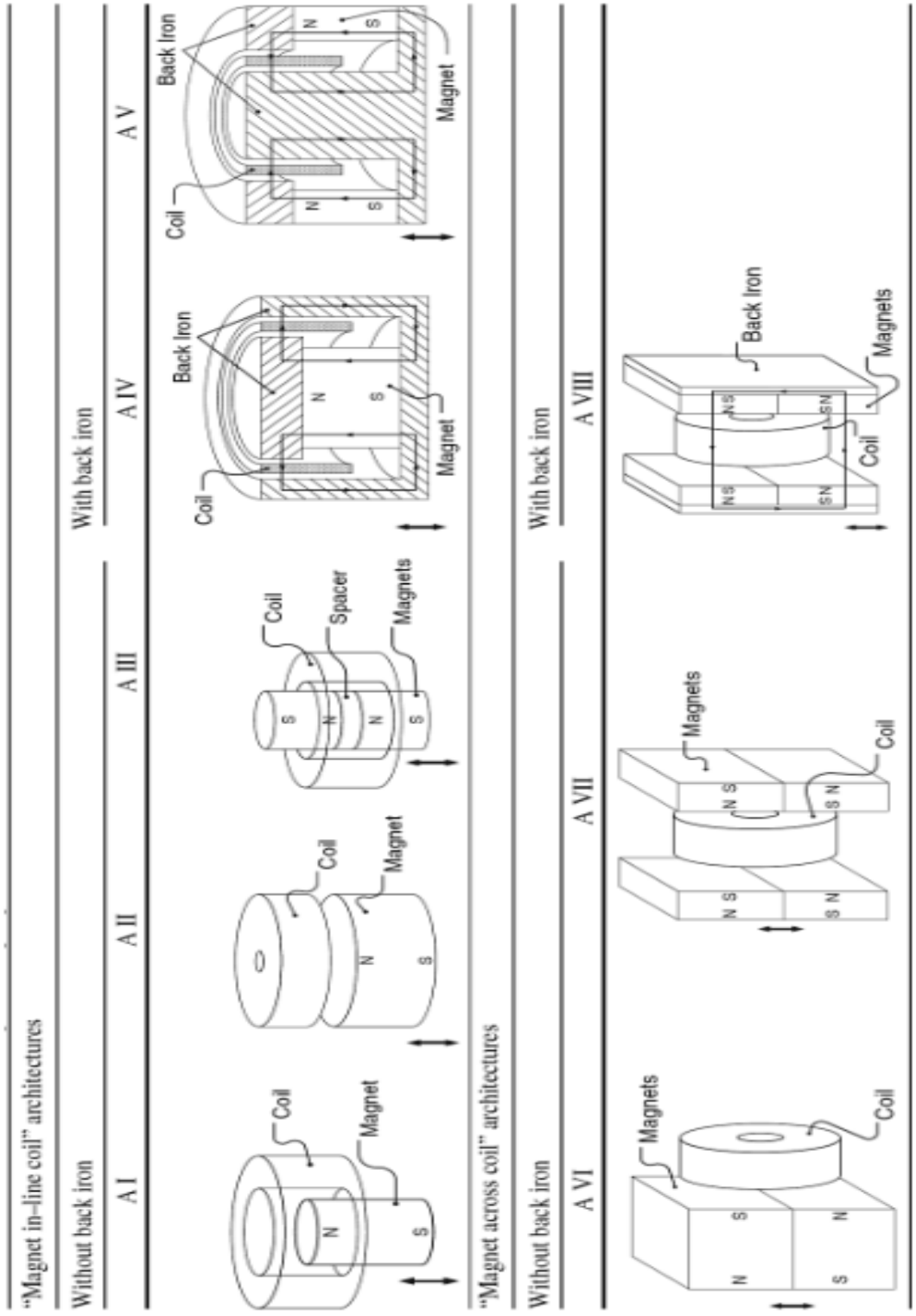

PEH systems as power generators and sensors could work with ambient vibration energy sources and provide advantages consisting of the ease of bulk to micro/nanosystems transformation and integration, having long lifetimes and the tendency of direct energy conversion [3]. The piezoelectric energy harvesting (PEH) systems use the piezoelectric effect of materials to scavenge energy from the system. Piezoelectricity is a material's feature that defines by applying strain energy from external vibration to deform the beam and produce a local charge separation in material's molecular structure [3]. This effect introduces electric charges to harvest from the system [3].

Vibration-based energy harvesting systems are more popular for using the piezoelectric and electromagnetic energy harvesting (PEH/EMEH) mechanism to harvest electrical energy because of high electromechanical coupling with no requirement to external voltage sources and their particular attention for use in microelectromechanical systems (MEMS) [15].

Torah et al. in 2006 reported an electromagnetic energy harvesting system that has four magnets mounted on a cantilever spring and a magnetic flux produced in the coil as the magnets are in opposite polarities and the device vibrates at the resonance frequency of 56.6Hz [16]. This generator generated the maximum output power of 17.8 μW at the acceleration of $0.6\ \mathrm{ms}^{-2}$ which rated as a low output generator.

Low output power and power density from a single mechanism of piezoelectric or electromagnetic components are problems for various applications. The solution to the stated problems could solve by hybrid energy harvesting devices to generate more energy to charge the output device and increase the reliability of the system.

Hybrid mechanisms of vibration harvester systems are using the coupling factor between mechanisms such as piezoelectric and electromagnetic energy harvesting system in this study. This idea is not new but it develops by new composite material for the piezoelectric material layer with high voltage capacity, numerical modelling for the new design in COMSOL and cheaper experimental set up for the prototype testing.

Yang et al. in 2010 proposed a hybrid electromagnetic and piezoelectric energy harvester that used a cantilever structure containing multilayer piezoelectric materials as a beam, magnets as a tip mass and coils near the magnets [17]. The relative position of

coil and magnets changes in the three types that show in Fig 2.1. They include type one and two, with magnetic pole direction using the z-axis and plane coils located in the horizontal and vertical plane. Type three has magnetic pole direction using along the y-axis and the plane coil located in the vertical plane. Each prototype uses 2, 4 and 6 magnets. Consequently, the output power of type III devices with 6 magnets and 2.5 g acceleration at 310Hz frequency for piezoelectric mechanism and electromagnetic mechanisms are 176 μW and 0.19μW respectively. Sang et al. in 2012 made a cantilever structure of hybrid energy harvesting system with maximum load power of 10.7mW at the resonance frequency of 50 Hz and the acceleration of 0.4g [18]. As a result, the output power from hybrid system with the optimal load of 50Ω increased by 81.4% in comparison to standalone electromagnetic mechanisms.

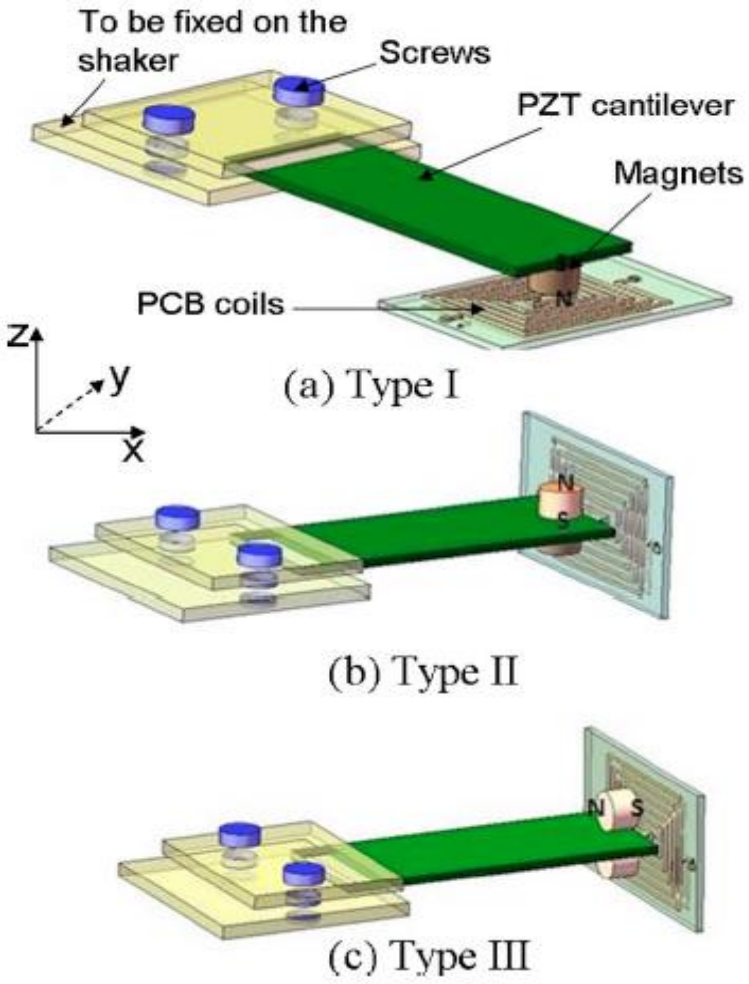


Figure 2.1: The hybrid PEH and EMEH system with a, b, c different positioning of magnet to coil [16].

## 2.3 Physical Design Structure

### 2.3.1 Electromagnetic Energy Harvester (EMEH)

There are three different structures for an EMEH system design including Cantilever beam structure (one clamped end and free on the other end) in Figure 2.2 with a beam[16, 19-23] or spring [24], cylindrical structure in Figure 2.3 with mechanical spring [13, 25] or magnetic spring [26] and disc structure in Figure 2.4 [27, 28].

#### 2.3.1.1Cantilever Beam Structure

In [16, 19] the architecture is "magnet across coil" with and without back iron (A-VIII) regarding Table 2.1 and using the cantilever beam structure. The beam vibrates with tip mass that is a coil or magnets depending on which one is moving. Developing an EMEH system including a coil between two magnets as the geometry requirement should involve winding a coil around magnets that are heavy and the motion result in low output voltage across the coil [19]. This structure showed in Fig 2.2 (a). Moreover, four magnets around a coil in Fig 2.2 (b) generates useful power of 157 µW tested in the engine block of a car [19]. This design also used in [16] by using a beam (a cantilever spring, dimensions optimised using ANSYS) with magnets (the size optimised using Ansoft Maxwell 3D) in opposite polarities above and below of the beam demonstrates in Fig 2.2(c) and a magnetic flux field produces electric current through the fixed coil. The device in [16] works in the frequency range of 50 Hz to 60 Hz with resonance in 56.6 Hz the optimised design generate the output power of 17.8 µW.

Above designs elucidate the magnetic field strength (H) regarding the following parameters:

a) Coil inductance (L) which increase by increasing the number of turns (N), bigger coil area including its diameter ($A = \pi r^2$), shorter length (l), higher coil's core

permeability ($\mu=\mu_r\mu_0$ where$\mu_r$ is relative permeability and $\mu_0 = 1$ for air) as mentioned below

$$L = \frac{N^2 \mu A}{l} \quad 2.1$$

$$emf = -L\frac{\Delta I}{\Delta t} \quad 2.2$$

b) Increasing in the magnet dimensions which means a larger proportion of coil intersects with the magnetic flux gradient.

c) The magnetic field strength the proportional to the inverse cube of the distance from dipole as mentioned in equation 2.3 which means adjusting the gap between magnets or magnets and the coil.

$$B\alpha\frac{1}{r^3} \quad 2.3$$

In [24] with the design in Fig2.2(e) the architecture is "magnet in-line coil" without back iron (A-II) regarding Table 2.1 and using the cantilever spring structure. There is a magnet as an inertial mass in the centre of spiral spring with fixed ends [24]. The function of this design is to increase electromagnetic forces by improving magnetic flux density and motion. Besides, the coil is fixed below the magnet and various vibration and load resistance applied. This design is good for low ambient vibration and acceleration devices that generate 115.1μW output power [24].

The efficiency and power density of vibration EMEH system depend on the value of vibration frequency [22]. The ambient low frequency usually extracted from the environment and mostly from human motion that is in the range of (1-10 Hz) [22]. So, there are several studies have worked on a mechanical frequency up-conversion method for EMEH as a frequency increased generator that either absorbs or convert mechanical energy into electrical one. The transferred energy to high-frequency oscillator mainly depend on the stiffness of the spring (spring constant, k) and this ratio changing by mass

(m) and damping ratio (c) [29]. This ambient low frequency could be for a resonance beam [30] or non-resonance oscillator [25] with limited force and displacement sources. The frequency up-conversion method utilises mechanical impact or magnetic attraction between a permanent magnet and a magnetic material to convert the low ambient frequency vibration ($w_n{}'$) to high natural frequency ($nw_n{}'$) [20, 21, 23, 25]. So, the duration ($\tau$) of this temporary motion in one cycle ($2\pi$) depend on the effective mass (m) which is express as equation 2.4 in [29].

$$\tau = \frac{2\pi}{n\omega_n{}'} = \frac{-2m\ln(^{Z}/_{Z_0})}{c} \qquad 2.4$$

Where $Z, Z0$ are displacements in $t = 1, t = 0$ and $c$ is damping coefficient.

In [20-23] the architecture is "magnet across coil" without back iron (A-VI) regarding Table 2.1 and using the cantilever beam structure. Their design structure as show in Fig 2.2(d) is a pickup coil on a cantilever beam as a tip mass and a magnet placed on a vibrating support across the coil [20-23]. There is a mechanical barrier arm on magnet's diaphragm with the function of up-conversion. The first attempt in [22] by increasing frequency from 10 Hz to 643 Hz provides the RMS (root mean squared) output power of 68.7 µW. However, in [23] the same structure design and technique used by conversion of 10 Hz to 394 Hz, which is lower value of conversion in comparison to previous work still 544.7 µW RMS power harvested. The evaluation of [22] and [23] highlighted the other effective parameters in design such as magnet configuration and number, coil geometry and scaled down the device dimensions.

| STRUCTURES | DESIGN | REFERENCES/METHODS |
|---|---|---|
| CANTILEVER | 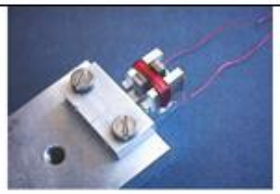 (a) | Using beam as a cantilever [19] |
| | 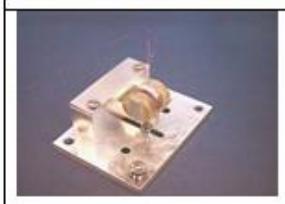 (b) | Using beam as a cantilever [19] |
| | 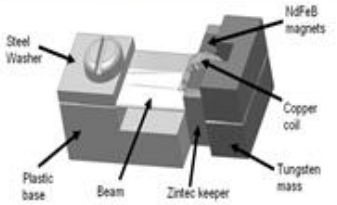  (c) | Using beam as a cantilever [16] |
| | 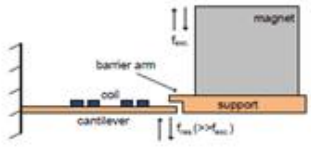  (d) | Using beam as a cantilever , frequency up-conversion [20-23] |
| | 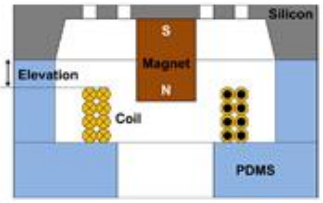  (e) | Using spring as a cantilever [24] |

Figure 2.2: Cantilever structure of EMEH system.

### 2.3.1.2 Cylindrical structure

The architecture of “magnet in-line coil” without back iron regarding Table 2.1 and the cylindrical structure applied in [13, 25, 26].

Using two helical compress springs and coupling them with two stationary NdFeB magnets at both ends of the thick hollow cylindrical tube (architecture of AII), wrapping coils around both ends and a moving non-magnetic ball in the middle of the structure mentioned in [25]. This non-resonant and up-converted system (the free ball impact the magnet by hitting it to vibrate at higher frequency) in Fig 2.3 generates 110μW average power and allows the powering of smart devices from low-frequency (<5 Hz) vibrations (shake hands, 2.5-6 Hz) [25].

Another design in [13] as demonstrates in Fig 2.3 is with one resonance spiral spring attached to a permanent magnet (architecture of AII) and a coil packed in inner and outer cylinder housing vibrates. This structure simulated using ANSYS and shown the spiral geometry of spring has lower spring constant and stress concentration that causes a larger displacement and useable in the applications with less than 100Hz input frequencies.

Lastly in [26, 31] a cylinder design proposed with one or two fixed permanent magnets at the ends (magnetic springs) of the tube and one or two moving magnets (mass) in the middle where a coil wrapped in series outside the tube (architecture AI). These EMEH tube designs show in Fig 2.3 (a-1), (a-2) and (b). The results in [26] show that the system vibrates with 8 and 6.5 Hz resonance frequency to move the magnets in middle and a voltage induces in the coil [26]. The results from [26] indicate the followings:

a) The cylindrical structure is beneficial in compare to the cantilever structure for random vibration signal

b) The magnetic spring with ease of construction, tenability and less prone to fatigue is better than mechanical spring

c) The average generated electrical power of the vibrational generator is proportional to the cube of the frequency

Munaz in 2013 adopted the design in [26] and the optimised EMEH generated 4.84 mW output power with the load resistance of 1 kΩ for three magnets at 6 Hz resonance frequency[31].

| STRUCTURES | DESIGN | REFERENCES/METHODS |
|---|---|---|
| Cylindrical | 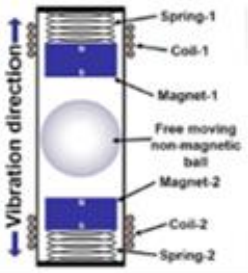 | Non resonance mechanical spring, frequency up-conversion by non-magnetic ball [25] |
| | 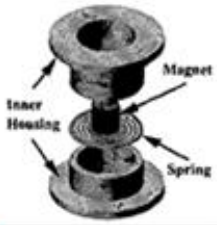 | Resonance mechanical spring [13] |
| | 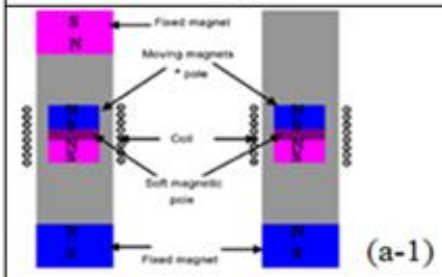 (a-1)<br> 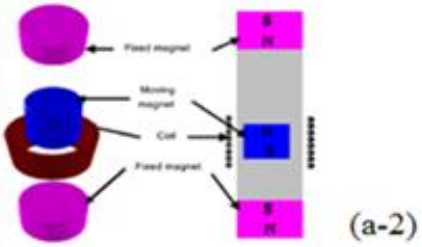 (a-2)<br> 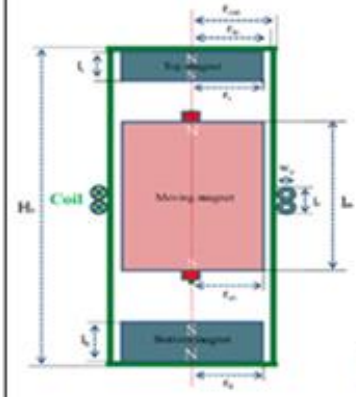 (b) | Magnetic spring and multipole magnet [26, 31] |

Figure 2. 3: Cylindrical structure of EMEH system.

### 2.3.1.3Disc structure

The “magnet in-line coil” architecture without back iron (AIII) regarding Table 2.1 and the disc structure used in [27, 28]. These articles utilise spiral springs connected to a plane winding the coil that is surrounding a movable permanent magnet of FePt membrane with spacers between them [27, 28]. The EMEH system displays in Fig 2.4. The results show that the EMEH system generates a nonlinear magnetic flux and maximum output power of 100 µW at 60 Hz [27, 28].

| STRUCTURES | DESIGN | REFERENCES/METHODS |
|---|---|---|
| Disc | 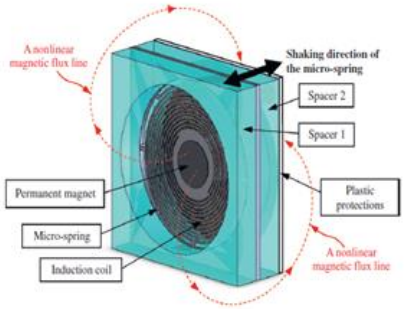 | Nonlinear magnetic flux with spiral spring [15, 16] |

Figure 2. 4: Disc structure of EMEH system.

### 2.3.2 Piezoelectric Energy harvesting (PEH)

There are several methods to design, improve and solve issues comprising the size and volume matter, low efficiency, small output power and voltage in piezoelectric power generators and scavenging energy from different kinds of ambient vibration source.

Firstly, it is important to select an efficient coupling mode of operation [32-35] or chose the proper device configuration [35-37] for the cantilever (piezoelectric layer and electrodes) of a vibration PEH system.

### 2.3.2.1The Coupling Modes of operation

The coupling modes of a cantilever in a PEH system are mostly either transverse 31-mode or longitudinal 33-mode. When the cantilever is in the transverse mode, the electric field is applied perpendicularly to the input strain. However, in the longitudinal mode, the electric field is applied parallel and in the same direction as the input strain.

Sood in [34] and Kim in [33] compared the 31-mode cantilever with two separate electrodes on top and bottom of the beam and the 33-mode cantilever with an interdigitated (IDT) electrode only on top of the beam. These two coupling modes introduced in Fig 2.5. The results of comparison between the features of 31-mode and 33-mode cantilever for a piezo-generator are following:

a. The distance between electrodes in the 31-mode beam is equal to the thickness of the piezoelectric layer while, in the 33-mode beam, it is independent and much larger than the piezoelectric layer thickness (~10 times of PZT thickness)[34].
b. Choice of the 31-mode cantilever beam over the other modes is due to its simple fabrication, lower chance of breakdown (electrodes distance as mentioned in "a") in the system with lower open-circuit voltage [38] and having typical higher power and efficiency in the output medium[33].
c. The 33- mode cantilever has a larger coupling coefficient (k) than the 31–mode as mentioned in equation 2.5 [32].

$$k = \sqrt{\frac{\text{Electrical Energy}-\text{Out}}{\text{Electrical Energy}-\text{In}}} \qquad 2.5$$

d. The 33-mode cantilever with the same dielectric constants ( $\varepsilon = \varepsilon_r \varepsilon_0$) as the 31-mode in the system has larger magnitude piezoelectric coefficients ($d_{33}, g_{33}$) of about 2 to 2.5 times and its open circuit voltage is about 20 times [33, 34].
e. The poles in 33-mode cantilever because of the electrode configuration can be harder than the 31-mode cantilever [33].

f. The PEH systems used the 31-mode cantilever more often with a small force and the low vibration system. Having higher capacitance in $d_{31}$mode PEH in compare to $d_{33}$ mode device conducts a better performance in transverse mode device[33]

The open-circuit voltage ($V_{oc}$) as mentioned above defined in [33, 34] as below

a) the applied stress ($\sigma_{ij}$[2])
b) The distance between electrodes ($L_x$, subscript x = 1 or 3)
c) The voltage constant $(g_{ij})$ Vm/N

and define as below equation 2.6

$$V_{oc} = \sigma_{ij} L_x g_{ij} \quad 2.6$$

Moreover, piezoelectric strain constant ($d_{ij}$) is proportional to the voltage constant $(g_{ij})$ Vm/N via the dielectric coefficient ( $\varepsilon = \varepsilon_r \varepsilon_0$) mentioned in equation 2.7.

$$g_{ij} = \frac{d_{ij}}{\varepsilon_r \varepsilon_0} \quad 2.7$$

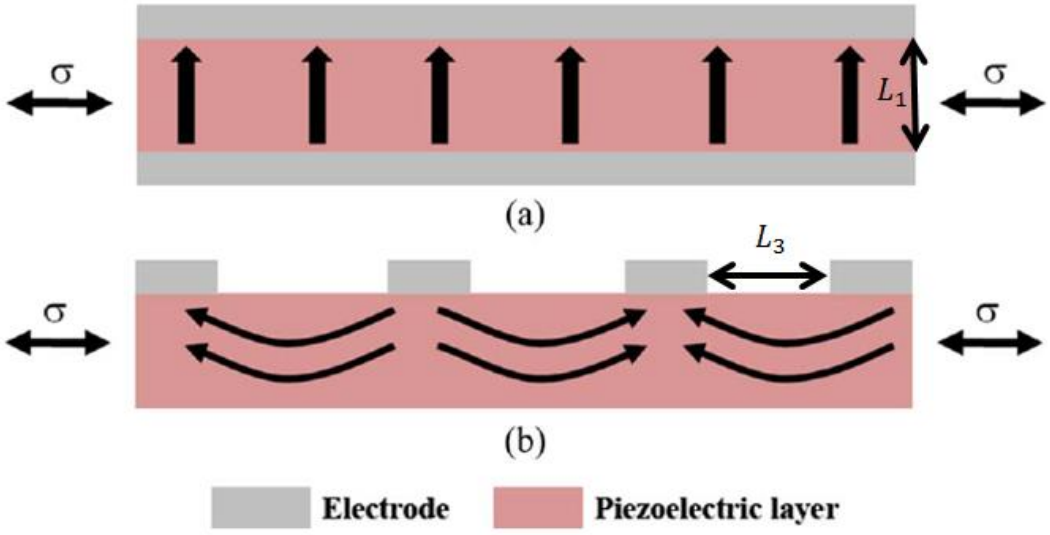


Figure 2.5: The coupling mode between piezoelectric layer and electrodes a) the $d_{31}$ mode with electrodes distance of $L_1$ b) the $d_{33}$ mode with electrodes distance of $L_3$ [33].

[2] Appendix B

Therefore, above relations confirm the importance of electrode factors, poling degree and simple fabrication in selecting the better performance in the design.

### 2.3.2.2 The Device Configurations

The configuration of piezoelectric energy harvesting systems could change using a uni-morph or triple layer bi-morph structure is shown in Fig 2.6 with one active layer and one inactive layer or an inactive layer between two active layers respectively [35]. The active layers consist of piezoelectric materials, and the inactive layer is a polymeric epoxy or metallic materials with elasticity [36].

The bimorph bending mode of active layers (piezoelectric patches) could design in series or parallel depending on polarisation direction and the applied field in the cantilevers [36]. In deformation of series layers, the electric field is applied perpendicular to the polarisation direction of an upper active layer, and its length expands while a lower active layer has a polarisation direction parallel to the applied electric field and condenses the layer [36]. However, parallel layers provide the same polarisation direction and electric field across the individual layers with opposite direction.

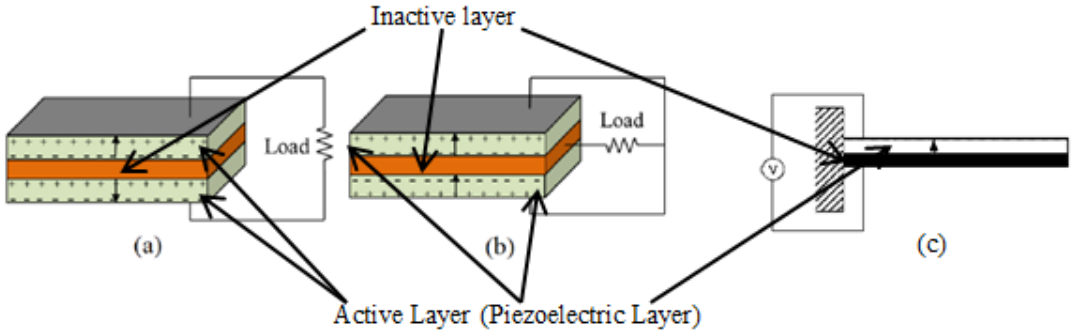


Figure 2.6: The piezoelectric layer configurations a) bi-morph in series electrical connection [37] b) bi-morph in parallel electrical connection [37] c) uni-morph [36].

The piezoelectric bender results in [35] show that the uni-morph structure generates maximum power of low excitation frequencies and load resistance while the

bimorph structures for parallel and series electrical connection generate highest power with medium and high excited frequency and load resistance respectively. In [36] they indicated that the bimorph benders are acceptable in many applications because of its features such as generative force (as actuators) and high sensitivity (as a sensor) and providing large displacement. They also deliver better reliability with an inner elastic layer that controls the deformation of both layers [36].

Also, it is important to alter the geometrical arrangement of the cantilever with mass function [35] or tuning the device using frequency matching and frequency band in a vibration PEH system.

#### 2.3.2.3 Geometrical Cantilever Arrangement with mass function

There could be different shapes of the cantilever such as rectangular [38], triangular [32], tapered [39] or trapezoidal [32, 40] with point mass or real end mass.

The mechanical construction in [39] has a tapered shape beam cantilever with a coated thick film (70µm) of lead zirconate titanate (PZT5H, piezoceramic). To test the design a shaker as a vibration source used and a mass as a supporting part attached to the beam tip with a short thread [39]. The shape of the beam (non-rectangular) has major edge effects such as boundary condition and damping that make the analytical modelling very complex. Consequently, a numerical modelling called Finite-element analysis (FEA) package of ANSYS software for the modification and testing of the system used [39]. The results demonstrate linear operation between deflection and stress of beam unless the increase of the beam amplitude results in higher stress level and nonlinear operation. Also, the evaluation of graphs in [39] highlighted the function of the electromechanical coupling coefficient ($k_{me}$) in the output power ($p_{out}$) which also indicates $k_{me} \propto (d_{31})^2$ ($d_{31}$ is piezoelectric transverse mode coefficient).

In [38] a rectangular shape beam cantilever with a thick film of PZT (1.64µm) and a nickel-metal mass on the free end tested. The functions of mass involve the mechanical strength improvement and the decrease in the natural frequency of the structure in low-frequency vibrations [41, 42]. The rectangular shape is a traditional and common beam geometry that provides large stress concentration at the cantilever. However, the area of maximum stress is small and the tip hardly strained. As mentioned

in [32] the rectangular cantilever beam needs modification for a more uniform strain distribution to generate more output power.

In both [38] and [39] a 31-mode, bi-morph power generator in micron scale was devised. While these systems have different geometrical cantilever and mass structure, the results in the system [39] with tapered shape cantilever provided 3µW output power and 80.1 Hz resonant frequency under maximum displacement. But, in the power generator developed by [38] just 2.16 µW power is generated within 608 Hz resonance frequency and 1g acceleration strength.

In [32] the cantilever beam with rectangular shape compared to the trapezoidal and triangular ones with point mass or real end mass depending on the cantilever structure. The results show around 30% higher output power in another shape than rectangular cantilever beam with uniform strain distribution.

#### 2.3.2.4 Frequency Matching and frequency band

Matching frequency between the natural and fundamental frequency of vibration is difficult. The matching needs i) precise material properties and regulating dimensions of the cantilever beam and mass in manufacturing ii) choose a frequency from several different fundamental frequencies of machine iii) choose an exact physical location such as in the corner or centre of air duct [32]. The frequency resonance with narrow bandwidth makes the system impracticable in general applications [38].

As mentioned in Shahruz's study in [43], different cantilever beams with different lengths and tip masses (beam-mass system) can be assembled parallel to each other and construct a mechanical bandpass filter shown in Fig 2.7. The advantage of this structure is surging of output power [38] while the disadvantages related to the size increases and not being cost-effective [43]. To study the frequency response of the filter an analytical modelling using a linear partial differential equation (PDE) which is an infinite dimension and a single degree of freedom (SDOF) is used [43]. The result from PDE model gives a transfer function that relates the displacement of the beam tip to the vibration source acceleration [41, 43] where the fundamental frequency is a function of the beam and mass dimensions.

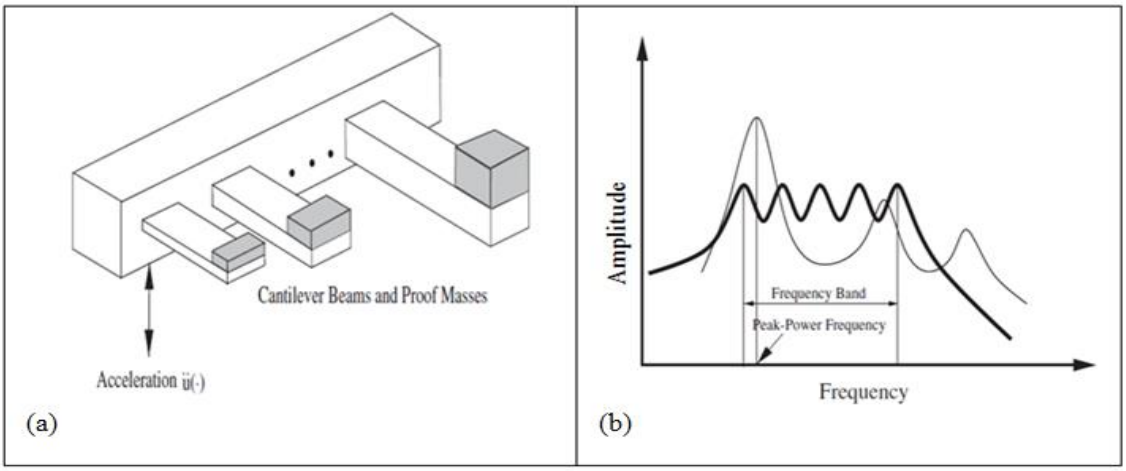


Figure 2.7: a) The mechanical band pass filter b) the frequency band and peak power frequency [43].

The quality factor (Q-factor) in [41] calculated by considering the phase angle peak between the fundamental frequency and the natural resonance frequency. The micro-scale PEH system in [41] obtained 2.15μW power at 461.15Hz resonance frequency with high Q-factor of 233. The high sensitivity and low loss from the calculated Q-factor demonstrate the inverse association between the Q-factor with damping and large differences in output power for small changes in Q-factor.

Finally, it is important to replace the materials of cantilever beam layers including a) active and b) inactive with more efficient one.

### 2.3.2.5 Materials of Cantilever Beam

There are many types of materials for cantilever beam to provide piezoelectric properties either naturally or are engineered [44]. In general, the output power depends on the frequency of vibration and the load resistance. Therefore, having the resonant frequency and an optimal load resistance are associated with the choice of the proper materials for the beam.

Various piezoelectric materials for active layer and a shim material (brass) as an inactive layer for a bi-morph in series electrically, transverse (31-mode) cantilever

beams considered in [45]. Tested active materials are Lead Zirconate Titanate (PZT), Lead Magnesium Niobate, Barium Titanate, Lead Titanate, Lead zirconate titanate and Lead Nickel Niobate. The differences of active materials are in their coupling factor ($k_{3i}$ i=1, 3), quality factor (Q-factor), relative dielectric constant ($\varepsilon_r$) and Young modulus($Y_p$). The inactive layer has a Young modulus (Y) of 110GPa.

Testing different active materials in [45] shows various connections between parameters. First, there is an exponential relation among each of the coupling factor (k), the Q-factor and the relative dielectric constant ($\varepsilon_r$) with the optimal resistance [45]. However, the Young modulus of materials (Y) is in direct relation to the resonance frequency [45]. Second, the output power of the materials parameters graphs affirms a direct correlation of the output power to the Q-factor, while has an inverse relation with relative dielectric constant ($\varepsilon_r$) and Young Modulus (Y) [45]. At the end, in [45] the dependence of output power on the vibration frequency (depending on the material) and load resistance indicated and with optimal resistance and at resonance frequency the best material performance belongs to the Lead Titanate.

The other thin active layer introduced in [46] which is zinc oxide (ZnO) and the inactive layer is silicon with a 33-mode cantilever beam and a mass at the free end of the cantilever. This vibration PEH system with z-direction displacement modelled numerically with FEA package of CoventorWare[2] software and provided the device resonance frequency at 34.4 kHz.

a) Type of Active Materials

Lead zirconate titanate is a material known as PZT, which is the most common and efficient example of piezoelectric ceramic used in power harvesting [4, 34]. However, the piezoceramic materials have some disadvantages such as their brittle nature and having a fatigue crack growth susceptibility because of applied strain or loading in the high frequency [4]. Poly vinylidene fluoride (PVDF) is also a piezoelectric polymer that exhibits better flexibility than the PZT for power generator applications. Additionally, there are fiber-based piezoelectric (piezo fiber) materials, which can contribute to higher power outputs, more efficient systems, larger

displacement capability in thicker plates, the highest piezoelectric coefficient ($d_{ij}$) and the lowest dielectric constant with the smaller diameter [4].

b) Type of Inactive Materials

The substrate of a piezoelectric layer of the cantilever beam with either uni-morph or triple layer bimorph configurations can change the amount of output power of vibration PEH system.

The substrate materials tested as shown in Fig2.8 for a 31 mode, uni-morph cantilever beam in vibration PEH system in [44] while the cantilever beam geometry, the active layer material (PZT) and the thicknesses of active/inactive layer fixed.

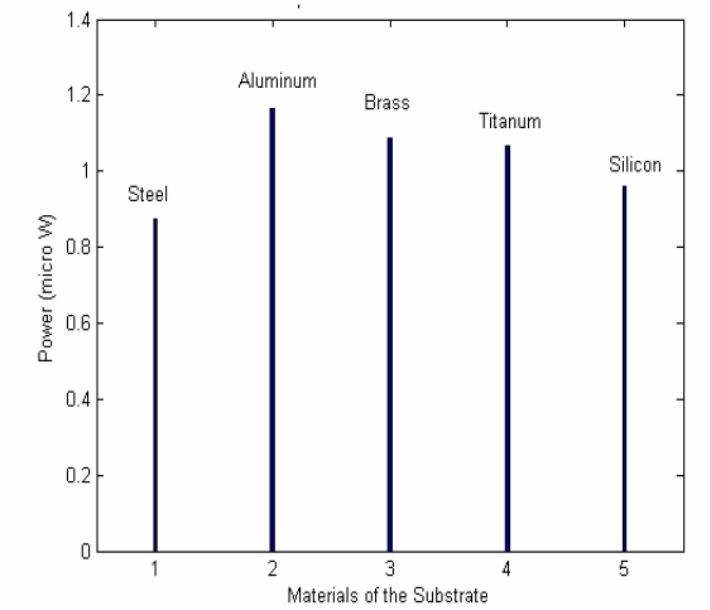


Figure 2.8: Effect of different substrate materials on the output power for the design in [44].

## 2.4 Modelling and Testing

To measure the parameters of the designs for PEH and EMEH systems, first the analytical (mathematical) modelling of the transducer, power converter and load separately is necessary. Second, the design should test with setting up the experiment for prototype and/or compare the numerical results with different analytical methods.

There is a source of excitation for any VEHS, which could be a shaker, an external force (shock with dropping from a given height or moving object hits the beam [47] ) or a motor with Harmonic motion.

### 2.4.1 Transducer

The transducer is a complex three-dimensional structure that is operating simultaneously in both the electrical and mechanical domains with lumped or distributed parameters. The distributed parameters use for modelling spatially or time-varying system that is difficult to integrate directly them into circuit analysis. However, lumped parameters model applicable for circuit analysis with multiple energy domain systems. In fact, the distributed electromechanical behaviour of the transducer is lumped into discrete circuit elements. However, this method is limited for systems with smaller dimensions than characteristic wavelength.

The piezoelectric transducers comprise of base, beam, mass and piezoelectric layer while for electromagnetic transducers consider spring/beam movement and coils - magnets. For modelling, a transducer three elements consider as mentioned with details below,

1. The mechanical parts:
   - I. There is a kinetic energy of a mass which is magnets or/and a coil in EMEH and it is proof mass (as an inductor in equivalent circuit element) for support in PEH
   - II. There is elastic energy (stiffness) of a spring (or beam/magnet spring) for either PEH or EMEH (as a capacitor in equivalent circuit element)
   - III. There are some damping coefficients (losses, as a resistor in equivalent circuit element) in the mechanical domain such as air and electrical one such as conversion mechanism or resistor in this domain.
   - IV. The deflection of the tip of bent beam generates charge flow in the mechanical domain in PEH and charge in EMEH is in the electrical domain for magnetic flux density in the area of coil and magnet to generate flux.

2. The electrical parts usually defined by circuit elements comprise of:

I. In EMEH, the coil modelled with a series RL circuit. L is self-inductance of coil and R internal resistance of the coil.

II. In PEH, the piezoelectric layer modelled with a series RC circuit. C is the piezoelectric layer capacitance and R is its dielectric of piezoelectric materials.

3. The coupling of mechanical and electrical domain ($k_{me}$) indicated as:

I. Base on Faraday's law of induction EMF is $\varepsilon(t) = -\frac{d\varphi}{dt}$ which can be rewrite as $\varepsilon(t) = G\frac{d(\text{motion plane})}{dt}$. So the coupling is factor "G" in EMEH.

II. An ideal transformer with (1(primary): N (secondary), step-up transformer $\frac{N_s}{N_p} = \frac{V_s}{V_p}$ ) turns ratio or a voltage source in mechanical domain and a current source in electrical domain with the different coefficient factor of $\alpha, \beta$ for a PEH.

The effective parameters indicate the use of motion equations in term of mass-spring-damper or linear beam theories [48] comprised of Euler-Bernoulli, Timoshenko, two-dimensional elasticity. The Kirchhoff's laws (KVL and/or KCL) for the equivalent circuit of the electromechanical system and Laplace transform of the output voltage to input force or vibration also could use. Any of the above techniques could be used in a single degree of freedom (SDOF) [1, 45, 47, 49-54] or multiple degrees of freedom (MDOF) [55, 56].

For the vibration PEH system bending of the beam while considering the boundary conditions can model by the (2, 3…, n) order ordinary differential equation (ODE with one independent variable) or/and the partial differential equation (PDE with more than one independent variable) [43, 57, 58]. The total energy conservation in active and inactive layer also helps to evaluate the bender system [44, 57]. However, bender modelling is out of the scope of this thesis.

#### 2.4.1.1 Vibration PEH Examples

In [47, 52, 53] the dynamic of a vibration PEH system with 31-mode and uni-morph cantilever beam and tip mass with SDOF are modelled in Fig 2.9. The

Kirchhoff's laws (KVL and/or KCL) for equivalent circuit and Laplace transform function are used to find deflection and output voltage relation in the frequency domain. The coupling coefficient defined by the transformer (turns ration-it shown in circle) where the average power dissipated in resistive load is $p = \frac{1}{R_L T}\int_0^T V(t)^2 dt$.

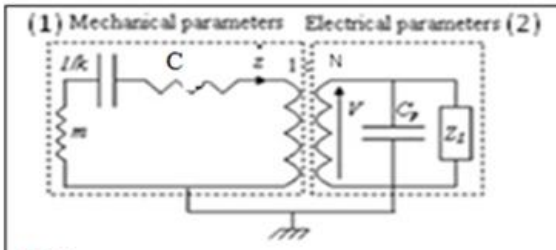


[47]

$$m\ddot{z} + c\dot{z} + kz + \textcircled{NV} = 0 \quad (1)$$
$$\textcircled{N\dot{z}} - C_p\dot{V} - \frac{V}{R_L} = 0 \quad (2)$$

displacement in z direction and assumption of zero initial condition except the velocity $\dot{z}$ (t=0 s) = $v_0$ .using laplace transform variable (s) to solve equations in frequency domain

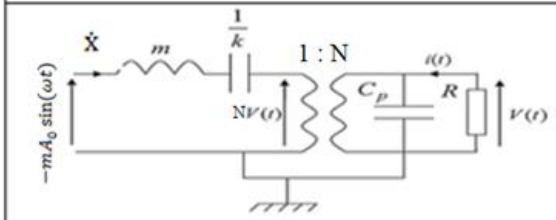


[50-52]

$$m\ddot{x} + kx + \textcircled{NV} = -mA_0\sin(\omega t) \quad (1)$$
$$\textcircled{N\dot{x}} - C_p\dot{V} - \frac{V}{R_L} = 0 \quad (2)$$

displacement in x direction and the input acceleration is $A_0\sin(\omega t)$. using laplace transform variable (s) to solve equations in frequency domain

Figure 2.9: The equivalent circuits of vibration PEH system with SDOF and resistive load ($R_L$) [47, 51-53].

Romani et al. in 2012 proposed a modelling technique suitable for envisaging the exact mechanical and electrical joint behaviour by coupling coefficient $\alpha$ *and* $\beta$ as piezoelectric effect coefficient instead of fixed transformer turn ratio (N) for a vibration PEH system in [51]. The piezoelectric transducer with 31-mode and bimorph configuration modelled as a lumped elements circuit [51]. The piezoelectric transducer in the situation of an open circuit as shown in Fig.2.10 (a) acts as an oscillator with resonance frequency $f_0$ and exponential damping coefficient ($\tau = \frac{2L_M}{R_M}$). On the other

hand, in the short circuit ($V_p \approx 0$) as shown in Fig.2.10 (b). A pure mechanical oscillator with resonance frequency $f_m$ is provided.

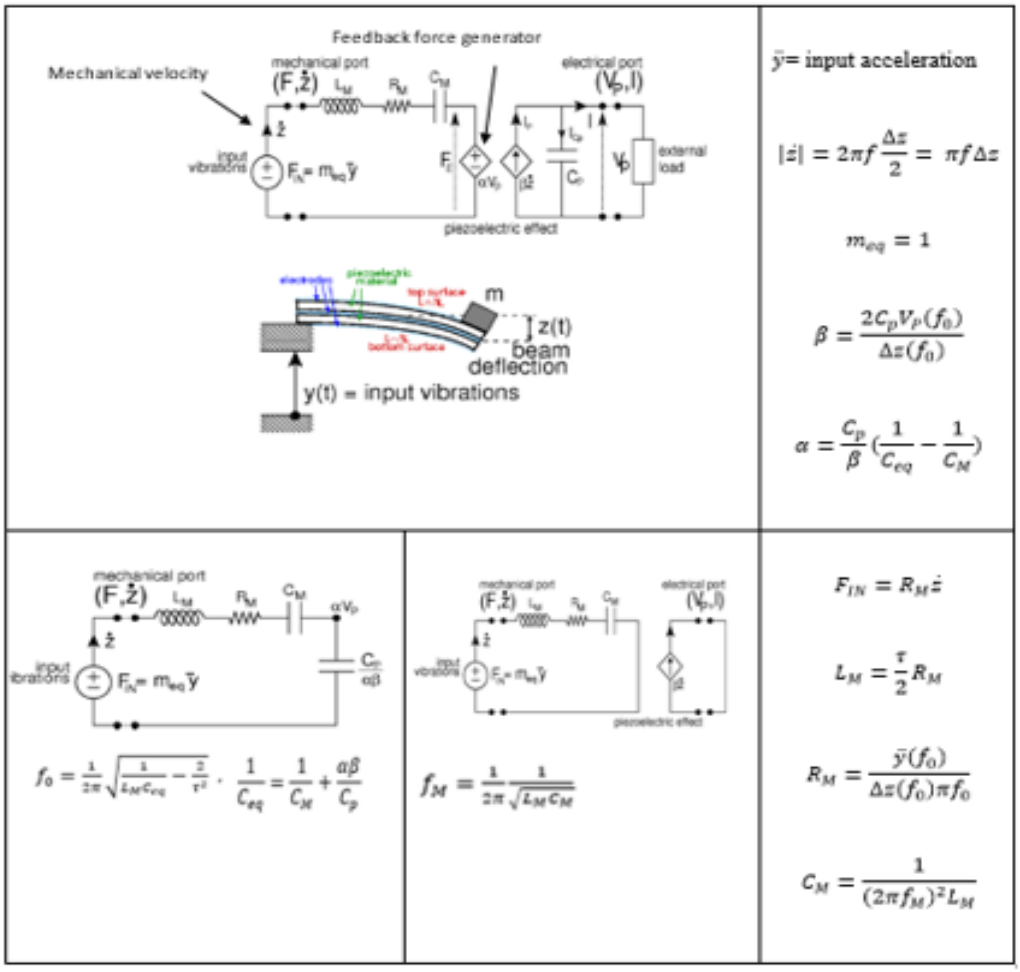


Figure 2.10: The complete equivalent circuits with a)open circuit b)short circuit of vibration PEH system with SDOF and resistive load ($R_L$) [51].

Roundy and Wright in 2004 use constitutive equations, equivalent circuit elements of a linear piezoelectric material and Euler-Bernoulli beam theory for a SDOF, 31-mode and bimorph configuration [45, 49, 50]. Based on the constitutive equations, the axial stress-stain relation defined as $\sigma = Y\varepsilon$ so the Young's modulus (Y) is the stress ($\sigma$) to strain ($\varepsilon$). The beam theory with the equation of $\frac{d^2z}{dx^2} = \frac{M(x)}{YI}$ defines a relation between strain ($\varepsilon$) and displacement ($z$) where M(x) is the moment and (I) is the effective moment of inertia. The KVL wrote for AC voltage source, mass-spring-damper with considering turn ratio as voltage source only in mechanical domain. On the

other hand, KCL in electrical domain calculated with total current through piezoelectric capacitance,$c_p$, and load resistance, $R_L$, as a resistive load. However, KCL considers piezoelectric capacitance,$c_p$, and storage capacitance,$c_s$, as the capacitive load with a rectifying situation in the electrical domain. This equivalent circuit did not consider the current through the secondary winding of transformer turns in comparison to above modelling. The Laplace transform of equations define in the frequency domain and relate output voltage (V) to input vibration (ÿ).

Park et al. in 2010 proposed a model for 33-mode, uni-morph vibration PEH with the help of the mass-spring-damper system, Euler-Bernoulli beam theory and equivalent circuit elements using Kirchhoff's law in [1] as shown in Fig2.11. This system in micro scale generates 1.41µW output power at 528Hz resonance frequency with less than 0.5g [1].

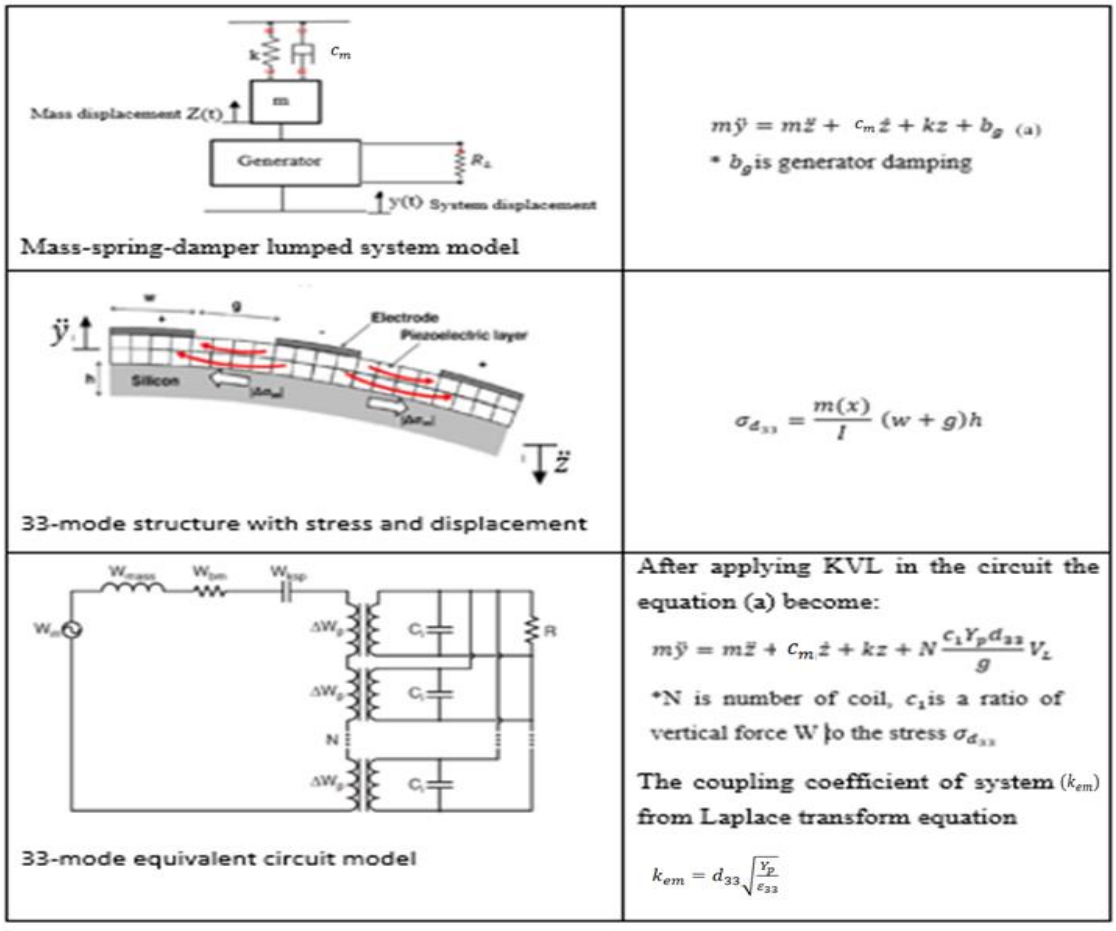


Figure 2.11: The summery of 33-mode vibration PEH system analytical modelling in [1].

In [59] regardless of mode and configuration of a piezoelectric layer for a general case of the PEH transducer modelled as shown in Fig 2.12. The mechanical variables force (F), displacement ($x$), and velocity ($\dot{x}$) represented with equivalent circuit elements of voltage($V_{eq}$), charge as a coupling factor of mechanical components ($\alpha$), and current ($i_{eq}$) [59]. The mass effect neglected, the losses measured separately and spring stiffness (k) represent by ($C_M$)[59]. The electrical domain modelled with single piezoelectric layer capacitance ($C_p$) and the coupling coefficient of mechanical and electrical domain as equation 2.8 [59],

$$k_{me=}\alpha\sqrt{\frac{1}{kC_p+\alpha^2}} \qquad 2.8$$

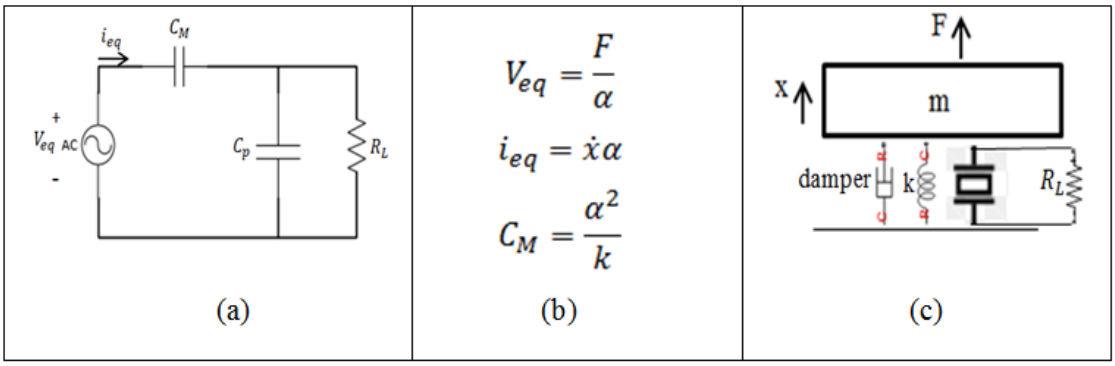


Figure 2.12:The modelling of vibration PEH system in [59] a) equivalent circuit b) equivalent equations c) mass-spring-damper schematic.

### 2.4.1.2 Vibration EMEH Examples

To model, a vibration EMEH system needs to identify the geometry of coil and magnet.

1) For coil is consisting number of turn of coil($N_c$) with height of coil ($l_c$), wire length ($l_w = N\pi\ 2r_c$; wire area $A_w = \pi {r_w}^2$), inner and outer diameter ($d_{in}$ and $d_{out}$) resulting in the average coil radios of $r_c = \frac{d_{in}+d_{out}}{4}$ . The area of the unit turn coil is $A_c = \pi {r_c}^2$
2) For magnet is either cylinder ($L_m, r_m, A = \pi {r_m}^2$) or cubic($L_x, L_y, L_z$)

In [22, 23] as shown in Fig 2.13 a moving cubic ($L_x, L_y, L_z$) magnet across a coil with an air gap distance from each other modelled. First, the magnetic field direction is going from further distance (d) to near the magnet $d_g$ [22, 23]. Second, the total magnetic flux density ($B = \mu (H + M)$, $^{Nm}/_{A}$) of the magnet is proportional to the magnetic field strength (density) of the magnet near coil (H, $^{A}/_{m}$) and magnetisation in the magnet (M). Third, the magnetic flux ($\varphi = \int B.dA$) so the Faraday's law of induction (Maxwell equations) states the open circuit voltage induced across the coil (electromotive force (EMF)) presented in equation 2.9

$$\varepsilon(t) = -\frac{d\varphi}{dt} = -N\frac{d(\overrightarrow{B_c}.\overrightarrow{A_c})}{dt} \qquad 2.9$$

The $\frac{d(\overrightarrow{B_c}.\overrightarrow{A_c})}{dt}$ defined as $\frac{d\overrightarrow{B_c}}{dt}\frac{dt}{dA} = \frac{d^2B(x)}{dxdy}$ and $\frac{d\overrightarrow{A_c}}{dt} = \frac{A_c}{L}\frac{dz}{dt}$.

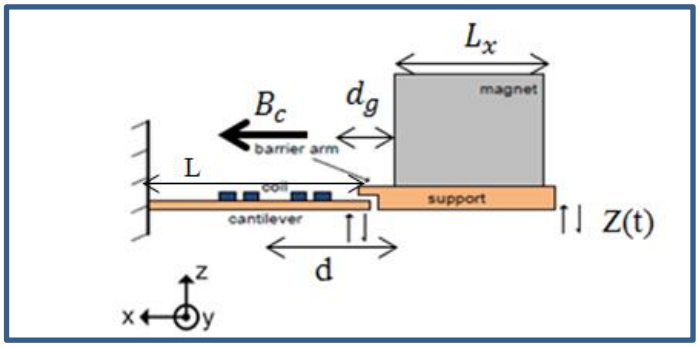


Figure 2.13: The vibration EMEH with mechanical frequency up-conversion method design in [22,23].

The $\frac{d\overrightarrow{A_c}}{dt}$ depends on the mechanical deflection of the cantilever beam. In [22, 23] z (t) is the function of sine wave displacement of the cantilever with the maximum value of Z with an input frequency of (f) and exponential effect of total damping on the wave. The equation indicates the z(t);

$$z(t) = Z\, e^{-\zeta\omega_n t}\sin(\omega_n t + \theta) \qquad 2.10$$

The RMS output voltage and power in the results decreased while the power density and resonance frequency increase with scaling down the harvester dimensions.

In [24] the vibration EMEH system is modelled with equivalent circuit elements as shown in Fig2.14(a). They are self-inductance of coil $L_c$, the internal resistance of coil $R_c$ and a voltage source $V_{emf}$. These components are in series with the load resistance$R_L$. So, we have equation2.11

$$V_{out} = V_{emf} - i(R_L + R_c + j\omega L_c) \qquad 2.11$$

$$\frac{|V_{out}|}{|V_{emf}|} = \frac{R_L}{R_L+R_c+j\omega L_c} \qquad 2.12$$

The $V_{emf} = \varphi\frac{dz(x)}{dt}$ and $\varphi = NBl_c$ , $\frac{dz}{dt} = \dot{z}$ and modelled with mass-spring-damper motion equation as shown in Fig2.14 (b). The motion equation with input vibration of $y = Y\sin\omega t$ is written in equation 2.13.

$$m\ddot{z} + (c_m + c_e)\dot{z} + kz = -m\ddot{y} \qquad 2.13$$

So the $|\dot{z}| = \frac{Y\left(\frac{\omega}{\omega_n}\right)\omega}{\sqrt{1-\left(\frac{\omega}{\omega_n}\right)^2+\left\{2(\zeta_m+\zeta_e)\left(\frac{\omega}{\omega_n}\right)\right\}^2}}$ where the $\zeta = \frac{c}{2\,M_{eq}\omega_n}$ and $M_{eq} = \frac{33}{140}m_{beam} + m_{coil}$. The assumption of fundamental frequency is the resonance frequency $(\omega = \omega_n)$.

Base on above equations $F_e = \frac{\varphi^2\dot{z}}{R_L+R_c+j\omega L_c}$ therefore $\zeta_e = \frac{\varphi^2}{2\,M_{eq}\omega_n(R_L+R_c+j\omega L_c)}$.

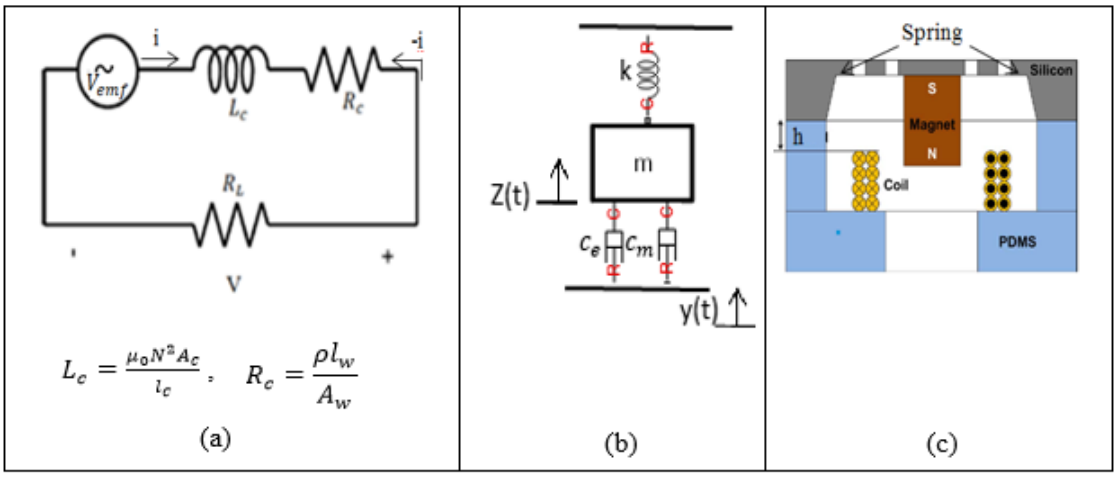


Figure 2.14: The modelled EMEH presented in [24] with a) equivalent circuit elements b)mass-spring-damper schematic c) the design.

Halim and Park in 2014 used the same modelling technique as in [24] for a non-resonance, frequency up conversion EMEH [25] with different motion equation as shown in Fig 2.15(a). In this design, the input force from a nonmagnetic ball generates the vibration of the magnet in a cylindrical helical spring beam (stiffness is k) structure shown in Fig2.15 (b). The EMF voltage $V_{emf}$, the cantilever beam velocity $\dot{x}$ and spring stiffness (k) modelled.

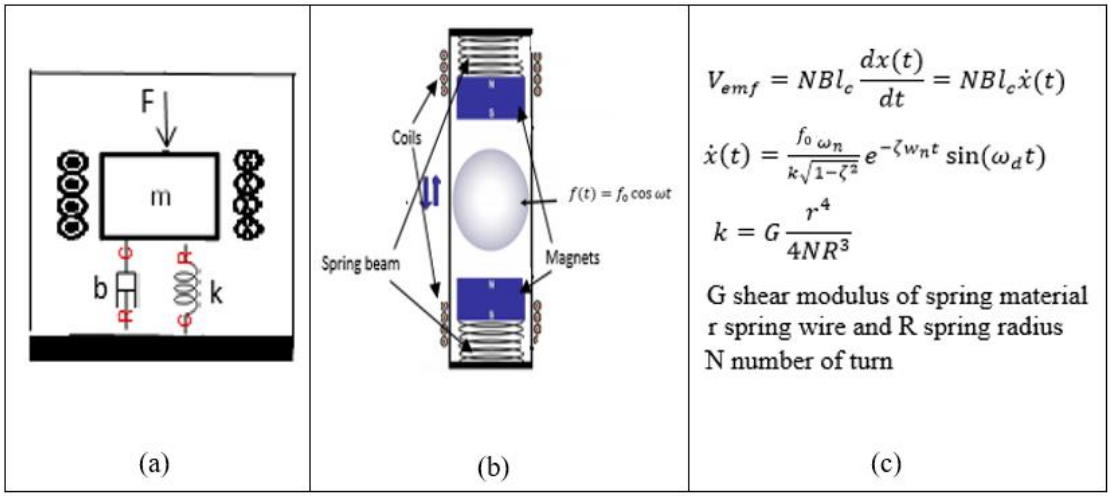


Figure 2.15: The cylinder tube, helical spring structure and up conversion, non-resonance vibration EMEH a) mass- spring-damper schematic b)the design c) the numerical analysis.

Where the $\zeta$ is damping ratio and natural frequency of damping ($\omega_d$) to the natural frequency of spring ($\omega_n$) is $\sqrt{1-\zeta^2}$.

Saha in 2008 modelled cylindrical structure with magnet springs in one or both end of the cylinder with finite element simulation of the force to displacement graph [26].There are one or two moving magnets with displacement in x-plane that defines by equation 2.14.

$$x(t) = \begin{cases} x\,, 0 < t < t_0 \\ Xe^{-\zeta\omega_n t}\sin(\omega_d t + \theta), \quad t > t_0 \end{cases} \qquad 2.14$$

$\omega_d, \zeta$ are as the same as the previous paper's definitions. The total force $F_T = kx(t) = F_{m1} + F_{m2}$ where $F_{m1}$and $F_{m2}$ are the repulsive force magnitude of middle magnets in respect to magnets at the ends.

Munaz et al. in 2013 followed the same design as [26] but for simplicity of modelling magnet-coil system assumed single turn coil moves through single magnet [31]. Basically, magnetic flux density defines $B = \mu_0 (H + M)$, $^{Nm}/_{A}$ and the point charge $q = BA$. In the magnet magnetization is $B_m = \mu_0 M$ and $q_m = B_m(\pi {r_m}^2)$ and for the coil $B_c = \mu_0 H$. The facts are a) the total magnetic flux is arising from point magnetic charge $q_m$, b) a single coil with a close loop according to Gauss's law (maxwell's equations, $\oint \vec{B} d\vec{A} = 0$) has the zero flux, c) the area around a point charge is sphere cap $A = \frac{2\pi R(R-H)}{4\pi R^2}$ as shown in Fig2.16 at both ends of magnet. So, the total magnetic flux indicated in equation2.15.

$$\varphi = q_m \frac{2\pi R(R-H)}{4\pi R^2} = \frac{q_m(R-h)}{2R} = \frac{q_m(\sqrt{{r_c}^2-h^2}-h)}{2\sqrt{{r_c}^2-h^2}} \qquad 2.15$$

Since the charges in poles are opposite signs indicated by $(q_m, -q_m)$ and magnetic flux through the wire changes modelled using a sign function in distance of $H + {l_m}/{2}$ and $H - {l_m}/{2}$ so with one magnet we have $\varphi = \varphi_1 + \varphi_2$ and with two magnets is $\varphi = \varphi_1' + \varphi_2' + \varphi_3' + \varphi_4'$.

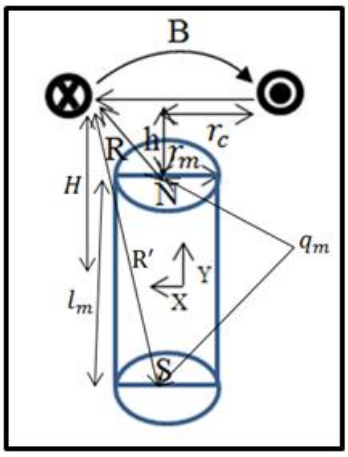


Figure 2.16: Schematic of the modelling parameters definitions.

The above model [31] was simulated using MATLAB software for open circuit voltage while examining the Finite element analysis (FEA) of ANSYS for the magnetic field area and flux line of the magnet. Besides, the mechanical vibration checked by running an experiment on the system. As the results, with the resonance frequency of 6

Hz the maximum RMS open circuit voltage is 3.4V, which has the potential applications in human wearable devices and wireless sensor nodes.

### 2.4.2 Power Converter interface and Load

The power converters as an electrical interface in power management circuit at the output channel comprise of AC/DC or/and DC/DC (control and voltage regulator) system. The electrical interface for PEH and EMEH is the same. They can be modelled with standard circuit elements to maximise the delivered energy to the load as power transfer electronics. On the other hand, a cantilever base PEH or EMEH system utilises as a transducer to harvesting energy from ambient vibration energy in the form of AC signal. Then, the energy stored in a load such as a capacitor, super capacitor or a rechargeable battery as a DC output voltage.

There have been several studies undertaken considering the problem of the low output voltage and developing passive and active power management circuit to supply the circuit and transfer the maximum harvested energy to the load [5, 21, 60-64].The passive circuitry commonly utilises a diode bridge rectifier (AC/DC converter) and an active circuitry represents by a switching power converter. In general, active circuits have some advantages such as the high capacity of harvesting energy even when the peak voltage of the transducer is lower than the output voltage of the interface circuit and provides high conversion efficiency. However, they imply more complexity, a necessity of power connection, cost and size issue in the system.

Two power conversion interface circuits tested for a piezoelectric energy harvester in [65] consisting a passive full-wave bridge rectifier (FWBR) and an active full-wave (the bridge could be H-bridge with CMOS or L-bridge with n-channel MOSFET) synchronous rectifier (FWSR) were both fabricated in a 0.25μm CMOS process. What is interesting in their performance is the 37% higher output power from the active FWSR than the passive FWBR circuit in the 82 kΩ load.

Furthermore, an electromagnetic energy harvester in [5] with a full-cycle inductive step-up AC/DC converter was manufactured, being a self-powered and an active electronic interface. This circuit with an electromagnetic transducer has been able to process every voltage pulse to harvest energy from human motion through several L-

C resonance cycles. The output data from [5] indicates 40% conversion efficiency, 1.4μW output power on a 18 kΩ load and 260mJ stored energy in a 1mF capacitor by applying 1 g of external acceleration in 240s at the mechanical resonance frequency of 10.4 Hz.

Above results clearly confirmed the improvement of the active interface circuit over the passive one. However, there is inconsistent evidence for the claim that modified passive and active interface circuitry perform counter wise as explained below [66].

A pulse width modulation (PMW) controller can add to a typical inductor switching mode DC-DC boost converter that commonly steps up the DC output of a passive rectifier. So, exploiting of a feed forward and feedback control as voltage mode controllers decrease the signal errors. This interface circuitry provides authority to the variety of the input voltage and results in the maximum output power of 35 mW. Moreover, diminishing of the duty ratio (D) which is the ratio of "on" time cycle to the total period can improve the conversion efficiency($\eta$) because of vice versa relation between them.

As mentioned before, the conventional passive rectifiers utilise diodes have mainly high voltage drops because of the direct relationship between the threshold voltage of diodes with the amount of output power loss [66]. In fact, This is the reason of low efficiency of the diode rectifiers while making them a suitable choice for low power systems without the need to be powered [66]. In [62, 66] a full wave bridge rectifier (FWBR) utilising a diode-connected PMOS transistors as low threshold voltage diodes instead of diodes were employed. This electronic interface was clamped and kept the output voltage at a certain level and decreased the input voltage to small voltage in output terminal. This structure reduced drain to source current ($I_{ds}$) and gave freedom to the output voltage to change without significant impedance in load. The other possible rectifier is a gate cross coupled (GCC) in [67] which is an improved version of FWBR, where a pair of diode-connected PMOS replaced with cross-connected NMOS transistors. In fact, the improvement of gate cross coupled rectifier (GCCR) comparing to a full wave bridge rectifier (FWBR) includes its conversion efficiency of the circuit to boost from 25% to 30% as reported in [21]. Replacing the threshold voltage of a pair

of diode-connected PMOS with the drain-source voltage of NMOS is the reason for this improvement, although both of these circuits suffer from high diode threshold voltage.

The boot strap rectifier (BSR) circuit in [21] which is a passive interface electronics for the vibration based electromagnetic energy harvester system fabricated in the 0.35µm standard CMOS process on the chip. This bridge rectifier circuitry used a pair of NMOS transistors of GCCR and replaced two other pairs with modified diode blocks with the internal 5 pF capacitor that connected to the bulk regulating transistors to avoid any latch up the effect of PMOS devices and work as DC/DC step-up converter. The quantities reported in this design are significant and comparable to results from [65] and [23], delivering the conversion efficiency of above 60%, minimum power losses, 128µW DC output power and 1.6 V DC voltage on the load across the 10µF external capacitor at the resonance frequency of 2 Hz.

The passive and active circuits at the load can be defined as purely resistive ones while approximation of the output is not convincing [49]. Contrarily, a capacitive load with a converter is the more realistic operational condition. In [49] a PEH system designed with an optimal density of $1cm^3$, 2.5 $^{m}/_{s^2}$ acceleration and 120 Hz frequency. The result from the system with the resistive load shows the transfer of $375Wcm^{-3}$power while only 190Wcm$^{-3}$ is transferred to the capacitive load. These statistics are justified by the effect of the Rectifier Bridge of diode's threshold voltage and power loss.

In [59] the PEH system's dissipation and harvesting concepts across loss factor studied with considering the power converter and storage units as a shunt circuit. The loss factor explained as a ratio of energy dissipation per cycle ($2\pi$) to maximum vibration energy. First, the shunt circuit defines as a nonlinear circuit composed of a filter capacitance parallel to a load as the output to an electronic interface of an AC/DC passive rectifier. Next, the piezoelectric transducer is connected to a single resistor as shunt damping. The result showed that the first circuit in [57, 59] has a maximum energy harvesting factor that is also the maximum energy loss factor without its dissipation. But, the resistive shunt circuit with zero harvesting of energy provides the maximum dissipation factor as the loss factor.

There are some other non-linear techniques that are implemented at the load to harvest more power from piezoelectric generators such as synchronous electric charge extraction (SECE) and synchronous switch harvesting on the inductor (SSHI). The synchronous switch harvesting on the inductor (SSHI) contains a switching device in series with an inductor parallel to the piezoelectric circuit before the bridge rectifier and a capacitor parallel to the battery after the bridge rectifier [4]. In [68] a SECE flyback converter is embedded at the load that stored about 55% more output power than the standard load (the circuit losses were not considered and acceleration is above 51mg). In this circuit, the bridge rectifier output is considered as the SECE flyback input voltage including a magnetised inductor that is charged by the piezoelectric capacitor. This part is connected in parallel to a transformer and series to two N-channels MOSFET that work as switches for the primary and secondary transformer. This circuit passes the generated gate-drive waveforms to a microcontroller to transmit the output. Although the second N-channel MOSFET is coupled in parallel with a diode to avoid losses, there are some power losses in the transformer and the microcontroller. These losses are inevitable for microcontroller but in the transformer's design effective parameters decreasing this effect such as geometry, the inductor magnetisation, the transformer core and turns are already included [68].

## 2.5 State of the Art and Potential Applications

### 2.5.1 PEH-shoe insert

One of the applications of piezoelectric energy harvesting system is in wearable electronics. Shenck and Paradiso in 2001 proposed an energy harvesting unit where a piezoelectric material installed at the heel or sole of a shoe and extract useful energy from the waste energy of walking [3]. The piezoelectric material is either a flexible, multilaminar polyvinylidene fluoride (PVDF) or a bimorph lead zirconate titanate (PZT) [3]. Starner in 1996 analysed various human activities and discovered the reason for embedding the piezoelectric materials in the heel of the shoe is that the heel strike has the most tapping source of waste energy[69].

### 2.5.2 PEH/EMEH-condition monitoring

Park et al. in 2008 reviewed low power embedded structural health monitoring SHM sensing system to develop energy harvesting [70]. In fact, a proper sensor network to detect damages and manage these data for signal processing for SHM is needed. Piezoelectric patches are usable as a sensor or actuator that is embedded in the structure to measure the mechanical strain. James et al. in 2004 introduced an electromagnetic generator power source for condition monitoring applications[10]. As a result, piezoelectric and electromagnetic energy harvesting system is used as a sensor network for condition monitoring applications.

### 2.5.3 PEH/EMEH in-ear device

Delnavaz and Voix in 2014 designed a hydro electromagnetic energy harvester and piezoelectric energy harvester which harvested energy from ear canal dynamic motion [71]. The experimental setup and the module of the hydro electromagnetic energy harvester shown in Fig 2.17, this device provides the maximum power of 2 μW from jaw joint motion. On the other hand, Piezoelectric energy harvester is a ring made of a flexible sheet of polyvinylidene fluoride (PVDF) which is a piezoelectric material mounted on a headset and generates 0.2μW power. As a result, ear canal dynamic motion can be used as a source of human power.

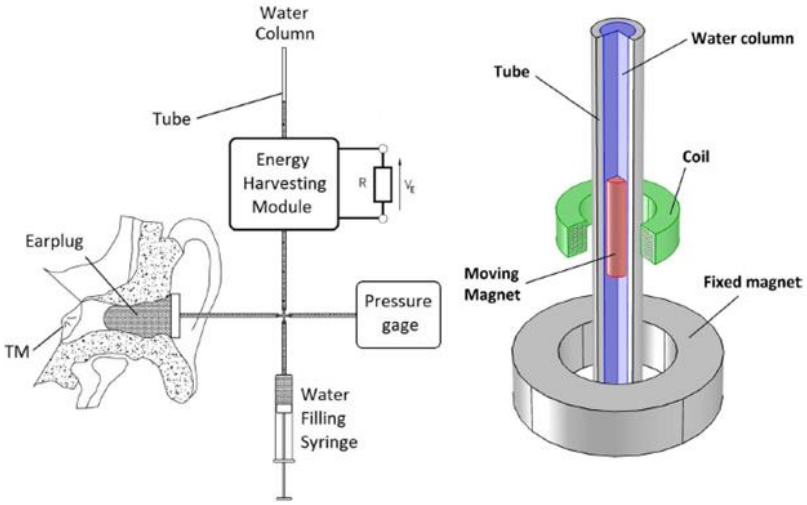


Figure 2.17: Hydro electromagnetic energy harvester. Experimental set up on the left and energy harvester module on the right [67].

### 2.5.4 EMEH-remote car key

Li et al. in 2013 proposed a novel non-resonance electromagnetic energy harvester which harvested the energy from a low frequency and large amplitude motion[72]. There is a round flat permanent magnet moving freely in a round flat cavity and packaged on both sides by printed circuit boards embedded with multi-layer copper coils[72]. This non-resonance electromagnetic energy harvester provides enough energy to used as a remote car key with maximum open circuit voltage of 1.1V. Therefore, integration and assembly of this energy harvester with a simple structure and comparable size to a coin battery CR2032 is not costly.

## 2.6 Summary

In this chapter, different parts and design process of existing piezoelectric and electromagnetic harvesting system from ambient vibration source reviewed and presented as a summary flowchart in Fig 2.18 and 2.19.

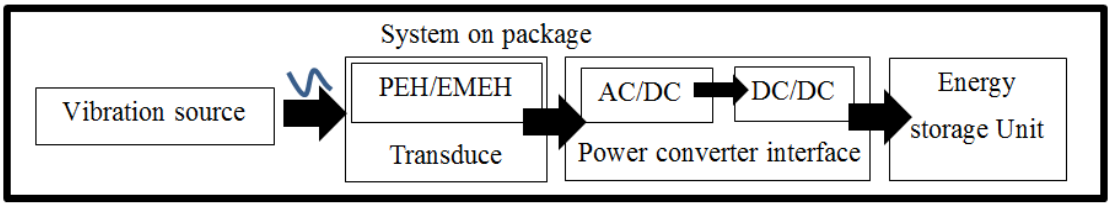


Figure 2.18: Schematic of parts in vibration energy harvesting system using piezoelectric and electromagnetic mechanisms.

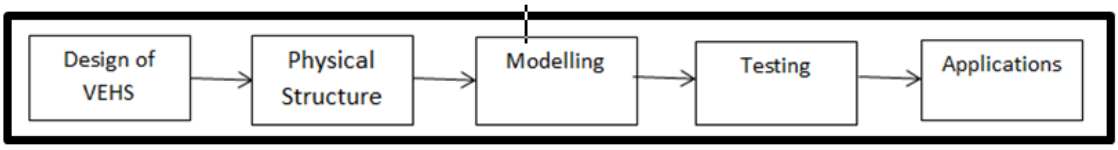


Figure 2.19: Flowchart of design process in vibration energy harvesting system.

# CHAPTER THREE

# DESIGN OF AN ELECTROMAGNETIC ENERGY HARVESTING SYSTEM

## 3.1 Synopsis

Firstly in this chapter presents the design and analytical modelling of the vibration based EMEH system. The scavenge of vibration energy from the system explained with a single degree of freedom (SDOF), spring-mass-damper system.These are used in the mechanical domain to explain the coil displacement and used Faraday's law to calculate the EMF voltage. The fundamental frequencies in the range of 2-56 Hz to evaluate output voltage at the up-converted frequency($f_n$) tested. The peak voltage of $V_{emf}$ with the effect of coil displacement has following changes. Firstly, decrease of the maximum output voltage with an increase of cantilever length. Then, rising of the maximum output voltage follows an increase in resonance frequency.

## 3.2 Vibration based EMEH

### 3.2.1 Design and modelling

The cantilever beam structure, up conversion mechanical frequency, resonance EMEH system is shown in Fig 3.1(b) with a pick up coil on the free end of a beam that has a clamped end on the other side mounted. There is a magnet on a diaphragm with low excitation frequency (f) and the mechanical barrier arm connected to it. The mechanical barrier when the diaphragm moved touches the cantilever beam on the opposite side that carry the coil as a tip mass. The generated vibration in cantilever is in resonance frequency ($f_n$) which is up converted frequency without driving force acting on the cantilever beam.

Above design as a vibration based EMEH with single degree of freedom (SDOF) can be modelled with analytical lumped parameters as spring-mass-damper system in Fig 3.1(a) and motion function define in equation 3.1as below,

$$m\ddot{z} + kz = -(c_m + c_e)\dot{z} \qquad 3.1$$

In the un-damped motion $c = c_m + c_e = 0$ so equation 3.1 written as,

$$\frac{d^2z(t)}{dt^2} = -\frac{k}{m}\, z(t) \qquad 3.2$$

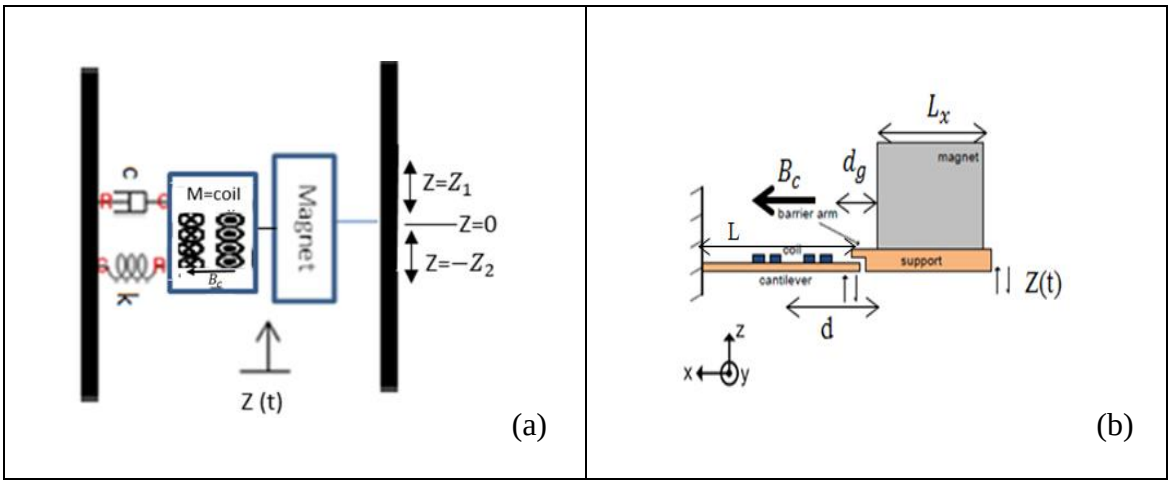


Figure 3.1: Schematic of tested model for EMEH a) mass-spring-damper equivalent b) the design parameters with magnet dimensions ($L_x, L_y, L_z$).

In equation 3.1 the mass at the tip (coil) is denoted by m where the $F = ma$. The total damping coefficient (c) denotes by mechanical damping coefficient, $c_m$, and electrical damping coefficient, $c_e$, ($c = c_m + c_e$). The k is the cantilever beam stiffness where $F = -kz$ based on Hook's law. There is no input excitation for cantilever beam movement $y(t) = 0$.

With boundary condition of at $t = 0, z = -Z_2$ the relative displacement of mass (coil) is given as:

$$z(t) = -Z_2 e^{-\zeta\omega_n t}\sin(\omega_n t + \theta) \qquad 3.3$$

The electromagnetic coupling in the mechanical domain for a magnet-coil system is only associated with the mass oscillation velocity (ż) while the energy from motion transferred to the electrical domain [51, 73].

The induced voltage ε(t) is expressed in equation 3.4 using the magnetic field in the coil $B_c$ in equation 3.6 (the constant value for magnetic field density in and around the coil assumed) where $B_m = \mu_0 M$. The coil surface area $A_c$ in the x-y plane on the cantilever with length (L) and coil radius ($r_c$)indicated in equation 3.5.

$$\varepsilon(t) = -\frac{d\emptyset}{dt} = -N\left|\overrightarrow{B_c}\right|\frac{dA_c}{dt} \quad 3.4$$

$$A_c(t) = \frac{|z(t)|}{L}\pi {r_c}^2 \quad 3.5$$

$$B_c = \frac{B_m}{\pi}\left[\tan^{-1}\left(\frac{L_y L_z}{2d\sqrt{{L_y}^2+{L_z}^2+4d^2}}\right) - \tan^{-1}\left(\frac{L_y L_z}{2(d+L_x)\sqrt{{d_y}^2+{d_z}^2+4(d+L_x)^2}}\right)\right] \quad 3.6$$

$$f_n = \frac{\omega_n}{2\pi} = \frac{1}{2\pi}\sqrt{\frac{k}{m_{eq}}} \quad 3.7$$

In equation 3.7 the quantity k is elastic energy of the spring which is defined in equation 3.8 as function of elastic module ($Y_c$), dimensions of cantilever (length (L), width (W), thickness (h)) and the coil radius ($r_c$) while $m_{eq}$ is coil mass ($m_c$) and $33/140$ cantilever mass ($m_{beam}$).

$$k = 2\,Y_c\frac{Wh^3}{L^3}\frac{1-(\frac{2r_c}{L})}{3-\left(\frac{2r_c}{L}\right)^3+\left(\frac{2r_c}{L}\right)^4} \quad 3.8$$

Since $\omega_n = \sqrt{\frac{k}{m_{eq}}}$, the damping ratio of cantilever beam, $\zeta = \frac{c}{2\sqrt{km_{eq}}}$

### 3.2.2 Testing and Simulation

#### 3.2.2.1 Input Vibration for Up Converted Frequency

The damped displacement of coil simulated in Simulink of MATLAB R2013b according to equations 3.9 and 3.10

$$Z(t) = A_0 e^{f(t)} \sin(2\pi f_n t) \quad 3.9$$

$$f_n = \frac{N_n}{T_n} \quad 3.10$$

In above equations, $A_0$ is maximum tip displacement, the algebra event converts to a repeated function f (t). Also, $f_n$ evaluates the periodic frequency consist of $N_n$ as the number of peaks and $T_n$ as the period in each time interval.

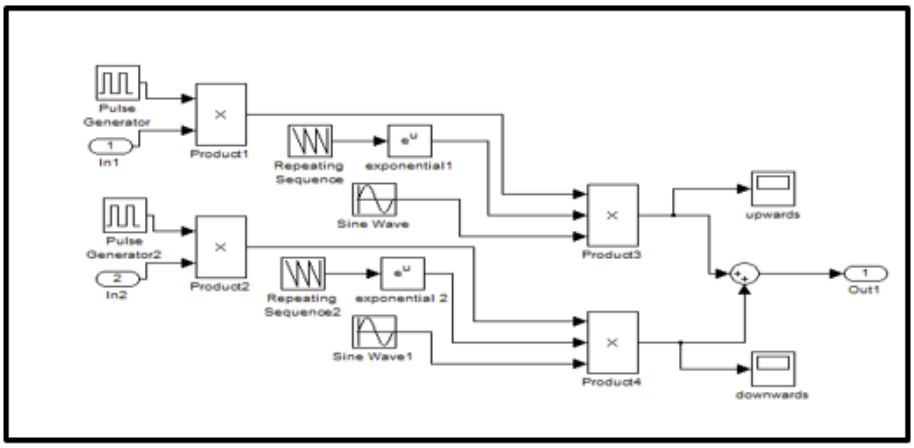


Figure 3.2: The Simulink block diagram of mass displacement z (t) in vibration based EMEH.

The block diagram shown in Fig 3.2 represents the upward and downward displacement of mass as shown in Fig 3.3 and Fig 3. 4.

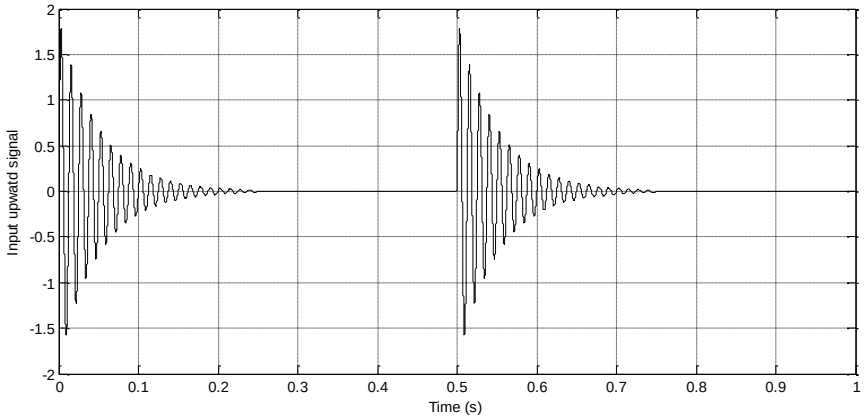


Figure 3.3: Upward $z = Z_1$ signal under vibration frequency of 2Hz

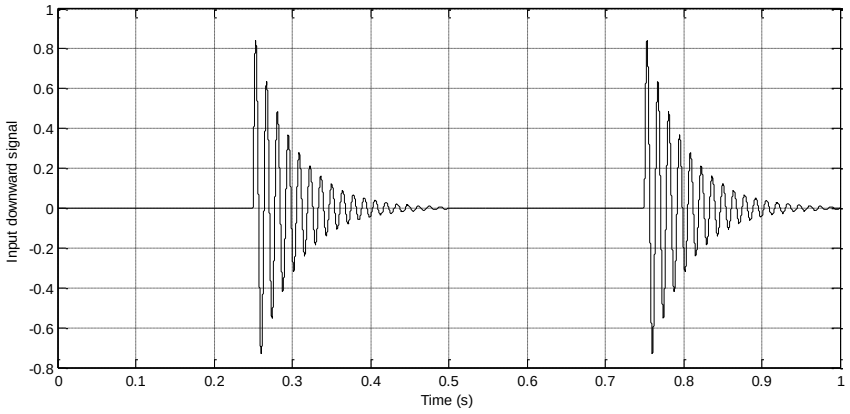

Figure 3.4: Downward $z = -Z_2$ signal under vibration frequency 2Hz.

The vibration of cantilever z (t) with up covered resonance frequency ($f_n$) when input frequency is $f = 2, 7, 56$ Hz shown in Fig 3.5, Fig 3.6, Fig 3.7.

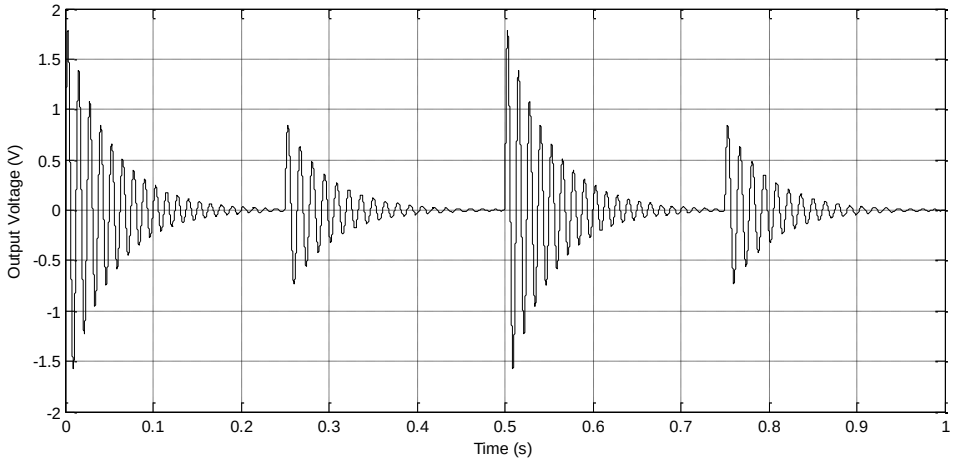


Figure 3.5: Simulated AC voltage signal $f = 2$ Hz.

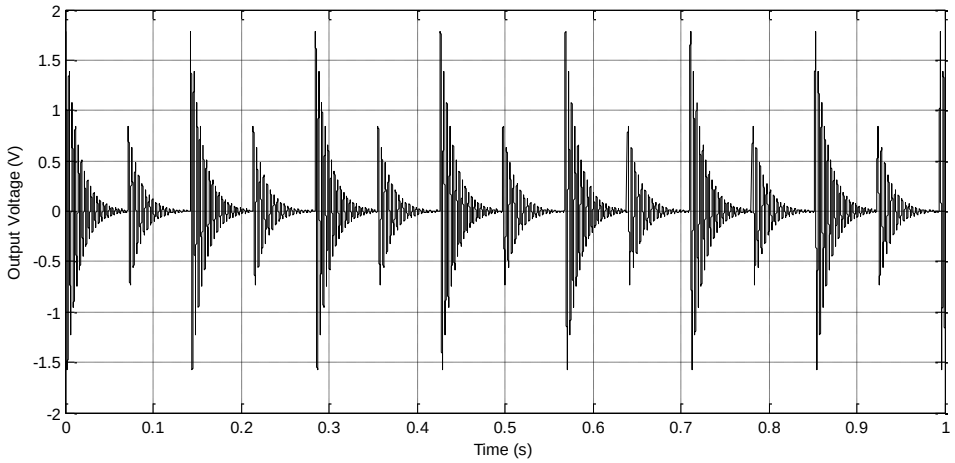


Figure 3.6: Simulated AC voltage signal $f = 7$ Hz.

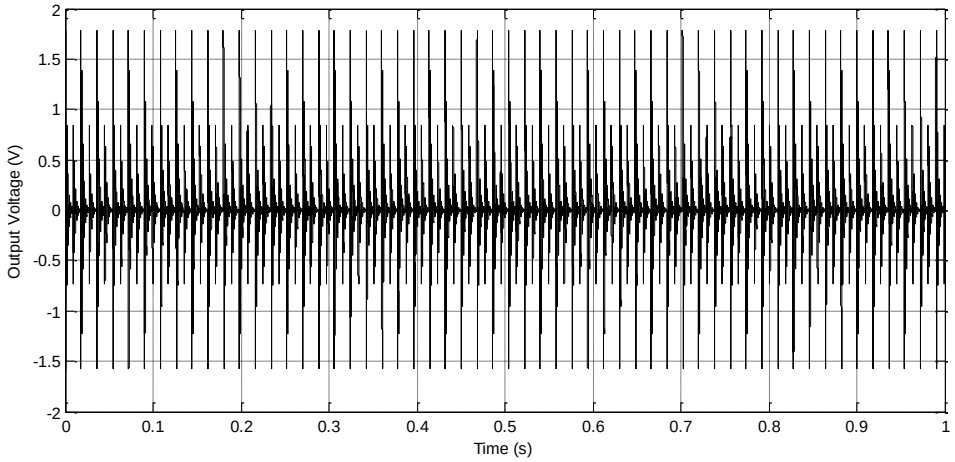


Figure 3.7: Simulated AC voltage signal f = 56 Hz.

### 3.2.2.2 Evaluation of EMEH System

The evaluation of EMEH is according to $\frac{V_{emf}}{A_c(t)}$, where $V_{peak} = \max(|V_{emf}|)$, cantilever length (L) , resonance frequency ($f_n = \sqrt{\frac{k}{m_{eq}}}$) and cantilever, coil and magnet parameters given in Table 3.1 .The Fig 3.8 and 3.9 show the variations of $V_{peak}$ with respect to L and $f_n$.

Table 3.1: The cantilever, coil and magnet parameters in simulation

| Coil | Magnet | Cantilever |
|---|---|---|
| Magnet-coil gap, $d_g = 2.2$mm so d=$d_g + r_c$<br>Coil turn radius, $r_c = 3.75$ mm<br>Coil wire radius, $r_w = 120$ μm<br>Coil turns numbers, N = 100<br>Coil resistance, $R_c = 3.54\ \Omega$<br>Coil density, $\rho_c = 8.92\ {}^{g}/_{cm^3}$ | $V_m = L_x \times L_y \times L_z = 7.5 \times 7.5 \times 7.5\ mm^3$<br>$B_m = 1.2$ T | Tip displacement, $A_0 = 2$mm<br>Mechanical Damping ratio, $\zeta_m$= 0.018<br>Elastic modulus, $Y_c$=3.2 GPa<br>Resonance frequency $f_n$<br>$V_{beam} = L \times W \times h = 9 \times 7.5 \times 0.5\ mm^3$<br>Cantilever density,$\rho = 1.2\ {}^{g}/_{cm^3}$ |

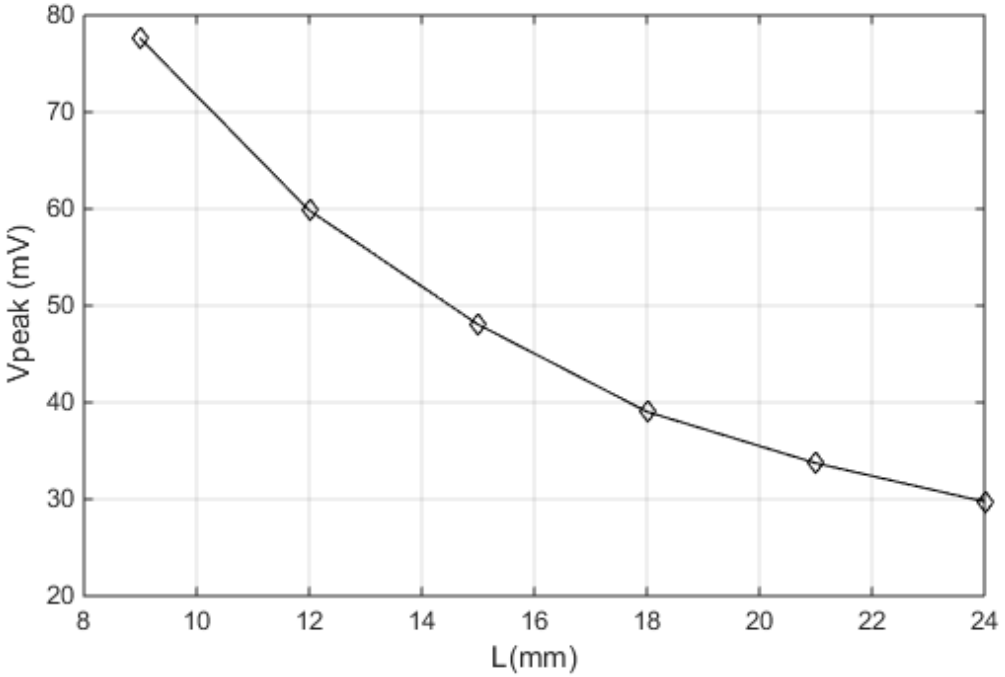


Figure 3.8: The changes of $V_{peak}$ to the length of cantilever (L).

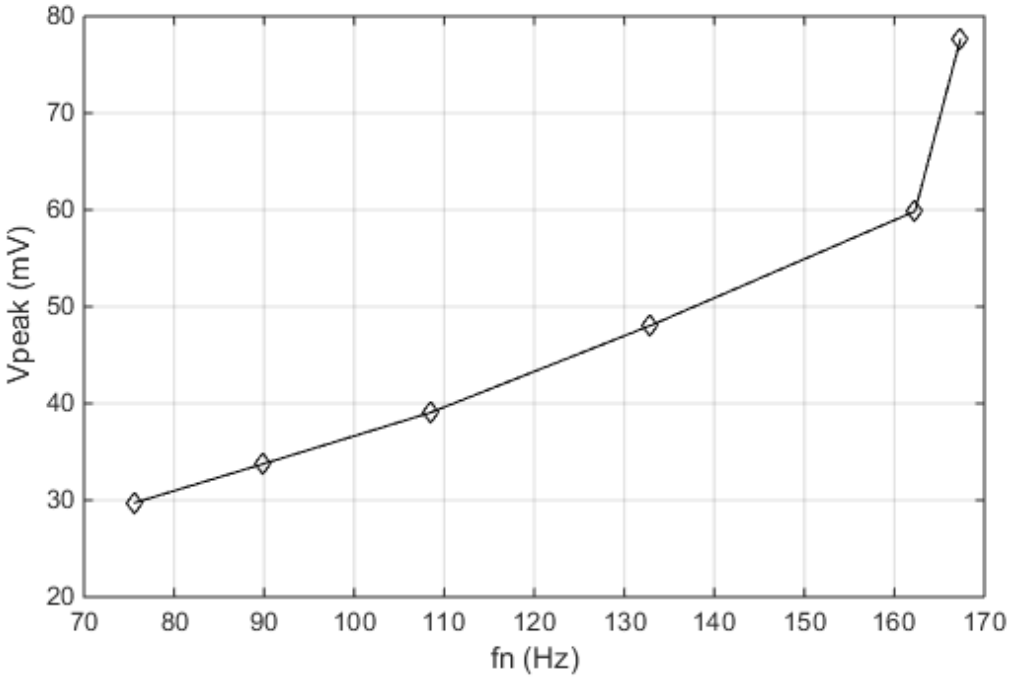


Figure 3.9: The changes of $V_{peak}$ to the resonance frequency ($f_n$).

## 3.3 Summary

The formulation of resonance, up-converted vibration based EMEH system with considering parameters variation by cantilever movement and coil-magnet movement and these movements related to each other are extracted and shown in Table 3.2.

Table 3.2: Outline of model

| | |
|---|---|
| Output voltage | $V_{emf} = -\mathrm{N}\left\vert\overrightarrow{\mathrm{B_c}}\right\vert \frac{\vert \mathrm{z(t)} \vert}{\mathrm{L}} \pi \mathrm{r_c}^2$ |
| Magnetic flux density in the coil | $B_c = \frac{B_m}{\pi}\left[\tan^{-1}\left(\frac{L_y L_z}{2d\sqrt{{L_y}^2 + {L_z}^2 + 4d^2}}\right) - \tan^{-1}\left(\frac{L_y L_z}{2(d+L_x)\sqrt{{d_y}^2 + {d_z}^2 + 4(d+L_x)^2}}\right)\right]$ |
| Coil displacements | $\mathrm{Z\ (t)} = \mathrm{A_0 e^{f(t)}} \sin(2\pi \mathrm{f_n\ t}) \qquad \mathrm{f_n} = \frac{\mathrm{N_n}}{\mathrm{T_n}}$ |

# CHAPTER FOUR

# DESIGN OF A PIEZOELECTRIC ENERGY HARVESTING SYSTEM

## 4.1 Synopsis

Firstly in this chapter presents the design and analytical modelling of the vibration based PEH system. The scavenges of vibration energy from the system with an equivalent circuit elements modelled. The circuit components for the mechanical domain of transducer defined with some ratio of stress to strain. The electrical function of piezoelectric material presented with single capacitor where the dielectric constant and dissipation in piezoelectric material neglected. The electrical interface for converting the AC output results to usable DC output and a regulator used at the output channel. The proposed model calculated the output current for a resistive load and a capacitive load. The results from Simulink tested for different piezoelectric materials and alternative size changes of the transducer. These changes are given different resonance frequency each time that shown the dependence of resonance frequency to material type and the size of them in the system.

## 4.2 Vibration based PEH

### 4.2.1 Design and modelling

Two layers of piezoelectric material as a cantilever beam with the structure of 31-mode as a bimorph (one inactive layer between two active layers) for the vibration PEH system designed as shown in Fig 4.1.

The piezoelectric effect in active layers can be explained by the coupling between internal dielectric polarisation from applying stress and the strain in the atomic arrangements of materials [74]. Based on the analytical formulation of piezoelectricity the constitutive equation of a linear piezoelectric material defines as mentioned in equation 4.1.

$$\begin{bmatrix} D \\ S \end{bmatrix} = \begin{bmatrix} d & \varepsilon^T \\ s^E & d^t \end{bmatrix} \begin{bmatrix} T \\ E \end{bmatrix}^{3} \qquad 4.1$$

T and E are the stress induced by mechanical and electrical effect respectively. E as electric field vector (a $3 \times 1$ matrix, $\frac{V}{m}$) and T is mechanical stress vector (a $6 \times 1$ matrix, $\frac{N}{m^2}$).The $s^E$ is the elasticity (a 6×6 matrix, $\frac{m^2}{N}$) for constant E while the $\varepsilon^T$is the dielectric constants (3×3 matrix, Farad/m) for constant T [75].

In the cantilever type, vibration based PEH considers firstly, the electrical field (E)/displacement (D, a 3×1 matrix, $\frac{C}{m^2}$) in the z-direction, the mechanical stress(σ)/strain (S, a 6×1 matrix) in the x-direction. Then, the electric field and stress variables are independent. So equation 4.1 can be written as below,

$$\begin{Bmatrix} S_1 = s_{11}^E T_1 + d_{31} E_3 \\ D_3 = \varepsilon_{33}^T E_3 + d_{31} T_1 \end{Bmatrix} \qquad 4.2$$

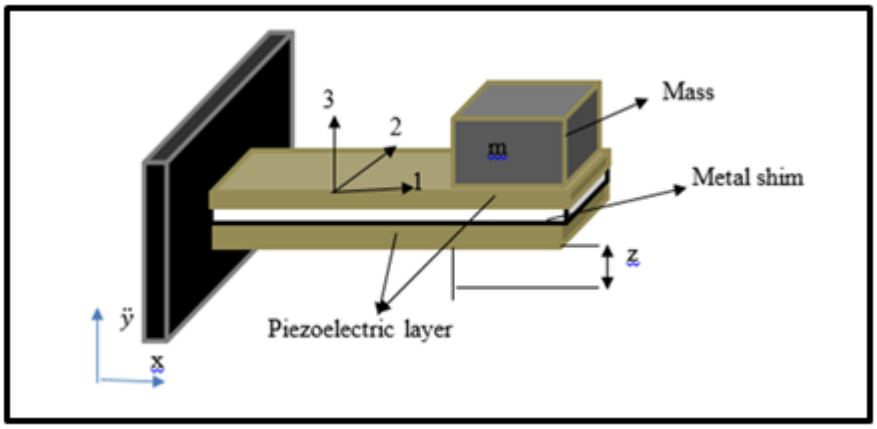


Figure 4.1: Schematic structure design of a 31-mode, bimorph vibration PEH system.

The physical relation of the stress(σ)/strain(S), in materials, is stated by Hooke's law that given in equation 4.3 and recognised as Young modulus or elasticity modulus(Y) in equation 4.4 for the active layer ($Y_p$) and inactive layer ($Y_c$).

[3] Appendix C

$$\{S\} = [s^E]\{\sigma\} \quad 4.3$$

$$\frac{\sigma}{S} = \frac{1}{s_{11}{}^E} = Y \quad 4.4$$

The vibration PEH transducer modelled with lumped parameters using mass-spring-damper schematic as given in Fig 4.2 (a) and its equivalent circuit elements for mechanical and electrical domains shown in Fig 4.2 (b).

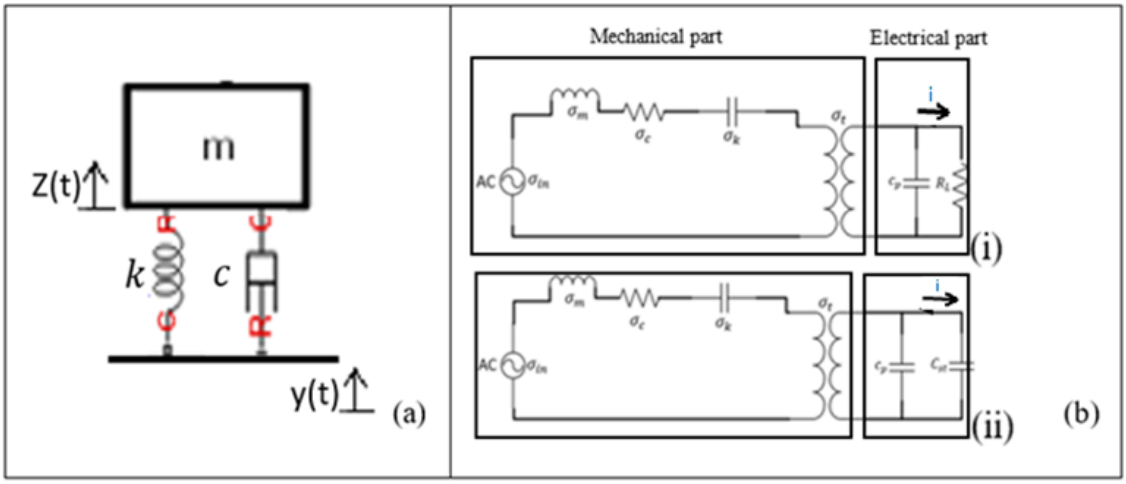


Figure 4.2: The lumped parameters for modelling PEH system a) mass-spring-damper model b) equivalent circuit elements (i) with resistive load ($R_L$) (ii) there is a full bridge diode rectifier with states of either $D_1$, $D_3$ conducting in positive cycle or $D_2$, $D_4$ conducting in negative cycle. There is a state where all four diodes are not conducting.

First, in the mechanical domain there is a relationship between the kinetic energy of inertia (m), elastic energy of spring stiffness (k) and energy dissipation of damper (c) of the design structure with stress and strain of the piezoelectric material. Moreover, the electromechanical coupling ($K_{31} = d_{31}\sqrt{\frac{Y_p}{\varepsilon}}$) is modelled as a transformer to relate stress to the electric field.

Last, in the electrical domain that usually modelled by an RC circuit, in this work, R that represents the dielectric of piezoelectric material neglected and ($C_p$) defines the piezoelectric layer capacitance. Since there are two piezoelectric layers with the same capacitance (C) (same piezoelectric material) in parallel or series poles relation, the piezoelectric capacitors are in the relation of equation 4.5 where C define in equation 4.6.

$$C_p = 2C \text{ or } C_p = \frac{C}{2} \quad 4.5$$

$$C = \frac{Q}{V} = \frac{\varepsilon A}{t} \quad 4.6$$

The parameters in capacitance (C) consist of the charge (Q) and voltage (V) of the capacitor that are equal to the physical feature of the capacitor including permittivity ($\varepsilon = \varepsilon_r \varepsilon_0$), the area between two plates (A), and the distance between plates (t).

The Power converter interface modelled with a purely resistive shown in Fig 4.2 (b-i) or a full wave bridge diodes rectifier (FWBR) for AC/DC convert with a capacitive load ($C_{st}$) shown in Fig 4.2 (b-ii) which could have a regulator (DC/DC converter) with a load after the storage capacitor.

The system equation 4.7 can be obtained by applying Kirchhoff's voltage law (KVL) for the circuit in Fig 4.2 (b).

$$\sigma_{in} = \sigma_m + \sigma_c + \sigma_k + \sigma_t \quad 4.7$$

The parameters $\sigma_{in}$, $\sigma_m$, $\sigma_c$, $\sigma_k$, $\sigma_t$ for equivalent circuit elements all well defined in Table 4.1.

Table 4.1: The lumped parameters model of a 31-mode, bimorph PEH system

| Variables | Components | Unit | Description |
|---|---|---|---|
| $\sigma_m = k_1 m\ddot{z} = k_1 k_2 m\ddot{S}$ | $L_m = k_1 k_2 m$ | $(\frac{kg}{m})$ | Inertia stress is function of cantilever displacement while base on the Euler-Bernoulli model [8, 9] $\frac{d^2z}{dx^2} = \frac{M(x)}{C_p I}$ ,where $\sigma_x = \frac{M}{I} z = -zC_p \frac{d^2w}{dx^2}$ and $\sigma = C_p S$ |
| $\sigma_c = c\, k_1 k_2 \dot{S}$ | $R_c = c\, k_1 k_2$ | $(\frac{N.s}{m^2})$ | Damping coefficient relation to stress and strain |
| $\sigma_k = Y_p S$ | $C_k = Y_p$ | $(\frac{N}{m^2})$ | Stiffness relation with stress and strain |
| $\sigma_t = -d_{31} Y_p E$ | $N = -d_{31} Y_p$ | - | Transformer relates stress to electric field at zero strain [10], considering equation (15) and $V = E t_p$ |
| $\sigma_{in} = k_1 m\ddot{y}$ | $\sigma_{in} = k_1 m\ddot{y}$ | $(\frac{kg}{m.s^2})$ | Input source is the stress which is function of input excitation |
| $k_1 = \frac{b(2l_p + l_m - l_e)}{2I}$ | $k_1$ | $(\frac{1}{m^2})$ | The first constant, which shows cantilever dimensions relation |
| $k_2 = \frac{l_b^2}{3b} \frac{(2l_p + \frac{3}{2} l_m)}{(2l_p + l_m - l_e)}$ | $k_2$ | (m) | The second constant, which shows cantilever dimensions relation |
| $F = F_{in} + F_m$ | $F=m(\ddot{y} + \ddot{z})$ | (N) | Total force = input excitation force+ mass force |
| $I = 2\left[\frac{w t_p^3}{12} + w t_p b^2\right] + \frac{Y_{sh} w t_{sh}^3}{12 Y_p}$ | I | $(m^4)$ | The effective moment of inertia is function of piezoelectric and the shim layer dimensions |
| $M(x) = m(\ddot{y} + \ddot{z})(l_p + \frac{1}{2} l_m - x)$ | M | $(\frac{N}{m})$ | The moment is the force multiplied by the distance |

$l_p, t_p, Y_p$ is the piezoelectric layer length, thickness and Young Modulus $t_{sh}, Y_{sh}$ is the shim layer thickness and Young Modulus, $b = \frac{t_p + t_{sh}}{2}$, $l_e$ is the electrode length, $l_m$ *is the mass length*, $m = \rho.l.w.t$ is the inertia

$$C_p = \frac{a^2 \varepsilon w l_e}{2t_p} \quad 4.8$$

The piezoelectric capacitance ($C_p$) in equation 4.8 defines base on equations 4.5 and 4.6 where $a = 1$ in series, $a = 2$ in parallel.

The electric field (E) in two active layers with thickness ($t_p$) defines in equation 4.9.

$$\mathrm{E} = \frac{\mathrm{aV}}{2\mathrm{t_p}} \quad 4.9$$

In equation 4.2 when E=0 the $\mathrm{S_1} = \mathrm{s_{33}^E T_1}\ and\ \mathrm{D_3} = \mathrm{d_{3i} T_1}$. With substituting $\mathrm{T_1}$ in $\mathrm{D_3}$ and with respect to equation 4.3 and 4.4 electrical displacement , $\mathrm{D_3}$, which is displacement in z direction according to coordinates in Fig 4.1define as equation 4.10.

$$\mathrm{D_3} = \mathrm{d_{3i}}\ \mathrm{S_1} Y_p \quad 4.10$$

The current in electrical domain in equation 4.11 is consist of charge ($\dot{D}$) in the density of electrodes ($w \times l_e$). So the current in equation 4.12 obtained by considering equation 4.10 in equation 4.11.

$$i = awl_e\dot{D} \quad 4.11$$

$$i = awl_e d_{31} Y_p \dot{S} \quad 4.12$$

The Kirchhoff's current law (KCL) applied in the electrical part that is the transducer's electrical domain, power converter interface and the storage element.

The current with considering a) the electrical domain of transducer only $C_p$ when FWBR is not conducting b) a resistive load $C_p R_L$ in parallel c) the power converter and capacitive load $C_{st}$ parallel to $C_p$, formulated in equation 4.13, 4.14 and 4.15 respectively. According to Kirchhoff's current law (KCL) in electrical part of circuit in Fig 4.2 (b) we have,

$$i = C_p\dot{V} \quad 4.13$$

$$i = C_p\dot{V} + \frac{V}{R_L} \quad 4.14$$

$$i = (C_p + C_{st})\dot{V} \qquad 4.15$$

### 4.2.2 Testing and Simulation

The PEH transducer's design is including a bimorph, 31-mode piezoelectric cantilever beam while the cantilever size parameters (active and inactive layers) and mass size varied as shown in Table 4.2. Then, different piezoelectric materials for cantilever are used which change the piezoelectric coefficients as given in Table 4.3 for four different materials.

As mentioned in chapter two there are different parameters that effect on the PEH transducer design. So the changes for cantilever and mass size and the piezoelectric material layer effect with above modelling investigated. The other parameters such as shim layer material, the number of active layers and inactive layers, the electrodes physical structure according to piezoelectric layer and the cantilever shape fixed.

#### 4.2.2.1 Changes in Piezoelectric Materials of the PEH Transducer

The circuit parameters in Fig 4.3 based on above model and assumption of input acceleration of 2.25 $\frac{\mathrm{m}}{\mathrm{s}^2}$ defined in m-file and simulated in Simulink. The Simulink in MATLAB R2013b used to evaluate the circuit performance that is a complete model of a bimorph, 31 mode vibration based PEH system.

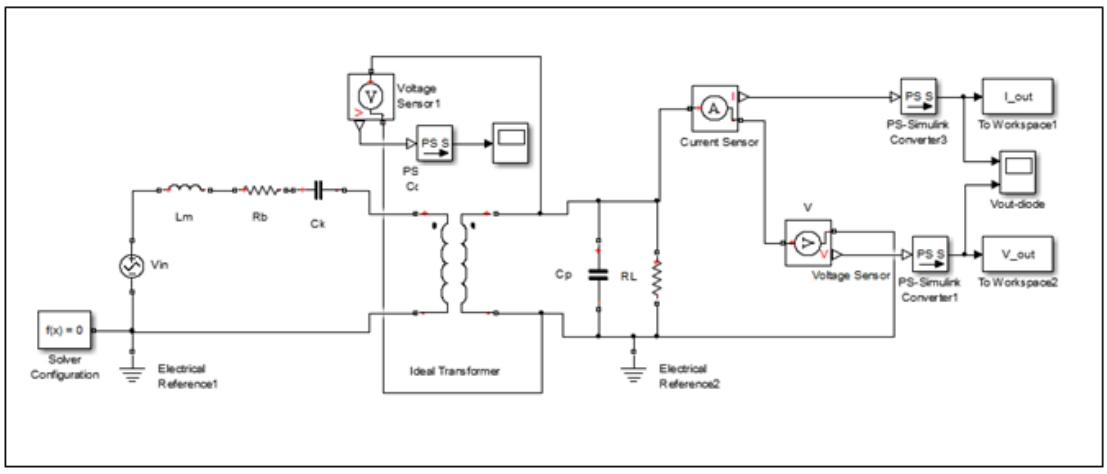


Figure 4.3: The Simulink circuit for resistive load.

The above code modified for four different materials to investigate the effect of parameters as given in Table 4.2 needed to consider for a piezoelectric material transducer for output results.

Table 4.2: The four different piezoelectric materials p [32].

| Piezoelectric materials | Strain coefficient ($d_{31} \times 10^{-12}$ $m/V$) | Density ($\rho_p \frac{kg}{m^3}$) | Quality factor $Q = \frac{1}{2\zeta}$ | Coupling coefficient ($K_{31}$) | Relative dielectric constant ($\varepsilon_r$) $\varepsilon = \varepsilon_r \varepsilon_0$ ($\varepsilon_0 = 8.85 \times 10^{-12}$ | Piezoelectric Young modulus ($Y_p \times 10^9$ $Pa$) |
|---|---|---|---|---|---|---|
| a. Lead Nickel Niobate | -310 | 1100 | 55 | $3.3\times10^{11}$ | 5500 | 55 |
| b. Lead Zirconate Titanate | -100 | 8000 | 900 | $2.8\times 10^{11}$ | 1050 | 73 |
| c. Barium Titanate | -32 | 6020 | 600 | $1.5\times 10^{11}$ | 640 | 125 |
| d. Lead Titanate | -3 | 7520 | 950 | $2.2\times 10^{10}$ | 270 | 128 |

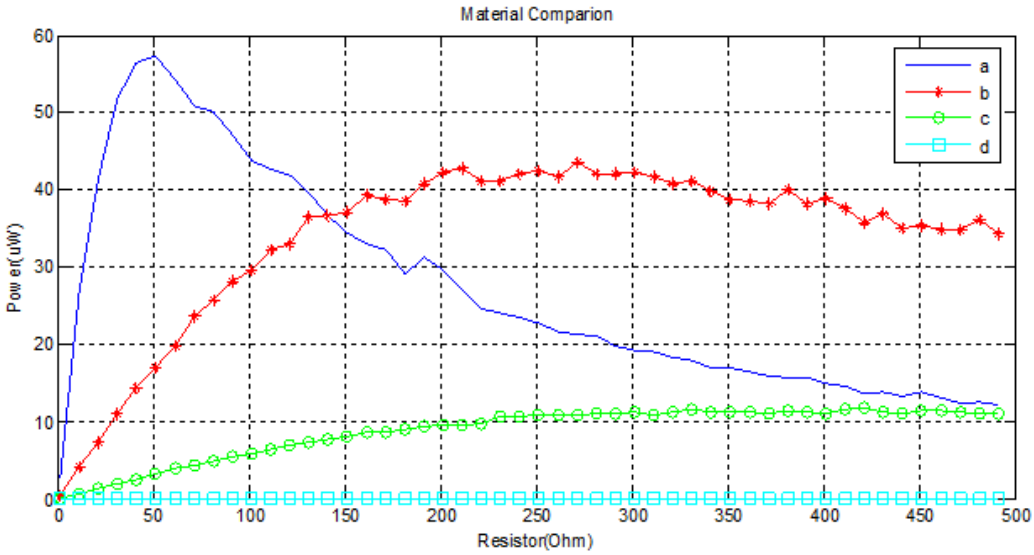


(a)

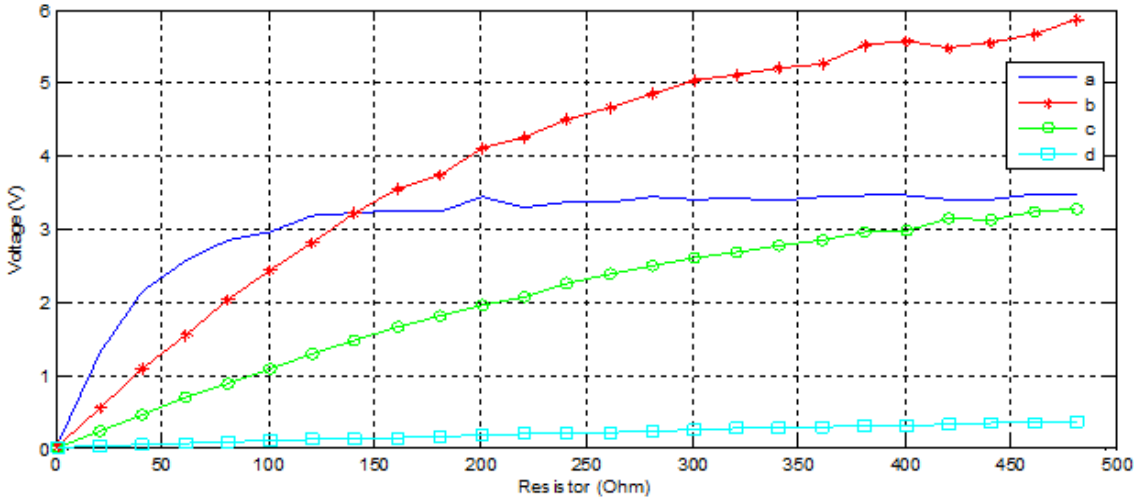


(b)

Figure 4.4: The graph of output parameters to the various load value ($R_L$) for different materials a) output power ($P_{out} = V_{out}I_{out}$) across ($R_L$) b) output voltage ($V_{out}$) in output part of circuit.

The output power in Fig 4.4(a) shows the optimal resistance at $R_L = 50\Omega$ with maximum output power at 58 µW for material (a) Lead Nickel Niobate. This material in the smallest resistance gives the maximum output peak power. While, the minimum output power in the range of 0.01 µW with different load resistance is belong to the material (d) Lead Titanate. The comparison between output power result and features of

materials in Table 4.2 shows that output power ($P_{out}$) proportional to strain coefficient of piezoelectric material in 31-mode beam ($d_{31}$) while the output power ($P_{out}$) relation to elasticity modulus of the piezoelectric beam ($Y_p$) is vice versa.

The output voltage in Fig 4.4(b) indicated output voltage for four material as a>b>c>d until R=100Ω but after that the material (b) Lead Zirconate Titanate output voltage has the significant increase in compare to Lead Nickel Niobate. The reason for these strange changes in the output voltage and power in piezoelectric materials is out of the scope of this thesis however it could be the objective of other projects.

#### 4.2.2.2 Physical Size effect in the (Lead Nickel Niobate) PEH Transducer

The effect of the cantilever and mass size adjustment in Table 4.3 as total density of PEH system for the piezoelectric material with maximum output power shown in Fig4.5.

Table 4.3: The physical cantilever and mass size parameters of the design.

| variables | Value(decrease) | Value [10] | Value(increase) | Unit |
|---|---|---|---|---|
| $l_p$ | 6.5 | 11 | 20 | mm |
| $t_p$ | 0.17 | 0.28 | 0.5 | mm |
| $t_{sh}$ | 0.08 | 0.1 | 0.2 | mm |
| $Y_{sh}$ | 110 | 110 | 110 | GPa |
| $w$ | 2.0 | 3.2 | 4.2 | mm |
| $l_e$ | 6.5 | 11 | 20 | mm |
| $\rho_m$ | 8800 | 8800 | 8800 | $\frac{kg}{m^3}$ |
| $l_m$ | 8.5 | 17 | 25 | mm |
| $t_m$ | 5.0 | 7.7 | 10 | mm |

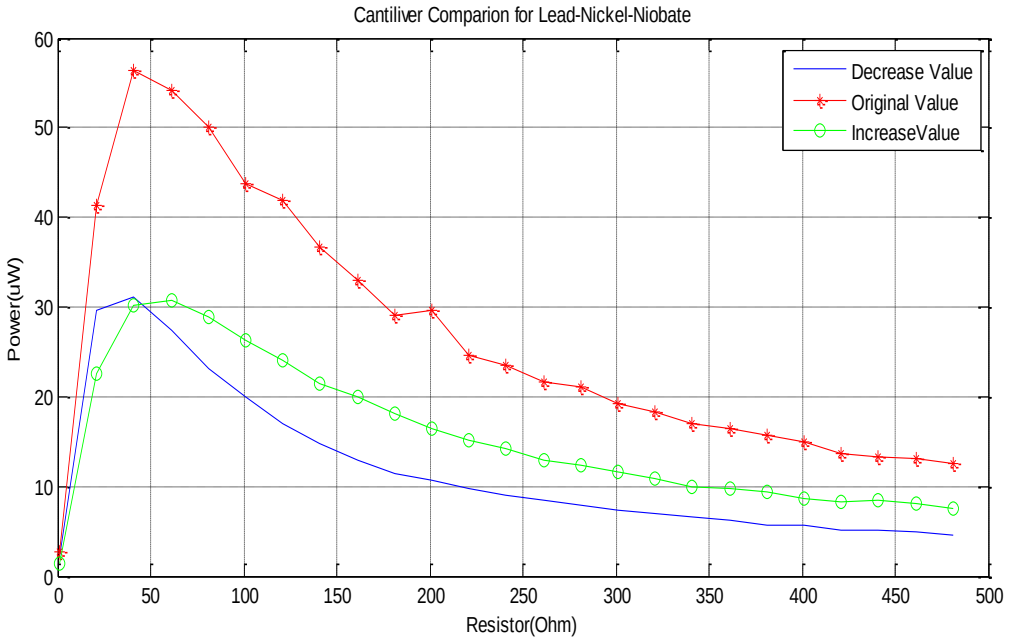


Figure 4.5: The graph of various load reistance to output power with respect to size modification of the PEH system.

The results of output power in Fig 4.5 for different output load shows the best size for the PEH system is the original one used by previous scholars since they optimise all the parameters. However increasing in the size has less exponential decreases in output power by increasing the load resistor.

#### 4.2.2.3 Evaluation of PEH System

The resonance frequency where the system size and materials are changing according to each other evaluated. The resonance frequency defines as equation 4.1

$$\omega_n = \sqrt{\frac{k}{m_{eq}}} \qquad 4.1$$

"K" is the spring stiffness and "$m_{eq}$" is a mass of point mass on the free end of cantilever and cantilever beam mass.

Table 4.4: the resonance frequency changes by four different materials (a, b, c, and d)[4] and changing of transducer size (decrease, original, increase)[5]

| | a | b | c | d |
|---|---|---|---|---|
| Decrease Value | 354.0686 | 399.3097 | 524.2945 | 528.2812 |
| Original Value | 172.9918 | 195.6027 | 256.9767 | 259.0363 |
| Increase Value | 131.4606 | 146.8573 | 193.4994 | 194.5633 |

## 4.3 Summary

The resonance, bimorph, 31-mode piezoelectric cantilever beam with tip mass at the free end design and modelling parameters in equivalent circuit parameters simulated. For testing the efficiency of the system the output results according to changes in some effective materials in PEH systems as mentioned in chapter two such as piezoelectric materials and size of cantilever and mass investigated. Solving the KVL and KCL of Kirchhoff's law in given circuit model gives the output voltage, current and the output power of the optimal resistance which is $R_L = 50\ \Omega$.

[4] Table 4.2
[5] Table 4.3

# CHAPTER FIVE

# DESIGN OF A HYBRID MECHANISMS OF PIEZOELECTRIC AND ELECTROMAGNETIC ENERGY HARVESTING SYSTEM

## 5.1 Synopsis

The model of an electromagnetic energy harvester and piezoelectric energy harvester investigated in chapters three and four. In this chapter the resonance frequency of piezoelectric transducer is estimated. The design flow of a hybrid electromagnetic and piezoelectric energy harvester using COMSOL 5 is proposed. The model analysis is used to calculate the output voltage and current from the hybrid system. The result from the experiment is in good agreement with the simulation results.

## 5.2 Hybrid Transducer Design and Modelling

The EMEH transducer in the proposed model has the magnet in-line with the coil architecture. There are seven NdFeB magnets in opposite poling attached to each other. The magnets attached to the free end of a cantilever as a tip mass where the other end of the cantilever beam clamped. In fact, the magnet is moving with respect to the fixed coil that located under the beam with the internal diameter larger than the magnet's diameter. As the result, the magnet can travel in the coil for the distance of (h).

The input vibration is from the beam that is the cantilever design structure[6]. The single piezoelectric material layer as an active layer and another inactive layer of steel are used in this design. This piezoelectric plate is chosen based on the maximum output voltage capacity $V_p \geq 10$ mV and current of $I_p = 12$mA. Which means the piezoelectric material is capable of generating output power in the range of 1.2 mW.

The input vibration is applied by the tip of a small motor to the free end of the beam (the mass that is magnet mounted on the bottom of the cantilever) with the total

[6] Figure 2.2

force of (F). while the effect of motor tip rotation is neglected and the maximum displacement assumed is downward as in model[7].

The proposed design is modelled using COMSOL 5.0 as given the details in the following section and this system prototype made and tested easily using basic materials and electronic lab equipment.

There are several capacity of developing this work by modelling with the help of an analytical model to use lumped parameters or distributed parameters using PDE for nonlinear motion equations.

## 5.3 Resonance Frequency

In a VEHS, the resonance frequency of the input vibration depends on the energy of elasticity and inertia of the total mass in the system. This parameter is one of the most important values since the maximum output power obtained from matching the fundamental frequency to the resonance frequency. To find the resonance frequency of the piezoelectric transducer we set up a circuit as is shown in figure 5.1(a). There is a sine wave function generator to model the input vibration. The AC voltage source is connected to an oscilloscope to record the input signal. A 100Ω resistance in series to the piezoelectric transducer is connected to an oscilloscope to measure the output signal voltage.

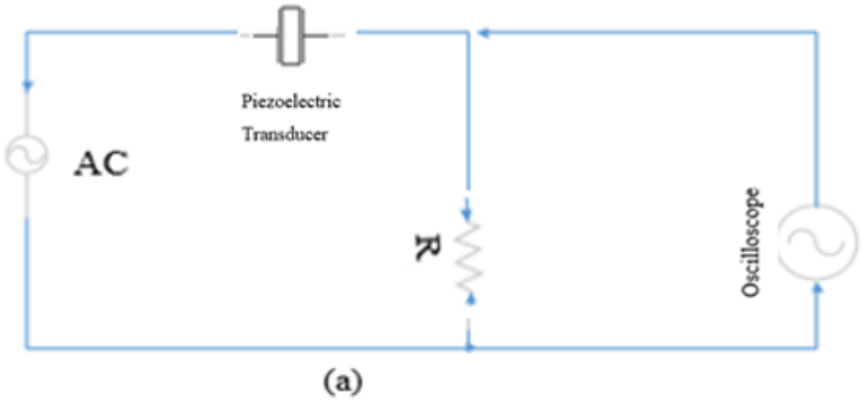

(a)

[7] Figure 3.1

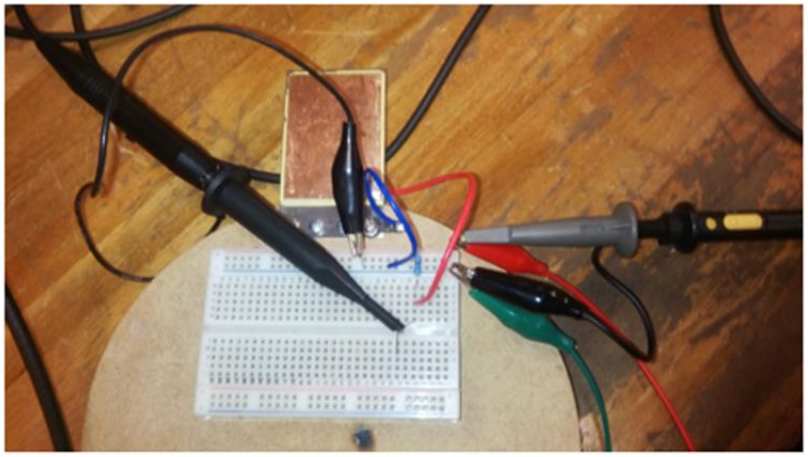

(b)

Figure 5.1: The electrical circuit to measure the resonance frequency a) the schematic b) the experiment set up.

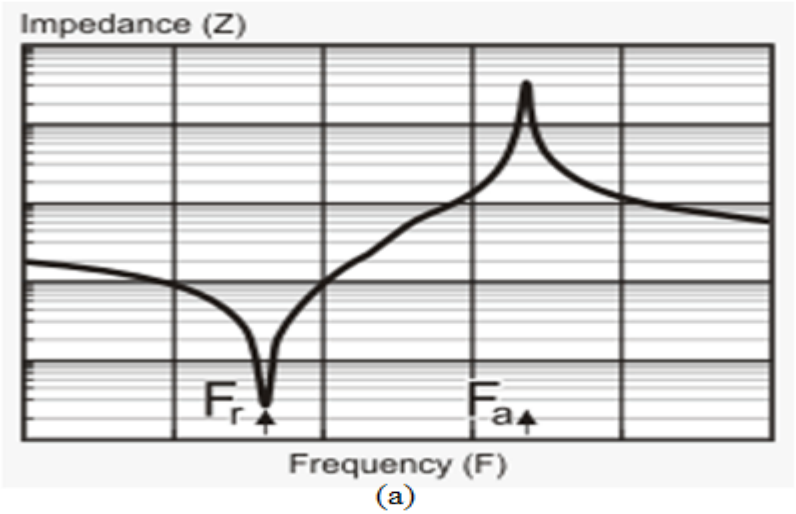


Figure 5.2: The variation of impedance (ohm) to frequency (Hz) a) Ref. [75] b) by simulation.

Fig 5.2 shows the variation of impedance as a function of frequency that $f_a$ is the parallel resonance (open circuit) and $f_r$ is the series resonance (short circuit) and the relation can explain with equation 5.1

$$Z(j\omega) = R + j\omega L + 1/(j\omega C) \qquad 5.1$$

Z is the impedance and R, L, C are resistance, inductance and capacitance respectively. The angular frequency is $(\omega)$ that is resonance when the $\omega_0 = \pm\frac{1}{\sqrt{LC}}$.

In the experiment in Fig 5.1, the input voltage $(V_{in})$ across the function generator and also the output voltage $(V_{out})$ across the piezoelectric transducer is recorded. The frequency at the minimum ratio of $V_{out}/V_{in}$ is the series resonance frequency $(f_r)$ which was measured to be 890 kHz for the piezoelectric composite layer (T-brass, G-Sus, N-ni-alloy).The experiment set up and the graph presented in Fig 5.3.

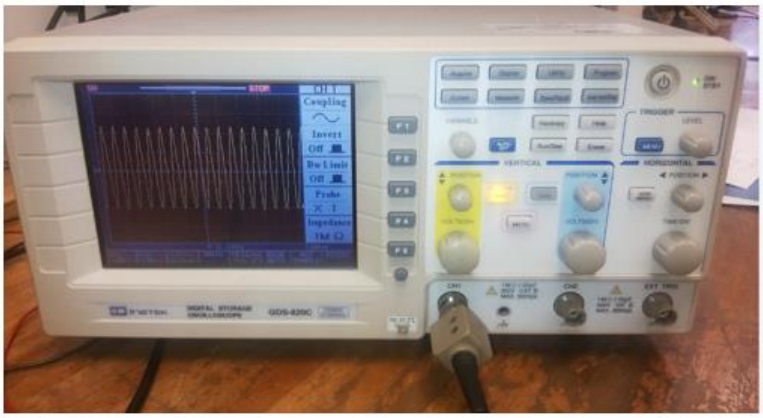

(a)

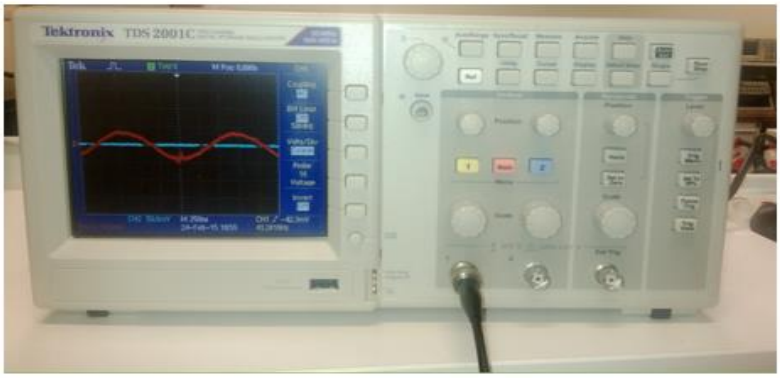


(b)


(c)

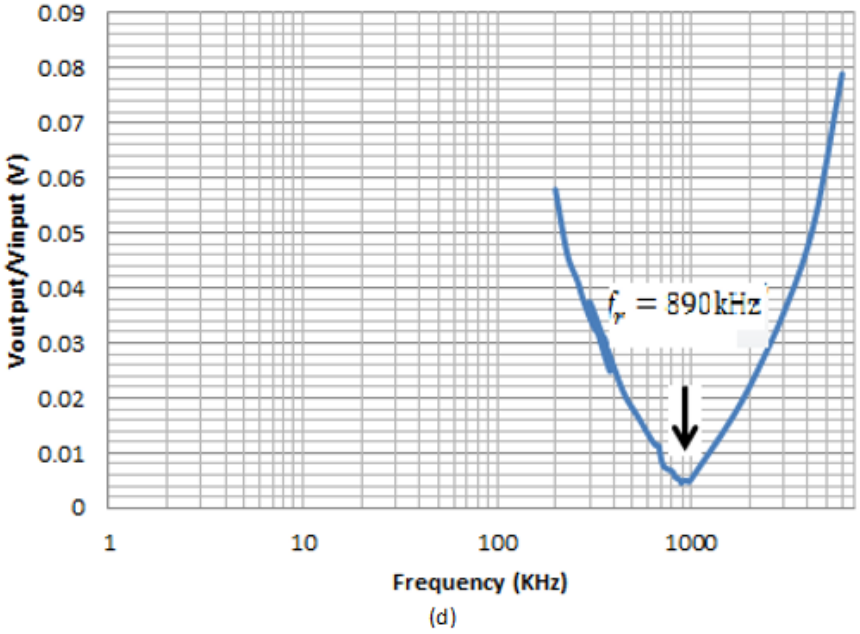


(d)

Figure 5.3: The input and output signal from oscilloscope and the resonance result a) input voltage b) output voltage c) input sine wave frequency d) the parallel resonance frequency at 890 kHz.

## 5.4 The COMSOL Software

The COMSOL Multiphysics is an engineering package that uses finite element analysis, solver and simulation to solve design problem for various applications. This software uses the finite element method (FEM) to solve nonlinear systems of differential equations in one, two or three dimensions with lumped parameter

modelling. Also, the software could solve problems related to electromagnetic, elastic and dynamic systems.

The key capabilities of the software are:

- Design and simulation projects in the fields such as electrical, mechanical, physics and chemistry
- Capability of interfacing with other engineering modelling software such as CATIA and MATLAB

In this thesis, COMSOL Multiphysics 5.0 is used to design and model the piezoelectric and electromagnetic transducer to harvest maximum output voltage from the mix mechanisms.

## 5.4 Geometry of Hybrid System

The design developed in the 3D environment and used the metric millimetre unit. There are a cantilever and a piezoelectric material layer that connected to a mass that is magnetic. The proof mass as a reference quantity not only increases the effective mass but also decreases the damping that results in the increase in output power. In the electromagnetic system design of a simulation, a moving part including cantilever, piezoelectric layer and magnet and a fixed part including coil and space are defined. To design the coil a workspace in the *xy* plane in the same plane as the cantilever and piezo with the plane geometry of circle with diagonal of 8.5 mm and 1 mm layer is chosen. Using “Extrude” drop down option from the list to brings out the coil 10 mm which modelled as the 3D coil. The design presented in Fig 5.3.

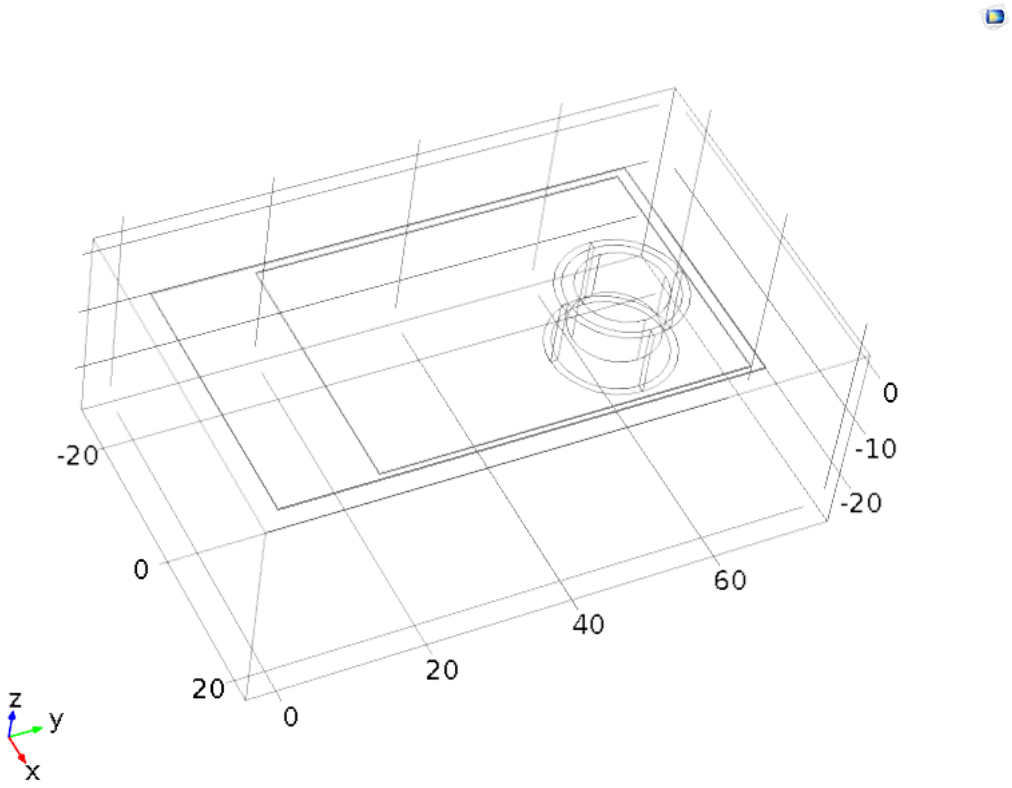


Figure 5.3: 3-D COMSOL design of hybrid piezoelectric and electromagnetic energy harvesting.

## 5.5 Physics used for Electromagnetic and Piezoelectric Energy Harvester

The electromagnetic energy harvester is a magnet with a remanent flux density of 10 T in the x-axis and a multi-turn coil with 306 turns. To describe the multi-turn coil and the magnet the magnetic field physics used. The maximum distance between the coil and piezo is 0.2 mm.

For the piezoelectric energy harvester, a base vector system is defined to ensure that the force from boundary load in the z-axis is in the same direction as the piezoelectric force. The piezoelectric layer is free from one end that is the boundary load in the *z*-axis where the force applied is given by $A.X.\sin(2 \times \text{pi} \times t \times f)$ with $A = 50000\ {}^{N}/_{m^3}$ and the fixed constraint is connected to the other end of piezoelectric material and cantilever. For this purpose, the solid mechanics physics is used. The floating potential and ground in the piezoelectric material are established using electrostatics physics. To show the current generated from the piezoelectric layer or

electromagnetic coil, this is measured across a resistor R=1000 Ω using electric circuit physics.

## 5.6 Meshing

In the meshing, we define how many parts will calculate. For meshing, the piezoelectric system the boundaries in the geometry are swept which allows the meshing to move and the element size set as fine. The electromagnetic system uses a deformed geometry with mesh displacement of $1e^{-3}\text{Ysin}\ (2 \times \text{pi} \times f_0 \times t)$ m (metre) and the meshing defined as physics controlled which is shown in Fig 5.4.

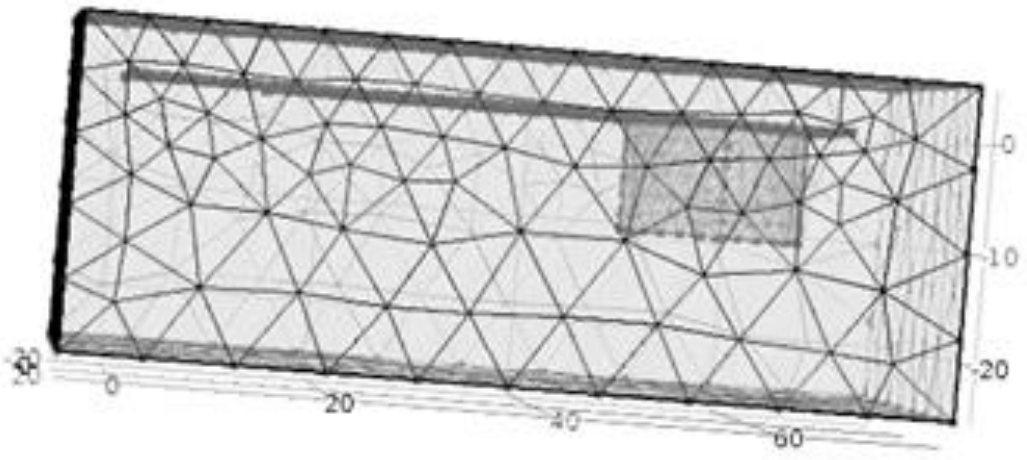


Figure 5.4: The meshing of hybrid piezoelectric and electromagnetic energy harvesting system.

## 5.7 Material Properties

The cantilever is stainless steel and the piezoelectric material is a T-brass, G-Sus, N-ni-alloy.

The magnet works as a proof mass with strong flux density that is rare earth magnet N35. This type of magnet offers up to five times the magnetic energy density of conventional Alnico magnets [19]. Neodymium Iron Boron (NdFeB) magnets have the most powerful magnetic properties per cubic centimetre known at this time [19].

The other properties of materials presented in Table 5.1.

Table 5.1: Specifications for device design and materials

| | |
|---|---|
| length of piezoelectric cantilever | $l_p = 50\text{mm}$ |
| width of piezoelectric cantilever | $W_p = 35\text{mm}$ |
| thickness of piezoelectric cantilever | $t_p = 0.2\text{mm}$ |
| length of electrode | $l_{e=}65\text{mm}$ |
| width of electrode | $W_e = 37\text{mm}$ |
| thickness of electrode | $t_{e=}0.2\text{mm}$ |
| Diameter of each magnet | $D_{magnet} = 12\text{mm}$ |
| Coil resistance | $R_{coil} = 0.001\Omega$ |
| height of each magnet | $t_{magnet} = 1\text{mm}$ |
| coil wire | $t_{coil} = 18\ \text{AWG}$ |
| Number of coil turn | $n_{coil} = 306$ |
| Resonance frequency of piezoelectric transducer (experimental) | $f_n = 890kHz$ |
| Electromechanical coupling coefficient of piezoelectric | $k_p \geq 0.60$ |
| Piezoelectric strain coefficient | $d_{33} \geq 0.60$ |
| Piezoelectric capacitance | $C_p = 220 \mp 15\%\ nF$ |
| Piezoelectric output voltage | $V_p \geq 10$ mV |
| Piezoelectric electric current | $I_p = 12mA$ |
| Piezoelectric material | T-brass, G-Sus,N-ni-alloy |

## 5.8 Simulation Result

The stationary and time-dependent studies were chosen to evaluate the system. The stationary is a steady state analysis to solve linear partial differential equations that do not consider time variation in the model while the time-dependent analysis uses distributed parameters to describe nonlinearity of the system parameters. Besides, the parametric sweep is used to study the voltage at different frequencies.

### 5.8.1 Stationary Analysis

The downward direction (-z) of the cantilever from the applied force results in the cantilever vibrating and deflecting the T-brass, G-Sus, N-ni-alloy piezoelectric film.

The stationary analysis shows that the beam deflected downward in (-z) direction is in the same direction of the applied external load. The maximum displacement of the cantilever observed in the free end at the value of $1.52 \times 10^{-3}$mm which is illustrated in Fig 5.5. It shows that the maximum displacement is at the free end and zero displacement is at the fixed end. As shown in Fig 5.6 the electric potential is scattered on the piezoelectric layer with the maximum value of $4.5 \times 10^{-1}$ V**.** The magnetic flux density in the coil is the maximum at the value of 8.36 T, which given in Fig 5.7**.**

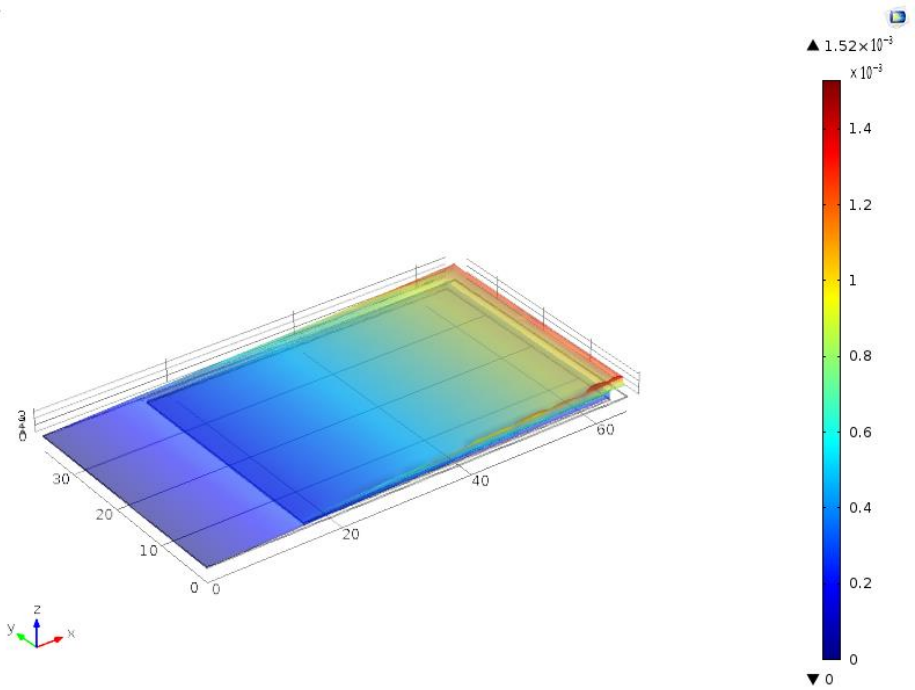


Figure 5.5: Simulation capture of cantilever's displacement at sine wave applied force with maximum displacement of $1.52 \times 10^{-3}$ mm at the free end.

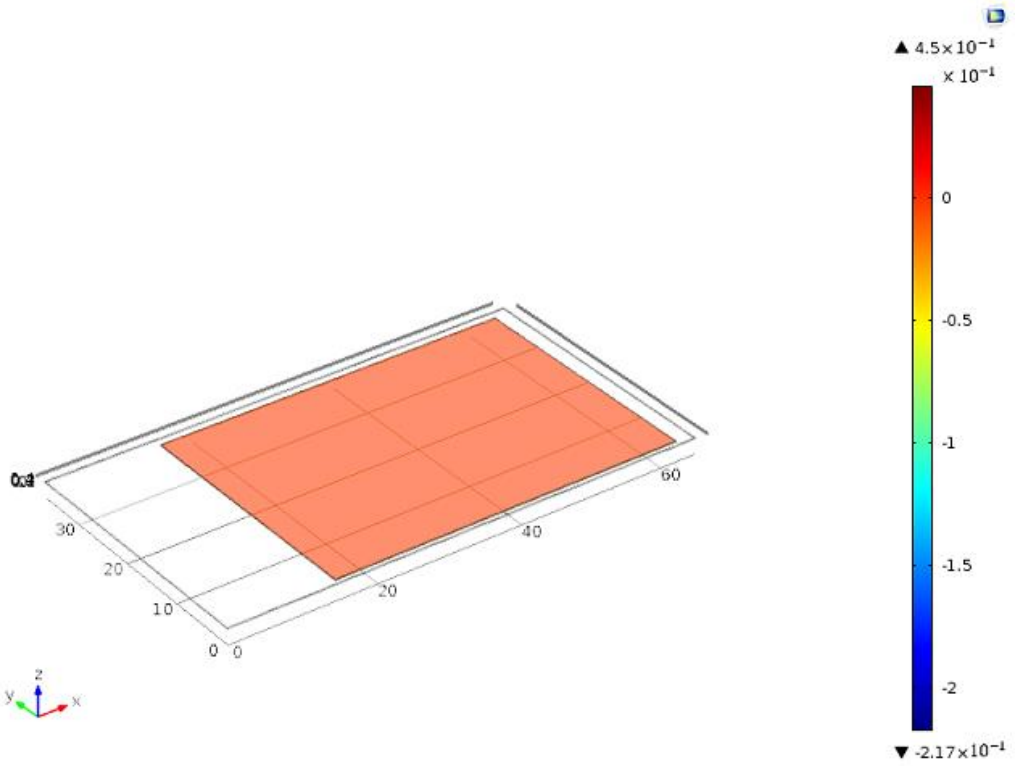


Figure 5.6: Simulation capture of general electrical potential with the sin wave applied force in piezoelectric film with maximum value of $4.5 \times 10^{-1}$(V).

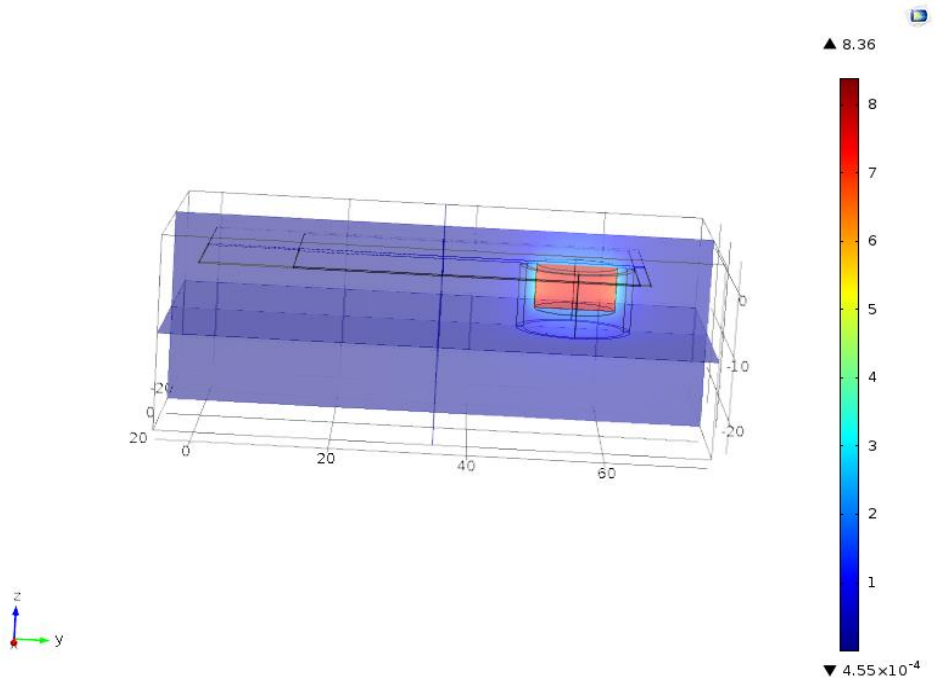


Figure 5.7: The 3D simulation of magnetic flux density distribution in hybrid system with maximum magnetic flux density of 8.36 T in the coil.

### 5.8.2 Parametric Sweep Analysis

The parametric sweep analysis for different frequencies to measure the output voltage and current of piezoelectric and electromagnetic energy harvester shown in Fig 5.8,

Fig 5.9 and Fig 5.10 and Fig 5.11. The results of the simulation are not well defined for the T-brass, G-Sus, N-ni-alloy piezoelectric film since we do not have enough information about the material specification. Fig 5.8 shows the maximum Voltage for 50 Hz frequency with the value of $4\,V$. The current from the piezoelectric energy harvester calculated along the 1000Ω resistor has a maximum value of $4\,mA$ at 50 Hz. We conclude that 50 Hz is the mechanical resonant frequency of the piezoelectric film when there is a maximum displacement of $1.52 \times 10^{-3}$ mm. There is a coil voltage illustrated in Fig 5.10 and Fig 5.11 which shows voltage of 0.23 V at the frequency of 10 kHz and 1.48 V voltage at 890 kHz. The current in the coil has the same value as the voltage while decrease depending on the internal resistance of coil that is following the $V = IR$ formula.

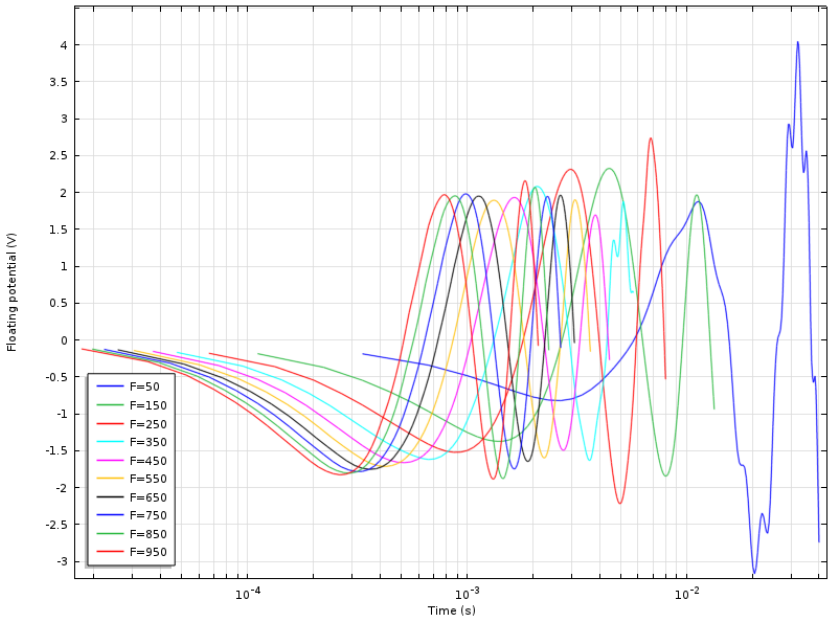


Figure 5.8: Simulation of piezoelectric system, graph of output AC voltage in the range of frequency from 50 Hz to 1 kHz.

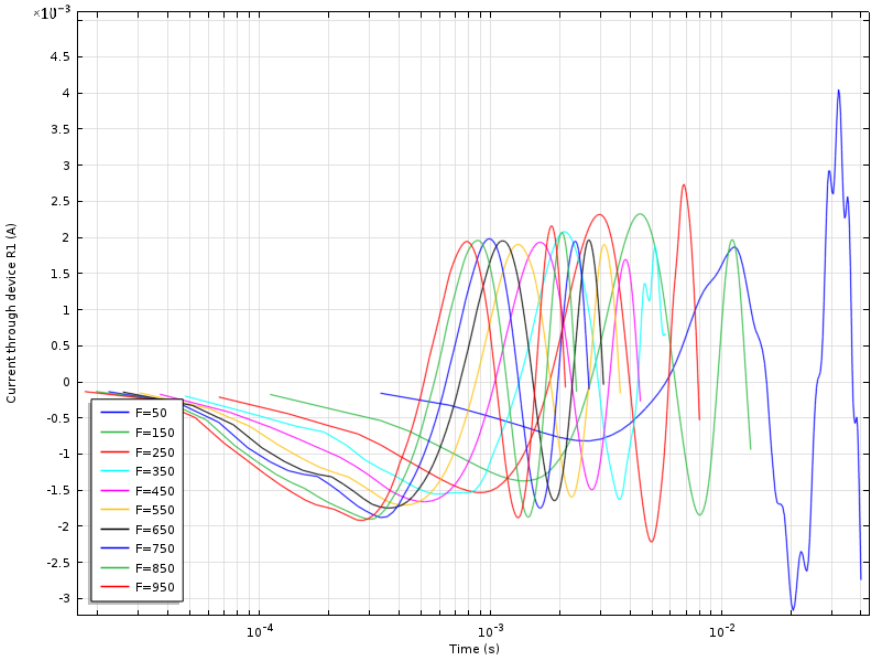


Figure 5.9: Simulation of piezoelectric system, graph of output AC current in the range of f=50 Hz to f=1 kHz and through $R_L = 1\ k\Omega$.

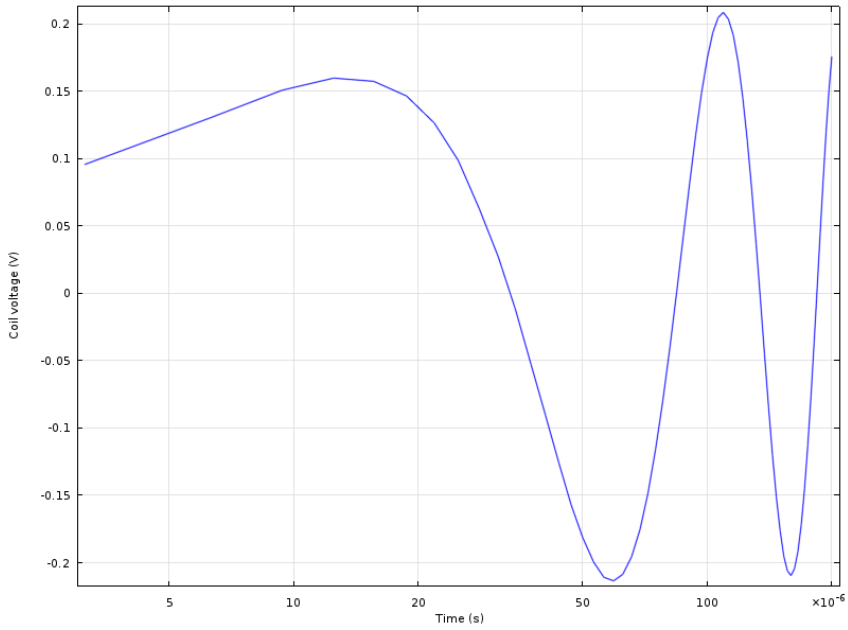


Figure 5.10: Simulation of electromagnetic coil system, graph of output AC voltage for frequency of 10 kHz.

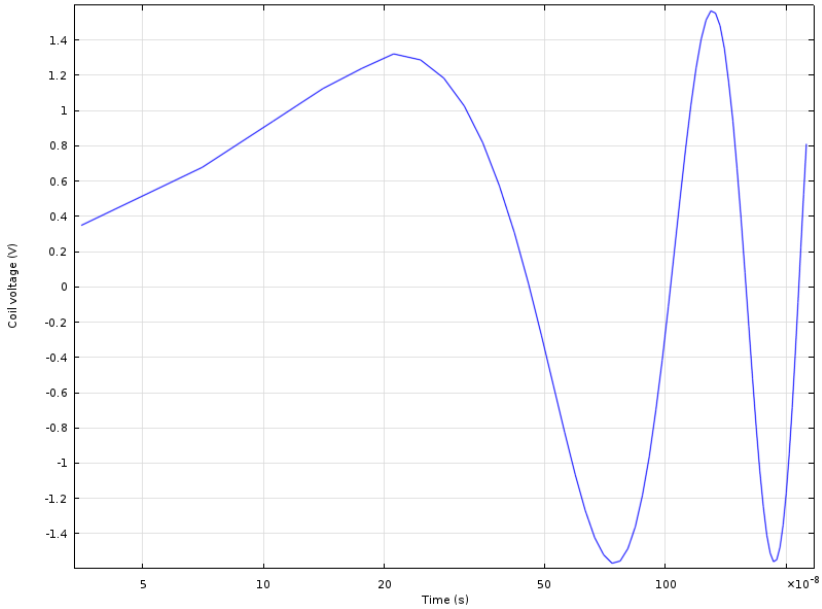


Figure 5.11: Simulation of electromagnetic coil system, graph of output AC voltage for frequency of 890 kHz.

## 5.9 Experimental Laboratory Work

Experimental Procedures was:

a. The piezoelectric beam is fixed using wood where the beam screwed onto the wood.

b. The motor that is a 5 V input voltage has a shaft that fixed beside the fixed beam and functions as a shaker.

c. Two wires were soldered from the beam, one from the piezoelectric layer as a positive side and the other one from the substrate that is steel and is connected to the negative side (ground).

d. The input frequency was measured using a digital tachometer with the frequency ranges from 50-200 Hz

e. There is a wire with 0.75 $mm^2$ thickness that is wound on a substrate to form a coil with 306 turns and resistance of approximately 0.001 Ω.

f. The cylindrical magnets used with 1mm height and 12 mm diameter are the disc of N35 NdFeB. There are seven magnets on each other and they all stick to the moving end of the beam.

g. The hand wound coil soldered to the wire and connected to the oscilloscope, which display the output voltage.

h. The experiment repeated for different input frequencies.

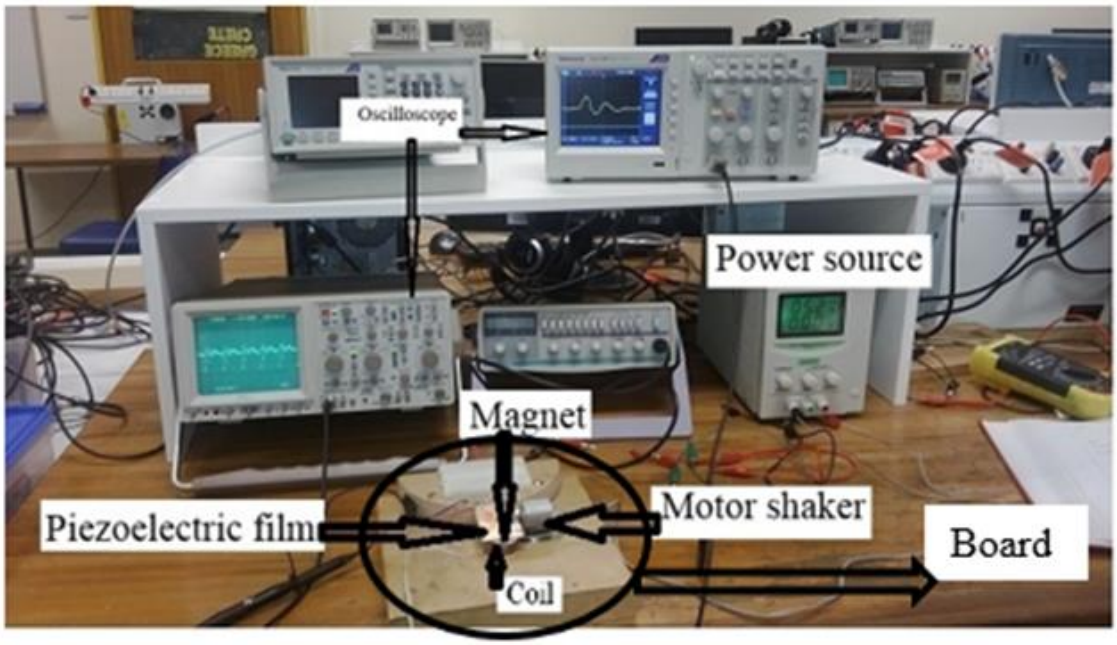


Figure 5.12: Experimental set up.

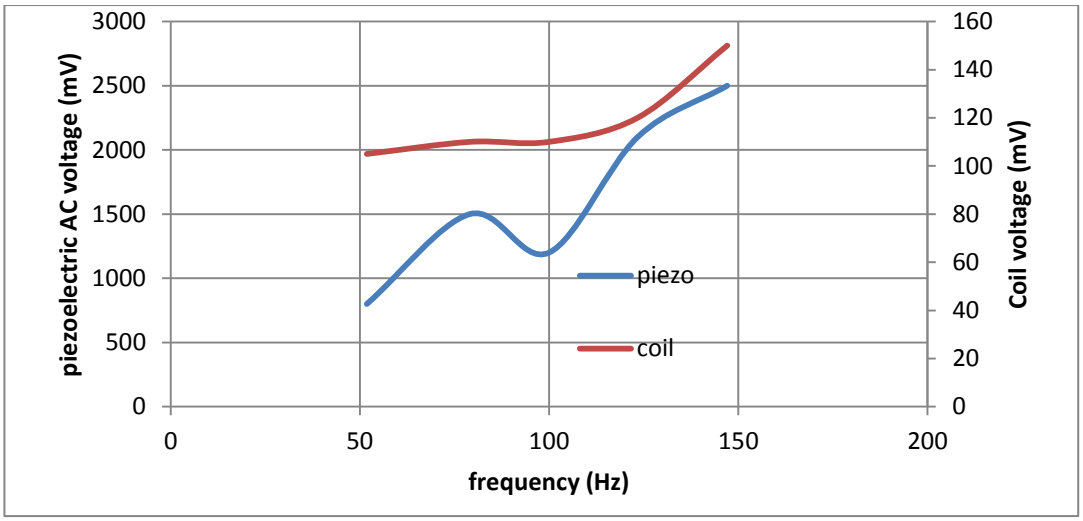


Figure 5.13: Experimental graph of frequency versus piezoelectric and coil AC voltage

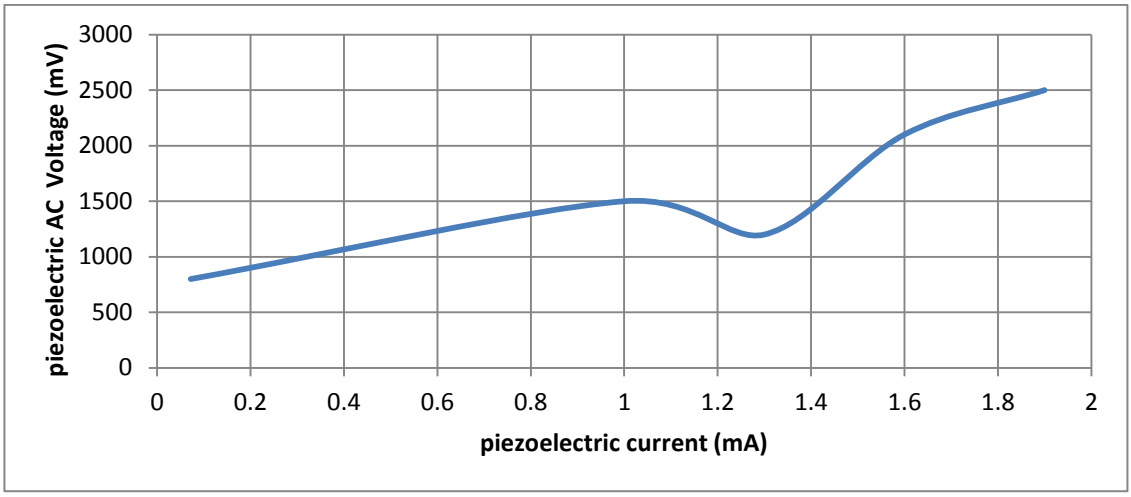


Figure 5.14: Experimental graph for piezoelectric AC voltage to the current.

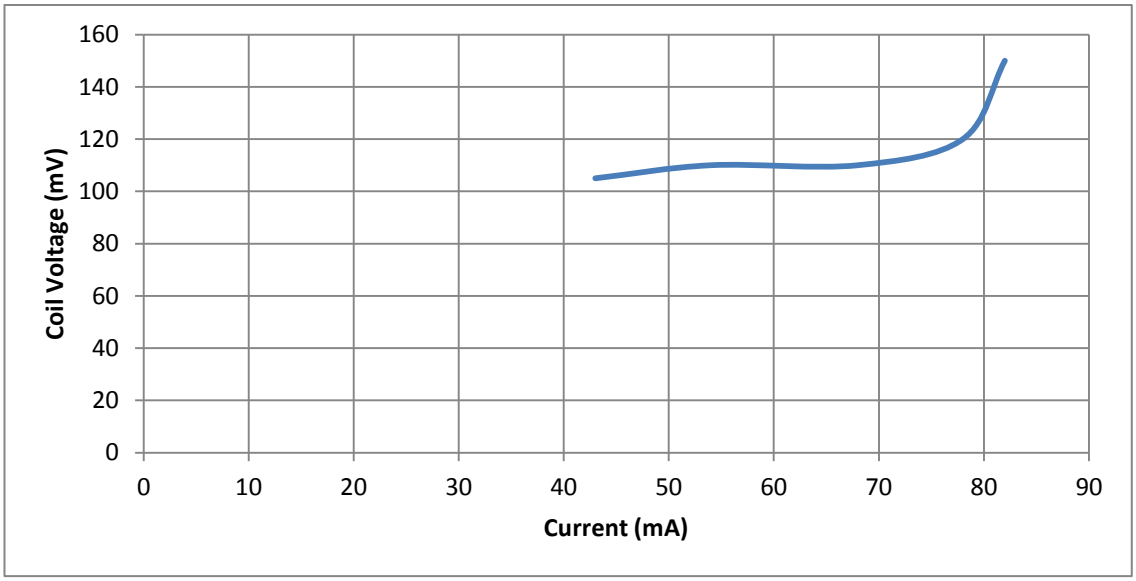


Figure 5.15: Experimental graph of coil voltage to current.

The experimental setup presented in Fig 5.11. The peak value of AC sine waves output voltage of coil and piezoelectric film measured in the experiment and the result of different frequency and current shown in Fig 5.12, Fig 5.13 and Fig 5.14. The voltage had an exponential trend and gradually increases with increasing frequency from 51.86 Hz to 147.16 and current from 43mA to 82mA as given in Fig 5.12 and Fig 5.14. The maximum coil voltage is 0.15V. The Fig 5.12 and Fig 5.13 show the piezoelectric output result that also had a growing trend with the increase of frequency and current. The maximum output extracted is at 2.5V voltage and 1.9mA current at 147.19Hz frequency. The piezoelectric film follows the piezoelectricity effect that makes the

piezoelectric film as a voltage source. Therefore, the voltage gain of the piezoelectric system is much higher than the current passing through the film.

The experimental results are more accurate than the result from COMSOL simulation since we do not have all the piezoelectric generator parameters to insert into the model. On the other hand, we cannot test the piezoelectric system in the experiment for high frequencies to confirm the 890 kHz electrical resonance frequency that we found in the different test on the piezoelectric film. The COMSOL simulation for piezoelectric energy harvester shows the maximum voltage of 4 V in 50 Hz frequency while the maximum voltage in experimental work appears at 2.5 V with 147.19 Hz frequency. The differences between the simulation and experiment can explain due to lack of cantilever beam coefficients and the limitations of the simulation software. The electromagnetic energy harvesting system works with the generated voltage in the coil that shows rising in the experiment and COMSOL simulations. The maximum voltage from the experiment is 0.15V at 147.16Hz while this value increase in the higher frequency which is 1.48 V at 890 kHz concluded from COMSOL simulation.

# CHAPTER SIX

# CONCLUSION AND RECOMMENDATIONS

## 6.1 Conclusion and Recommendations

This thesis is focused on propose an effective design for a hybrid piezoelectric and electromagnetic energy harvester to increase the output result consist of voltage and mainly the output power which presents the capacity of charges storage. To shows the increases of output result in the hybrid system the efficient piezoelectric and electromagnetic energy harvesting transducer based on the literature in chapter two chosen and the output results base on one or two system parameters tested separately. The project supported is carried out mainly by experimental work and some simulation and modelling using MATLAB 2013b and COMSOL 5.

The results showed that it is possible to harvest energy from piezoelectric and electromagnetic device at the same time using the design introduced in this thesis. The MATLAB simulation result from single electromagnetic energy harvester shows the maximum output result belongs to the highest tested frequency with BSR rectifier as the most efficient rectifier. The generated power from single piezoelectric energy harvester is a maximum for Lead-Nickel-Niobate as the material with the highest strain coefficient and lowest density and Young modulus among other materials. In fact, different materials were investigated to establish a relationship between beam vibrations and piezoelectric materials. The electrical, mechanical and electromechanical interaction of piezoelectric and electromagnetic vibration energy harvester has thoroughly had been investigated.

Furthermore, this thesis used COMSOL software to design a hybrid electromagnetic and piezoelectric energy harvester device successfully where the output results illustrated in chapter 5. The piezoelectric film in our design is different from previous research and it has an electrical resonance frequency much higher than the other piezoelectric materials. The previous work has the resonance frequency in the

range of Hz while the experimental electrical resonance frequency for the alloy that we used in our design is in kHz. The configuration of PEH system is a uni-morph beam bending mode with one active layer and one inactive layer. The vibration coupling mode of a cantilever in a PEH system is longitudinal 33-mode where the electric field is applied parallel and in the same direction as the input strain. The mass material and shape in the hybrid system is magnetic and circular. The EMEH system is including a fixed magnet on the tip of the cantilever and a coil below the magnet where the magnet goes inside the coil that induces a voltage and a current in the coil. The COMSOL model for a hybrid system can apply to any other piezoelectric material that would generate an AC output result.

The initial purpose of this thesis was to design a sensor to monitor the health of the building. The piezoelectric system embedded in concrete that lasts for decades as powered by on-demand. In this study, due to resource limitations, examined the mechanical, electrical and electromechanical structure of electromagnetic and piezoelectric energy harvester. This study designed a hybrid system of piezoelectric and electromagnetic energy harvesting system combination. The system with high electrical resonance frequency investigated that limits its application to wearable technology. It may be developed in future with other advances in chopper circuits to create electromagnetically coupled system. The future works could be investigating of the device capacity in different applications, measuring the other parameters of this piezoelectric film alloy that has a high resonance voltage around 10 V with a current as high as 12mA as mentioned in the data sheet. It is possible to work on the hybrid COMSOL model of the electromagnetic system to work on the low frequency by changing different parameters, and this could also continue in a future study.

# References:


[1] J. C. Park, J. Y. Park, and Y. P. Lee, "Modeling and characterization of piezoelectric d33-Mode MEMS energy harvester," *Journal of Microelectromechanical Systems*, vol. 19, pp. 1215-1222, 2010.

[2] S. C. L. Yuen, J. M. H. Lee, W. J. Li, and P. H. W. Leong, "An AA-sized vibration-based microgenerator for wireless sensors," *IEEE Pervasive Computing*, vol. 6, pp. 64-72, 2007.

[3] N. S. S. a. J. A. Paradiso, "Energy scavenging with shoe-mounted piezoelectrics," *IEEE Micro*, vol. 21, pp. 30-42, 2001.

[4] S. R. Anton and H. A. Sodano, "A review of power harvesting using piezoelectric materials (2003-2006)," *Smart Materials and Structures*, vol. 16, pp. R1-R21, 2007.

[5] E. Dallago, A. Danioni, M. Marchesi, V. Nucita, and G. Venchi, "A self-powered electronic interface for electromagnetic energy harvester," *IEEE Transactions on Power Electronics*, vol. 26, pp. 3174-3182, 2011.

[6] M. C. Francesco Cottone, "Introduction to Vibration Energy Harvesting," ed: NiPS Energy Harvesting Summer School, August 2011.

[7] P. C. P. Chao, "Energy Harvesting Electronics for Vibratory Devices in Self-Powered Sensors," *Sensors Journal, IEEE*, vol. 11, pp. 3106-3121, 2011.

[8] J. Tsai, J. Wang, and Y. Su, "Piezoelectric rubber films for human physiological monitoring and energy harvesting," in *Micro Electro Mechanical Systems (MEMS), 2013 IEEE 26th International Conference on*, 2013, pp. 841-844.

[9] J. Kymissis, C. Kendall, J. Paradiso, and N. Gershenfeld, "Parasitic power harvesting in shoes," in *Wearable Computers, 1998. Digest of Papers. Second International Symposium on*, 1998, pp. 132-139.

[10] E. P. James, Tudor, M. J., Beeby, S. P., Harris, N. R., Glynne-Jones, P.,Ross, J. N., and White, N. M., "An investigation of selfpowered systems for condition monitoring applications," *Sensors & Actuators A*, vol. 110, pp. 171–176, 2004.

[11] N. Elvin, A. Elvin, and D. H. Choi, "A self-powered damage detection sensor," *Journal of Strain Analysis for Engineering Design*, vol. 38, pp. 115-124, 2003.

[12] R. O. Robert GHERCA, "HARVESTING VIBRATION ENERGY BY ELECTROMAGNETIC INDUCTION " Annals of the university of Craiova ,2011.

[13] J. M. H. Lee, S. C. L. Yuen, W. J. Li, and P. H. W. Leong, "Development of an AA size energy transducer with micro resonators," in *Proceedings - IEEE International Symposium on Circuits and Systems*, 2003, pp. IV876-IV879.

[14] Y. M. Dirk Spreemann, "power and voltage optimization approach," in *Electromagnetic Vibration Energy Harvesting Devices : Architectures, Design, modeling and optimization*

ed Germany: Springer, 2012, pp. 38-40.

[15] P. Li, S. Gao, S. Niu, H. Liu, and H. Cai, "An analysis of the coupling effect for a hybrid piezoelectric and electromagnetic energy harvester," *Smart Materials and Structures*, vol. 23, p. 065016, 2014.

[16] R. Torah, Beeby, S, P,Tudor, M, J, O'Donnell, T, Roy, S, , "Development of a Cantilever Beam Generator Employing Vibration Energy Harvesting," presented

at the The 6th Int. Workshop on Micro and Nanotechnology for Power Generation and Energy Conversion Applications (PowerMEMS 2006), 2006.

[17] B. Yang, C. Lee, W. L. Kee, and S. P. Lim, "Hybrid energy harvester based on piezoelectric and electromagnetic mechanisms," *Journal of Micro/Nanolithography, MEMS, and MOEMS*, vol. 9, 2010.

[18] S. Yingjun, H. Xueliang, L. Hexiang, and J. Ping, "A Vibration-Based Hybrid Energy Harvester for Wireless Sensor Systems," *Magnetics, IEEE Transactions on*, vol. 48, pp. 4495-4498, 2012.

[19] P. Glynne-Jones, M. J. Tudor, S. P. Beeby, and N. M. White, "An electromagnetic, vibration-powered generator for intelligent sensor systems," *Sensors and Actuators, A: Physical*, vol. 110, pp. 344-349, 2004.

[20] A. Rahimi, O. Zorlu, H. Kulah, and A. Muhtaroglu, "An interface circuit prototype for a vibration-based electromagnetic energy harvester," in *2010 International Conference on Energy Aware Computing, ICEAC 2010*, 2010.

[21] A. Rahimi, Ö. Zorlu, A. Muhtaroğlu, and H. Külah, "An electromagnetic energy harvesting system for low frequency applications with a passive interface ASIC in standard CMOS," *Sensors and Actuators, A: Physical*, vol. 188, pp. 158-166, 2012.

[22] O. Zorlu, E. T. Topal, and H. Kulah, "A mechanical frequency up-conversion mechanism for vibration based energy harvesters," in *Sensors, 2009 IEEE*, 2009, pp. 1366-1369.

[23] Ö. Zorlu, E. T. Topal, and H. Külah, "A vibration-based electromagnetic energy harvester using mechanical frequency up-conversion method," *IEEE Sensors Journal*, vol. 11, pp. 481-488, 2011.

[24] J. C. Park, D. H. Bang, and J. Y. Park, "Micro-fabricated electromagnetic power generator to scavenge low ambient vibration," *IEEE Transactions on Magnetics*, vol. 46, pp. 1937-1942, 2010.

[25] M. A. Halim and J. Y. Park, "A non-resonant, frequency up-converted electromagnetic energy harvester from human-body-induced vibration for hand-held smart system applications," *Journal of Applied Physics*, vol. 115, 2014.

[26] C. R. Saha, T. O'Donnell, N. Wang, and P. McCloskey, "Electromagnetic generator for harvesting energy from human motion," *Sensors and Actuators A: Physical*, vol. 147, pp. 248-253, 9/15/ 2008.

[27] W. L. Lu and Y. M. Hwang, "Analysis of a vibration-induced micro-generator with a helical micro-spring and induction coil," *Microelectronics Reliability*, vol. 52, pp. 262-270, 1// 2012.

[28] C. T. Pan, Y. M. Hwang, H. L. Hu, and H. C. Liu, "Fabrication and analysis of a magnetic self-power microgenerator," *Journal of Magnetism and Magnetic Materials*, vol. 304, pp. e394-e396, 2006.

[29] K. Ashraf, M. H. M. Khir, and J. O. Dennis, "Analysis of frequency up-conversion based vibration energy harvesting," in *Micro and Nanoelectronics (RSM), 2011 IEEE Regional Symposium on*, 2011, pp. 305-309.

[30] I. Sari, T. Balkan, and H. Kulah, "An Electromagnetic Micro Power Generator for Low-Frequency Environmental Vibrations Based on the Frequency Upconversion Technique," *Microelectromechanical Systems, Journal of*, vol. 19, pp. 14-27, 2010.

[31] A. Munaz, B. C. Lee, and G. S. Chung, "A study of an electromagnetic energy harvester using multi-pole magnet," *Sensors and Actuators, A: Physical*, vol. 201, pp. 134-140, 2013.

[32] D. S. R. Jessy Baker, Prof. Paul Wright, "Alternative Geometries for Increasing Power Density in Vibration Energy Scavenging for Wireless Sensor Networks," presented at the 3rd International Energy Conversion Engineering Conference, San Francisco, California, August 2005.

[33] S. B. Kim, H. Park, S. H. Kim, H. C. Wikle, J. H. Park, and D. J. Kim, "Comparison of MEMS PZT cantilevers based on d31 and d 33 modes for vibration energy harvesting," *Journal of Microelectromechanical Systems*, vol. 22, pp. 26-33, 2013.

[34] Y. B. J. R. Sood, J.-h. Jeong and S.G. Kim, "PIEZOELECTRIC MICRO POWER GENERATOR FOR ENERGY HARVESTING," in *Solid-State Sensor and Actuator Workshop*, 2004.

[35] S. Saadon and O. Sidek, "Environmental vibration-based MEMS piezoelectric energy harvester (EVMPEH)," in *Proceedings - 4th International Conference on Developments in eSystems Engineering, DeSE 2011*, 2011, pp. 511-514.

[36] Q. M. Wang and L. Eric Gross, "Constitutive equations of symmetrical triple layer piezoelectric benders," *IEEE Transactions on Ultrasonics, Ferroelectrics, and Frequency Control*, vol. 46, pp. 1343-1351, 1999.

[37] H. B. N. S. Kundu, "Piezoelectric Vibration Energy Harvester Based On Thickness-Tapered Cantilever," 2015.

[38] H. B. Fang, J. Q. Liu, Z. Y. Xu, L. Dong, L. Wang, D. Chen, *et al.*, "Fabrication and performance of MEMS-based piezoelectric power generator for vibration energy harvesting," *Microelectronics Journal*, vol. 37, pp. 1280-1284, 2006.

[39] P. Glynne-Jones, S. P. Beeby, and N. M. White, "Towards a piezoelectric vibration-powered microgenerator," *IEE Proceedings: Science, Measurement and Technology*, vol. 148, pp. 68-72, 2001.

[40] H. P. Hu, Z. J. Cui, and J. G. Cao, "Performance of a piezoelectric bimorph harvester with variable width," *Journal of Mechanics*, vol. 23, pp. 197-202, 2007.

[41] D. Shen, J. H. Park, J. Ajitsaria, S. Y. Choe, H. C. Wikle, and D. J. Kim, "The design, fabrication and evaluation of a MEMS PZT cantilever with an integrated Si proof mass for vibration energy harvesting," *Journal of Micromechanics and Microengineering*, vol. 18, 2008.

[42] P. Pillatsch, E. M. Yeatman, and A. S. Holmes, "A piezoelectric frequency up-converting energy harvester with rotating proof mass for human body applications," *Sensors and Actuators, A: Physical*, vol. 206, pp. 178-185, 2014.

[43] S. M. Shahruz, "Design of mechanical band-pass filters for energy scavenging," *Journal of Sound and Vibration*, vol. 292, pp. 987-998, 2006.

[44] T. J. Johnson, D. Charnegie, W. W. Clark, M. Buric, and G. Kusic, "Energy harvesting from mechanical vibrations using piezoelectric cantilever beams," 2006, pp. 61690D-61690D-12.

[45] A. Mukherjee and U. Datta, "Comparative study of piezoelectric materials properties for green energy harvesting from vibration," in *Proceedings of the 2010 Annual IEEE India Conference: Green Energy, Computing and Communication, INDICON 2010*, 2010.

[46] A. A. Md Ralib, A. Nurashikin Nordin, and H. Salleh, "Simulation of a MEMS piezoelectric energy harvester," in *Symposium on Design, Test, Integration and Packaging of MEMS/MOEMS, DTIP 2010*, 2010, pp. 177-181.

[47] R. Michael, F. Paolo, and H. Chris van, "Optimization of a piezoelectric unimorph for shock and impact energy harvesting," *Smart Materials and Structures*, vol. 16, p. 1125, 2007.

[48] N. F. J. v. R. A. Labuschagne , A.J. van der Merweb, "Comparison of linear beam theories," *Mathematical and Computer Modelling*, vol. 49, p. 2030, 2009.

[49] S. Roundy and P. K. Wright, "A piezoelectric vibration based generator for wireless electronics," *Smart Materials and Structures*, vol. 13, pp. 1131-1142, 2004.

[50] K. R. Vidya Balasubramanyam, Suresh Bala,Volker Zerbe. Modeling and Simulation of an Energy Harvesting System [Online].

[51] A. Romani, m., Paganelli, R.,P., Sangiorgi, E.,Tartagni, M., "Joint Modeling of piezoelectric Transducers and power conversion circuits for energy harvesting applications," *IEEE Sensoors Journal*, vol. 13, pp. 916-925, 2013.

[52] M. Renaud, T. Sterken, A. Schmitz, P. Fiorini, C. Van Hoof, and R. Puers, "Piezoelectric harvesters and MEMS technology: Fabrication, modeling and measurements," in *TRANSDUCERS and EUROSENSORS '07 - 4th International Conference on Solid-State Sensors, Actuators and Microsystems*, 2007, pp. 891-894.

[53] M. Renaud, K. Karakaya, T. Sterken, P. Fiorini, C. Van Hoof, and R. Puers, "Fabrication, modelling and characterization of MEMS piezoelectric vibration harvesters," *Sensors and Actuators, A: Physical*, vol. 145-146, pp. 380-386, 2008.

[54] M. Renaud, R. Elfrink, M. Jambunathan, C. De Nooijer, Z. Wang, M. Rovers, *et al.*, "Optimum power and efficiency of piezoelectric vibration energy harvesters with sinusoidal and random vibrations," *Journal of Micromechanics and Microengineering*, vol. 22, 2012.

[55] N. G. Elvin and A. A. Elvin, "A general equivalent circuit model for piezoelectric generators," *Journal of Intelligent Material Systems and Structures*, vol. 20, pp. 3-9, 2009.

[56] Y. Y. A. L. TANG, "Equivalent Circuit Modeling of Piezoelectric Energy Harvesters," *JOURNAL OF INTELLIGENT MATERIAL SYSTEMS AND STRUCTURES*, vol. 20, December 2009.

[57] J. Ajitsaria, S. Y. Choe, D. Shen, and D. J. Kim, "Modeling and analysis of a bimorph piezoelectric cantilever beam for voltage generation," *Smart Materials and Structures*, vol. 16, pp. 447-454, 2007.

[58] H. M. Wang and L. Zou, "The performance of a piezoelectric cantilevered energy harvester with an imperfectly bonded interface," *Smart Materials and Structures*, vol. 22, 2013.

[59] J. Liang and W. H. Liao, "Energy harvesting and dissipation with piezoelectric materials," in *Proceedings of the 2008 IEEE International Conference on Information and Automation, ICIA 2008*, 2008, pp. 446-451.

[60] X. Cao, W. J. Chiang, Y. C. King, and Y. K. Lee, "Electromagnetic energy harvesting circuit with feedforward and feedback dc-dc PWM boost converter

for vibration power generator system," *IEEE Transactions on Power Electronics*, vol. 22, pp. 679-685, 2007.
[61] E. Lefeuvre, D. Audigier, C. Richard, and D. Guyomar, "Buck-boost converter for sensorless power optimization of piezoelectric energy harvester," *IEEE Transactions on Power Electronics*, vol. 22, pp. 2018-2025, 2007.
[62] A. Rahimi, O. Zorlu, A. Muhtaroğlu, and H. Külah, "A vibration-based electromagnetic energy harvester system with highly efficient interface electronics," in *2011 16th International Solid-State Sensors, Actuators and Microsystems Conference, TRANSDUCERS'11*, 2011, pp. 2650-2653.
[63] Y. K. Ramadass and A. P. Chandrakasan, "An efficient piezoelectric energy harvesting interface circuit using a bias-flip rectifier and shared inductor," *IEEE Journal of Solid-State Circuits*, vol. 45, pp. 189-204, 2010.
[64] S. Xu, K. D. T. Ngo, T. Nishida, G. B. Chung, and A. Sharma, "Converter and controller for micro-power energy harvesting," in *Conference Proceedings - IEEE Applied Power Electronics Conference and Exposition - APEC*, 2005, pp. 226-230.
[65] T. T. Le, J. Han, A. Von Jouanne, K. Mayaram, and T. S. Fiez, "Piezoelectric micro-power generation interface circuits," *IEEE Journal of Solid-State Circuits*, vol. 41, pp. 1411-1419, 2006.
[66] M. Marzencki, Y. Ammar, and S. Basrour, "Integrated power harvesting system including a MEMS generator and a power management circuit," *Sensors and Actuators, A: Physical*, vol. 145-146, pp. 363-370, 2008.
[67] A. Rahimi, Ö. Zorlu, A. Muhtaroğlu, and H. Külah, "A compact electromagnetic vibration harvesting system with high performance interface electronics," in *Procedia Engineering*, 2011, pp. 215-218.
[68] T. Paing and R. Zane, "Design and optimization of an adaptive non-linear piezoelectric energy harvester," in *Conference Proceedings - IEEE Applied Power Electronics Conference and Exposition - APEC*, 2011, pp. 412-418.
[69] T. Starner, "Human Powered Wearable Computing," *IBM Systems*, vol. 35, pp. 618-629, 1996.
[70] T. R. Gyuhae Park, Michael D. Todd, Charles R. Farrar, William Hodgkiss, "Energy Harvesting for Structural Health Monitoring Sensor Networks," *INFRASTRUCTURE SYSTEMS*, vol. 14, pp. 64-79, 2008.
[71] A. Delnavaz and J. Voix, "Energy Harvesting for In-Ear Devices Using Ear Canal Dynamic Motion," *Industrial Electronics, IEEE Transactions on*, vol. 61, pp. 583-590, 2014.
[72] X. Li, T. Hehn, M. Thewes, I. Kuehne, A. Frey, G. Scholl, *et al.*, "Non-resonant electromagnetic energy harvester for car-key applications," *Journal of Physics: Conference Series*, vol. 476, 2013.
[73] G. D. Szarka, S. G. Burrow, P. P. Proynov, and B. H. Stark, "Maximum power transfer tracking for ultralow-power electromagnetic energy harvesters," *IEEE Transactions on Power Electronics*, vol. 29, pp. 201-212, 2014.
[74] S. Senturia, D, *Microsystem design*. Boston, Dordrecht, London: Kluwer Academic Publisher, 2003.
[75] W. H. L. T. H. Ng, "Sensitivity analysis and energy harvesting for a self-powered piezoelectric sensor," vol. 16, pp. 785-797, October 2005.

# Appendix A
# Source code

## A.1 EMEH SYSTEM

```
clc
clear all

dg = 2.2; % mm
rc = 3.75; % mm
d = dg + rc;
rw = 120; % um
N = 100;
Rc = 3.54; % ohm
rho_coil = 3.92; % g/cm^3

lx = 7.5; % mm
ly = 7.5; % mm
lz = 7.5; % mm
Bm = 1.2; % Tesla

A0 = 2; % mm
zeta = 0.018;
Yc = 3.2; % GPa
% L = 9; % mm
W = 7.5; % mm
h = 0.5; % mm
rho_g = 1.2; % g/cm^3


Bc = (Bm/pi)*(atan(ly*lz/(2*d*sqrt(ly^2+lz^2+4*d^2)))-
atan(ly*lz/(2*(d+lx)*sqrt(ly^2+lz^2+4*(d+lx)^2))));

%%

A1 = 0.75*A0; % first part amplitude
A2 = A0; % second part amplitude

f= 10;
T = 1/f; % period

T1= T/2; % first part duration (sec)
T2= T/2; % second part duration (sec)

L = [9, 12, 15, 18, 21, 24]; % mm
% L = 8:30; % mm
for i = 1:length(L)

m_coil = rho_coil*(N*(pi*(rw*1e-4)^2)*(2*pi*rc*1e-1));
m_cant = rho_g*(L(i)*W*h)*1e-3;

meq = m_coil + (33/140)*m_cant; % geram
```

```
k = 2*Yc*1e9*(W*h^3/L(i)^3)*(1-(2*rc/L(i)))/(3-
(2*rc/L(i))^3+(2*rc/L(i))^4);

fn = (1/(2*pi))*sqrt(k/meq);
f_n(i) = fn;

N1 = T1*fn; % No. of first part peaks
N2 = T2*fn; % No. of second part peaks

T_run=1/f-1e-4;

sim('input_signal');

Z = downward;
Vemf = -N*abs(Bc)*abs(Z)*pi*rc^2/L(i);
Vpeak(i) = max(abs(Vemf));
end
figure(1);
plot(L,Vpeak)
xlabel('Length mm')
ylabel('Vpeak mV')

figure(2);
plot(f_n,Vpeak)
xlabel('fn Hz')
ylabel('Vpeak mV')
```

## A.2 PEH SYSTEM

```
clc
clear all
close all;

%% varaiable parameters of cantilever
tp = [0.17,0.28,0.5]*10^-3;       % piezo thickness
tsh = [0.08,0.1,0.2]*10^-3;       % shim  thickness
tm = [5.0,7.7,10]*10^-3;          % mass  thickness
lp = [6.5,11,20]*10^-3;           % length of piezoelectric
lm = [8.5,17,25]*10^-3;           % length of mass
w = [2,3.2,4.2]*10^-3;            % width of all layers
%% variable parameters of piezo layer
Yp = [55,73,125,128]*10^9;        % young modulus of piezoelectric
d31 = [-310,-100,-32,-3]*10^-12; % strain coefficient of piezoelectric
ru_p = [1100,8000,6020,7520];     % piezo density
Q = [33,900,600,950];             %quality factor
epsilon_r = [5500,1050,640,270]; % relative dielectric constant
%% equivalent circuit elements of model
k=0;
for ii=1:numel(tp)
    for j=1:numel(Yp)

        k=k+1;
```

```
        [cp, Ck, N, Lm, Rc, sigma_in, f_n] =
PEH_fun(tp(ii),tsh(ii),tm(ii),lp(ii),lm(ii),w(ii),Yp(j),d31(j),ru_p(j)
,Q(j),epsilon_r(j));

        R_L_t = [1:20:500];
        for i=1:numel(R_L_t)

           R_t=R_L_t(i);
           sim('resistive_load_revised');
           V_R(k,i) = rms(V_out);
           P_out_R(k,i) = (V_R(k,i)^2/(2*R_t))*1000;

        end

    end
end

figure(1);
plot(R_L_t,P_out_R(5,:),R_L_t,P_out_R(6,:),'-r*',R_L_t,P_out_R(7,:),'-
go',R_L_t,P_out_R(8,:),'-cs');
title('Material Comparion');
ylabel('Power(uW)');
xlabel('Resistor(Ohm)');


figure(2);
plot(R_L_t,P_out_R(1,:),R_L_t,P_out_R(5,:),'-r*',R_L_t,P_out_R(9,:),'-
go');
title('Cantiliver Comparion for Lead-Nickel-Niobate');
ylabel('Power(uW)');
xlabel('Resistor(Ohm)');
```

### A.3 The PEH Function

```
function [cp, Ck, N, Lm, Rc, sigma_in, f_n] =
PEH_fun(tp,tsh,tm,lp,lm,w,Yp,d31,ru_p,Q,epsilon_r)


Ysh = 110*10^9;                    % young modulus of shim
eta_s = Ysh/Yp;                    % young modulus ratio
le = lp;                           % length of electrodes = length of
lsh = lp;                          % length of shim layer = length of
L = lp+lm;                         %% the system length= length of piezo
layer+ length of mass
b = (tp+tsh)/2;                    %% average thickness of cantilever
ru_m = 8800;                       % mass density
ru_sh = 8800;                      % shim density
m_p =(ru_p*lp*w*tp);               % mass of piezo layer kg
m_sh =(ru_sh*lsh*w*tsh);           % mass of shim layer kg
m_m =(ru_m*lm*w*tm);               % mass of proof mass kg
m_total = (2*m_p)+m_sh+m_m;        %% total mass kg
epsilon_0 = 8.85*10^-12;           % air dielectric constant
epsilon = epsilon_r*epsilon_0;     %% dielectric constant
```

```
k31 = d31*sqrt(Yp/epsilon);      % coupling coefficient,conversion
ability
n= 2;                            % number of piezoelectric layer
Ip = n*(((w*tp^3)/12)+(w*tp*b^2))+(eta_s*w*tsh^3)/12;    % moment of
inertia
k1 = (b*(2*lp+lm-le))/(2*Ip);                            % design
constant k1
k2 = ((lp^2)*(2*lp+(3/2)*lm))/((3*b)*((2*lp)+lm-le));    % design
constant k2
k = Yp/(k1*k2);                  % spring constant
w_n = sqrt(k/m_total);           %resonance wn
f_n = w_n/(2*pi);                %resonance frequency
Ain = 2.25;                      % input acceleration m/s^2
zeta = 1/(2*Q);                  %damping ratio
c = 2*m_total*w_n*zeta;          %mechanical damping coefficient
a = 2;                           % piezo layers capacitance in series
connection a=1; parallel a=2
sigma_in = k1*m_total*Ain*10^-3;
Lm = k1*k2*m_total*10^-6;
Rc = k1*k2*c*10^-6;
Ck = 1/Yp;
N = (a/2)*-d31*Yp;
cp = (a^2*epsilon*w*le)/(2*tp);


end
```

# Appendix B[8]

# STRESS AND ELECTRIC FIELD

**Piezoelectricity**

The piezoelectric effect is a property that exists in many materials. The name is made up of two parts; piezo, which is derived from the Greek work for pressure, and electric from electricity. The rough translation is, therefore, pressure - electric effect. In a piezoelectric material, the application of a force or stress results in the development of a charge in the material. This is known as the direct piezoelectric effect. Conversely, the application of a charge to the same material will result in a change in mechanical dimensions or strain. This is known as the indirect piezoelectric effect.

Several ceramic materials have been described as exhibiting a piezoelectric effect. These include lead-zirconate-titanate (PZT), lead-titanate ($PbTiO_3$), lead-zirconate ($PbZrO_3$), and barium-titanate ($BaTiO_3$). These ceramics are not actually piezoelectric but rather exhibit a polarized electrostrictive effect. A material must be formed as a single crystal to be truly piezoelectric. Ceramic is a multi crystalline structure made up of large numbers of randomly orientated crystal grains. The random orientation of the grains results in a net cancelation of the effect. The ceramic must be polarized to align a majority of the individual grain effects. The term piezoelectric has become interchangeable with polarized electrostrictive effect in most literature.

**Piezoelectric Effect**

It is best to start with an understanding of common dielectric materials in order to understand the piezoelectric effect. The defining equations for high permittivity dielectrics are:

$$C = \frac{K \varepsilon_r A}{t} = \frac{\varepsilon_o \varepsilon_r A}{t} = \frac{\varepsilon A}{t}$$

and

$$Q = C V \longrightarrow Q = \frac{\varepsilon A V}{t}$$

where:

$C$ = capacitance
$A$ = capacitor plate area
$\varepsilon_r$ = relative dielectric constant
$\varepsilon_o$ = dielectric constant of air = $8.85 \times 10^{-12}$ farads / meter
$\varepsilon$ = dielectric constant
$V$ = voltage
$t$ = thickness or plate separation
$Q$ = charge

In addition, we can define electric displacement, D, as charge density or the ratio of charge to the area of the capacitor:

$$D = \frac{Q}{A} = \frac{\varepsilon V}{t}$$

[8] PIEZOELECTRIC TECHNOLOGY PRIMER James R. Phillips
Sr. Member of Technical Staff, CTS Wireless Components,4800 Alameda Blvd. N.E., Albuquerque, New Mexico 8711390

and further define the electric field as:

$$E = \frac{V}{t} \qquad \text{or} \qquad D = \varepsilon E$$

These equations are true for all isotropic dielectrics. Piezoelectric ceramic materials are isotropic in the unpolarized state, but they become anisotropic in the poled state. In anisotropic materials, both the electric field and electric displacement must be represented as vectors with three dimensions in a fashion similar to the mechanical force vector. This is a direct result of the dependency of the ratio of dielectric displacement, D, to electric field, E, upon the orientation of the capacitor plate to the crystal (or poled ceramic) axes. This means that the general equation for electric displacement can be written as a state variable equation:

$$D_i = \varepsilon_{ij} E_j$$

The electric displacement is always parallel to the electric field, thus each electric displacement vector, $D_i$, is equal to the sum of the field vector, $E_j$, multiplied by its corresponding dielectric constant, $\varepsilon_{ij}$:

$$D_1 = \varepsilon_{11} E_1 + \varepsilon_{12} E_2 + \varepsilon_{13} E_3$$
$$D_2 = \varepsilon_{21} E_1 + \varepsilon_{22} E_2 + \varepsilon_{23} E_3$$
$$D_3 = \varepsilon_{31} E_1 + \varepsilon_{32} E_2 + \varepsilon_{33} E_3$$

Fortunately, the majority of the dielectric constants for piezoelectric ceramics (as opposed to single crystal piezoelectric materials) are zero. The only non-zero terms are:

$$\varepsilon_{11} = \varepsilon_{22} \ , \ \varepsilon_{33}$$

**Axis Nomenclature**

The piezoelectric effect, as stated previously, relates mechanical effects to electrical effects. These effects, as shown above, are highly dependent upon their orientation to the poled axis. It is, therefore, essential to maintain a constant axis numbering scheme.

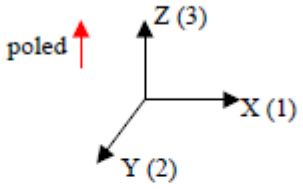


| # | Axis |
|---|---|
| 1 | X |
| 2 | Y |
| 3 | Z (poled) |
| 4 | Shear Around X |
| 5 | Shear Around Y |
| 6 | Shear Around Z |
| P | Radial Vibration |

for electro-mechanical constants:

$d_{ab}$, a = electrical direction; b = mechanical direction

**Electrical - Mechanical Analogies**

Piezoelectric devices work as both electrical and mechanical elements. There are several electrical - mechanical analogies that are used in designing modeling the devices.

| Electrical Unit | | Mechanical Unit | |
|---|---|---|---|
| e | Voltage (Volts) | f | Force (Newtons) |
| i | Current (Amps) | v | Velocity (Meters / Second) |
| Q | Charge (Coulombs) | s | Displacement (Meters) |
| C | Capacitance (farads) | $C_M$ | Compliance (Meters / Newton) |
| L | Inductance (henrys) | M | Mass (Kg) |
| Z | Impedance | $Z_M$ | Mechanical Impedance |

$$i = \frac{dQ}{dt} \qquad v = \frac{ds}{dt}$$

$$e = L\frac{di}{dt} = L\frac{d^2Q}{dt^2} \qquad f = M\frac{dv}{dt} = M\frac{d^2s}{dt^2}$$

**Coupling**

Coupling is a key constant used to evaluate the "quality" of an electro-mechanical material. This constant represents the efficiency of energy conversion from electrical to mechanical or mechanical to electrical.

$$k^2 = \frac{\text{Mechanical Energy Converted to Electrical Charge}}{\text{Mechanical Energy Input}}$$

or

$$k^2 = \frac{\text{Electrical Energy Converted to Mechanical Displacement}}{\text{Electrical Energy Input}}$$

**Electrical, Mechanical Property Changes With Load**

Piezoelectric materials exhibit the somewhat unique effect that the dielectric constant varies with mechanical load and the Young's modulus varies with electrical load.

Dielectric Constant

$$\varepsilon_{T\,\text{FREE}}(1 - k^2) = \varepsilon_{T\,\text{CLAMPED}}$$

This means that the dielectric "constant" of the material reduces with mechanical load. Here "Free" stands for a state when the material is able to change dimensions with applied field. "Clamped" refers to either a condition where the material is

physically clamped or is driven at a frequency high enough above mechanical resonance that the device can't respond to the changing E field.

Elastic Modulus (Young's Modules)

$$Y_{OPEN}\,(1-k^2) = Y_{SHORT}$$

This means that the mechanical "stiffness" of the material reduces when the output is electrically shorted. This is important in that both the mechanical $Q_M$ and resonate frequency will change with load. This is also the property that is used in the variable dampening applications.

**Elasticity**

All materials, regardless of their relative hardness, follow the fundamental law of elasticity. The elastic properties of the piezoelectric material control how well it will work in a particular application. The first concepts, which need to be defined, are stress and strain.

for a given bar of any material:

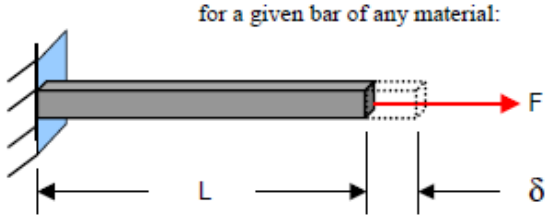


F = Applied Force
A = Area To Which Force Is Applied
δ = Elongation

$$\text{Stress} = \sigma = F / A$$
$$\text{Strain} = \lambda = \delta / L$$

The relationship between stress and strain is Hooke's Law which states that, within the elastic limits of the material, strain is proportional to stress.

$$\lambda = S\,\sigma$$

or, for an anisotropic material

$$\lambda_i = S_{ij}\,\sigma_j$$

Note: The constant relating stress and strain is the modulus of elasticity or Young's modulus and is often represented by S, E or Y.

**Piezoelectric Equation**

It has been previously shown that when a voltage is applied across a capacitor made of normal dielectric material, a charge results on the plates or electrodes of the capacitor. Charge can also be produced on the electrodes of a capacitor made of a piezoelectric material by the application of stress. This is known as the Direct Piezoelectric Effect.

Conversely, the application of a field to the material will result in strain. This is known as the Inverse Piezoelectric Effect. The equation, which defines this relationship, is the piezoelectric equation.

$D_i = d_{ij}\,\sigma_j$ where: $D_i \equiv$ Electric Displacement (or Charge Density)

$d_{ij} \equiv$ Piezoelectric Modulus, the ratio of strain to applied field or charge density to applied mechanical stress

Stated differently, d measures charge caused by a given force or deflection caused by a given voltage. We can, therefore, also use this to define the piezoelectric equation in terms of field and strain.

$$Di = \frac{\sigma_i \lambda_j}{E_j}$$

Earlier, electric displacement was defined as

$$Di = \varepsilon_{ij}\,E_j$$

therefore,

$$e_{ij}\,E_j = d_{ij}\,\sigma$$

and

$$Ej = \frac{d_{ij}\,\sigma_j}{\varepsilon_{ij}}$$

which results in a new constant

$$gij = \frac{d_{ij}}{\varepsilon_{ij}}$$

This constant is known as the piezoelectric constant and is equal to the open circuit field developed per unit of applied stress or as the strain developed per unit of applied charge density or electric displacement. The constant can then be written as:

$$g = \frac{\text{field}}{\text{stress}} = \frac{\text{volts / meter}}{\text{newtons / meter}^2} = \frac{\Delta L / L}{\varepsilon\, V / t}$$

Fortunately, many of the constants in the formulas above are equal to zero for PZT piezoelectric ceramics. The non-zero constants are:

$$s_{11} = s_{22},\ s_{33},\ s_{12},\ s_{13} = s_{23},\ s_{44},\ s_{66} = 2\,(s_{11} - s_{12})$$

$$d_{31} = d_{32},\ d_{33},\ d_{15} = d_{24}$$

**Basic Piezoelectric Modes**

Thickness Expansion

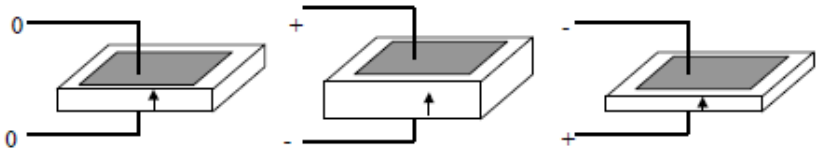


Thickness Shear

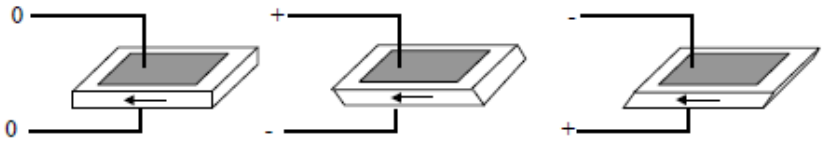


Face Shear

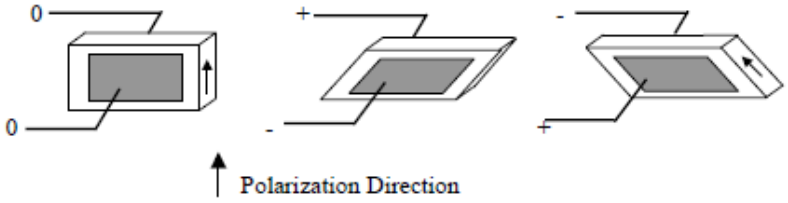


**Poling**

Piezoelectric ceramic materials, as stated earier, are not piezoelectric until the random ferroelectric domains are aligned. This alignment is accomplished through a process known as "poling". Poling consists of inducing a D.C. voltage across the material. The ferroelectric domains align to the induced field resulting in a net piezoelectric effect. It should be noted that not all the domains become exactly aligned. Some of the domains only partially align and some do not align at all. The number of domains that align depends upon the poling voltage, temperature, and the time the voltage is held on the material. During poling the material permanetly increases in dimension between the poling electrodes and decreases in dimensions parallel to the electrodes. The material can be de-poled by reversing the poling voltage, increasing the temperature beyond the materials Currie point, or by inducing a large mechanical stress.

**Post Poling**

Applied Voltage:
Voltage applied to the electrodes at the same polarity as the original poling

voltage results in a further increase in dimension between the electrodes and decreases the dimensions parallel to the electrodes. Applying a voltage to the electrodes in an opposite direction decreases the dimension between the electrodes and increases the dimensions parallel to the electrodes.

Applied Force:

Applying a compressive force in the direction of poling (perpendicular to the poling electrodes) or a tensile force parallel to the poling direction results in a voltage generated on the electrodes which has the same polarity as the original poling voltage. A tensile force applied perpendicular to the electrodes or a compressive force applied parallel to the electrodes results in a voltage of opposite polarity.

Shear:

Removing the poling electrodes and applying a field perpendicular to the poling direction on a new set of electrodes will result in mechanical shear. Physically shearing the ceramic will produce a voltage on the new electrodes.

**Piezoelectric Benders**

Piezoelectric benders are often used to create actuators with large displacement capabilities. The bender works in a mode which is very similar to the action of a bimetallic spring. Two separate bars or wafers of piezoelectric material are metallized and poled in the thickness expansion mode. They are then assembled in a + -+ - stack and mechanically bonded. In some cases, a thin membrane is placed between the two wafers. The outer electrodes are connected together and a field is applied between the inner and outer electrodes. The result is that for one wafer the field is in the same direction as the poling voltage while the other is opposite to the poling direction, This means that one wafer is increasing in thickness and decreasing in length while the other wafer is decreasing in thickness and increasing in length, resulting in a bending moment.

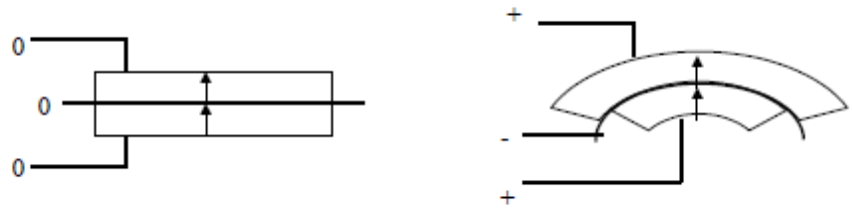


**Loss**

There are two sources for loss in a piezoelectric device. One is mechanical, the other is electrical.

Mechanical Loss: $Q_M = \frac{\text{Mechanical Stiffness Reactance or Mass Reactance}}{\text{Mechanical Resistance}}$

Electrical Loss: $\tan \delta = \frac{\text{Effective Series Resistance}}{\text{Effective Series Reactance}}$

**Simplified Piezoelectric Element Equivalent Circuit**

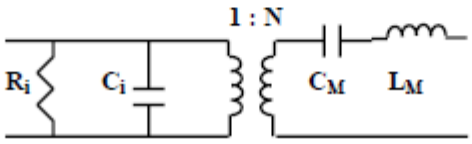


$R_i$ = Electrical Resistance

$C_i$ = Input Capacitance = $\frac{\varepsilon_O \varepsilon_r A}{t}$

$\varepsilon_O$ = 8.85 X 10-12 farads / meter
A = Electrode Area
t = Dielectric Thickness

$L_M$ = Mass (Kg)

$C_M$ = Mechanical Compliance = 1 / Spring Rate (M / N)

N = Electro-mechanical Linear Transducer Ratio (newtons/volt or coulomb/meter)

This model has been simplified and it is missing several factors. It is only valid up to and slightly beyond resonance. The first major problem with the model is related to the mechanical compliance ($C_M$). Compliance is a function of mounting, shape, deformation mode (thickness, free bend, cantilever, etc.) and modulus of elasticity. The modulus of elasticity is, however, anisotropic and it varies with electrical load. The second issue is that the resistance due to mechanical $Q_M$ has been left out. Finally, there are many resonant modes in the transformers, each of which has its own $C_M$ as shown below.

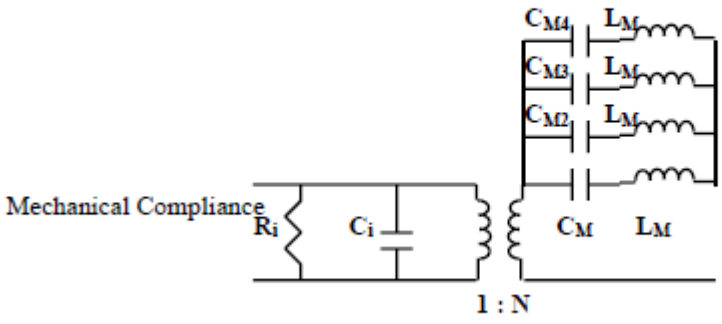

Mechanical compliance, which is the inverse of spring constant, is a function of the shape, mounting method, modulus and type of load. Some simple examples are shown below.

Simple Beam - Uniform End Load

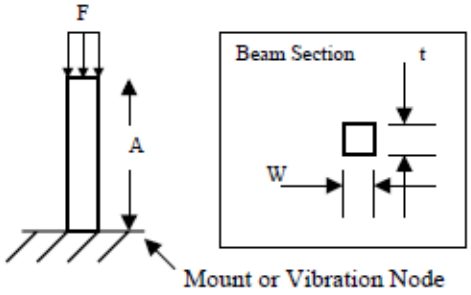


$$C_M = \frac{A}{AY_{ij}} = \frac{A}{W\,t}$$

$$L_M = \rho\, A\, W\, t$$

Simple Beam - Uniform Load - End Mounts

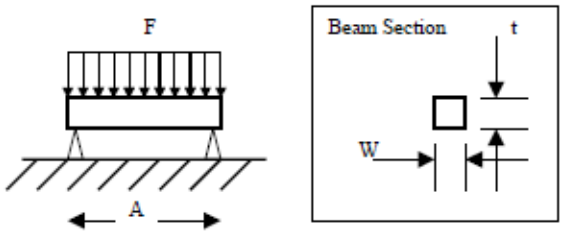


$$C_M = \frac{5\ A^3}{384\ Y_{ij}\ I}$$

I = Moment of Inertia

$$= \frac{W\,t3}{12}$$

$$C_M = \frac{5\ A^3}{32\ W\ t^3}$$

Simple Beam - Uniform Load - Cantilever Mount

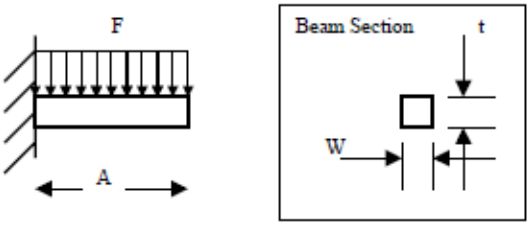


$$C_M = \frac{A^3}{8Y_{ij}I}$$

$$= \frac{3\ A^3}{2\ Y_{ij}\ W\ t^3}$$

The various elements that have been explained can now be combined into the design of a complete piezoelectric device. The simple piezoelectric stack transformer will be used to demonstrate the way they are combined to create a functional model.

**Simple Stack Piezoelectric Transformer**

The piezoelectric transformer acts as an ideal tool to explain the modeling of piezoelectric devices in that it utilizes both the direct and indirect piezoelectric effects. The transformer operates by first converting electrical energy into mechanical energy in one half of the transformer. This energy is in the form of a vibration at the acoustic resonance of the device. The mechanical energy produced is then mechanically coupled into the second half of the transformer. The second half of the transformer then reconverts the mechanical energy into electrical energy. The figure below shows the basic layout of a stack transformer. The transformer is driven across the lower half (dimension $d_1$) resulting in a thickness mode vibration. This vibration is coupled into the upper half and the output voltage is taken across the thinner dimension $d_2$.

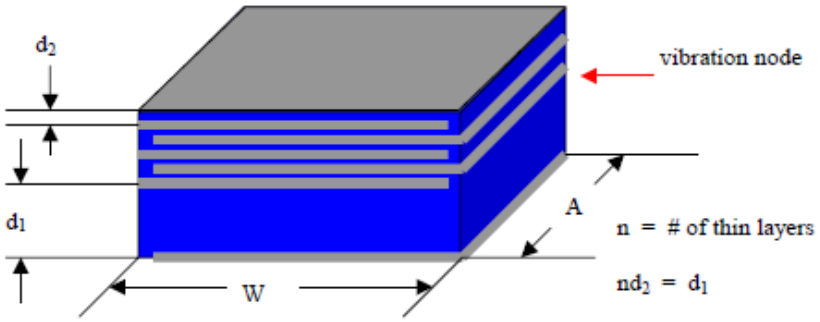


Equivalent Circuit:

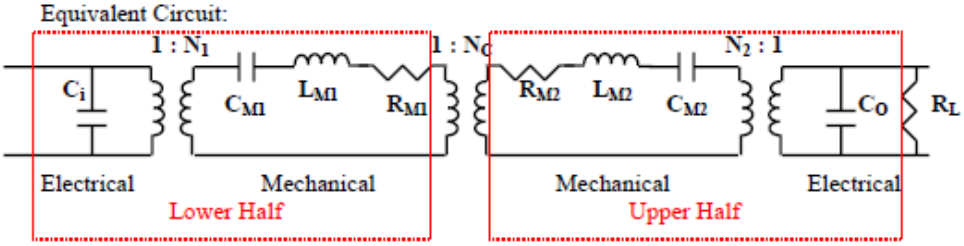


The equivalent circuit model for the transformer (shown above) can be thought of as two piezoelectric elements that are assembled back to back. These devices are connected together by an ideal transformer representing the mechanical coupling between the upper and lower halves. The input resistance, $R_i$, and the output resistance, $R_O$, are generally very large and have been left out in this model. The resistor RL represents the applied load. Determining the values of the various components can be calculated as shown previously.

Input / Output Capacitance:

$$Ci = \varepsilon_O \varepsilon_r \frac{\text{Input Area}}{\text{Input Thickness}} = \varepsilon_O \varepsilon_r \frac{A\,W}{d_1}$$

similarly,

$$C_O = \varepsilon_O \varepsilon_r \frac{\text{Output Area}}{\text{Output Thickness}} = \varepsilon_O \varepsilon_r \frac{n A W}{d_2}$$

Mechanical Compliance:

The mechanical compliance, $C_M$, can be represented by a simple beam subjected to a uniform axial load. This is because the thickness expansion mode will apply uniform stress across the surface. It should be noted that the beam length is measured with respect to the vibration node. The vibration node is used as this is the surface which does not move at resonance and can, therefore, be thought of as a fixed mounting surface.

$$C_M = \frac{\text{Beam Length}}{\text{Beam Area } Y_{33}}$$

$$C_{M1} = \frac{d_1}{A W Y_{33}}$$

$$C_{M2} = \frac{d_2}{A W Y_{33}}$$

Note: Even if $nd_2 \neq d_1$ the vibration node will still be located in the mechanical center of the transformer.

Mass:

$$L_{M1} = \rho A W d_1$$

$$L_{M2} = \rho A W nd_2 = \rho A W d_1$$

Resistance:

The resistances in the model are a function of the mechanical $Q_M$ and Q of the material at resonance and will be calculated later.

Ideal Transformer Ratio:

The transformer ratio, $N_1$, can be thought of as the ratio of electrical energy input to the resulting mechanical energy output. This term will then take the form of newtons per volt and can be derived form the piezoelectric constant, g.

as before:

$$g = \frac{\text{Electric Field}}{\text{Stress}} = \frac{\text{Volts / Meter}}{\text{Newtons / Meter}^2}$$

therefore:

$$\frac{1}{g} = \frac{n/m}{V/m}$$

$$N_1 = \frac{1}{g}\frac{\text{Area Of Applied Force}}{\text{Length Of Generated Field}}$$

or

$$N_1 = \frac{A\ W}{g_{33}\ d_1}$$

The output section converts mechanical energy back to electrical energy and the ratio would normal be calculated in an inverse fashion to $N_1$. In the model, however, the transformer ratio is shown as $N_2$ : 1. This results in a calculation for $N_2$ that is identical to the calculation of $N_1$.

$$N_2 = \frac{1}{g}\frac{\text{Area Of Applied Force}}{\text{Length Of Generated Field}}$$

or

$$N_2 = \frac{A\ W}{g_{33}\ d_2}$$

The transformer 1 : $N_C$, represents the mechanical coupling between the two halves of the transformer. The stack transformer is tightly coupled and the directions of stress are the same in both halves. This results in $N_C \equiv 1$.

Model Simplification:

The response of the transformer can be calculated from this model, but it is possible to simplify the model through a series of simple network conversion and end up in an equivalent circuit whose form is the same as that of a standard magnetic transformer.

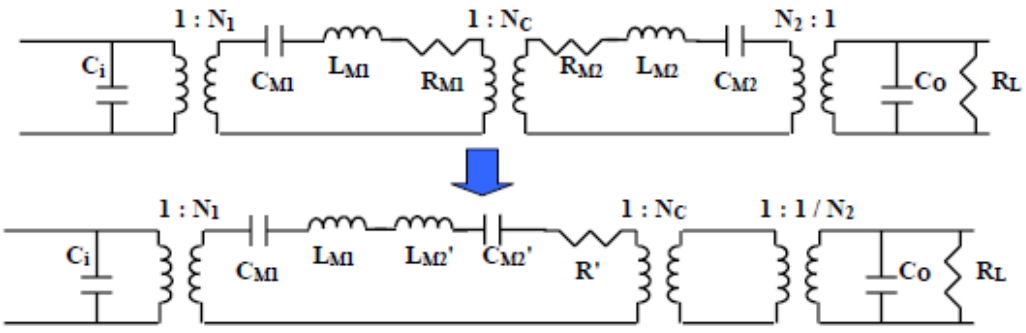

where, due to translation through the transformer,

$$C_{M2}' = N_C^2 C_{M2} \quad \text{and} \quad L_{M2}' = L_{M2} / N_C^2$$

but $N_C^2 \equiv 1$, therefore

$$C_{M2}' = C_{M2} = C_{M1} \quad \text{and} \quad L_{M2}' = L_{M2} = L_{M1}$$

which allows the next level of simplification

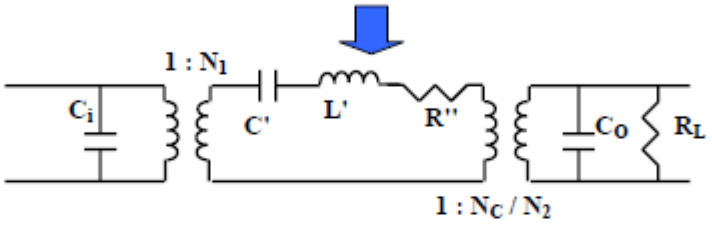


here

$$L' = L_{M1} + L_{M2}' = 2 L_1 = 2 \rho A W d_1$$

$$C' = \frac{(C_{M1} C_{M2}')}{(C_{M1} + C_{M2}')} = \frac{C_{M1}^2}{2C_{M1}} = \frac{C_{M1}}{2} = \frac{d_1}{2 A W Y_{33}}$$

Final simplification

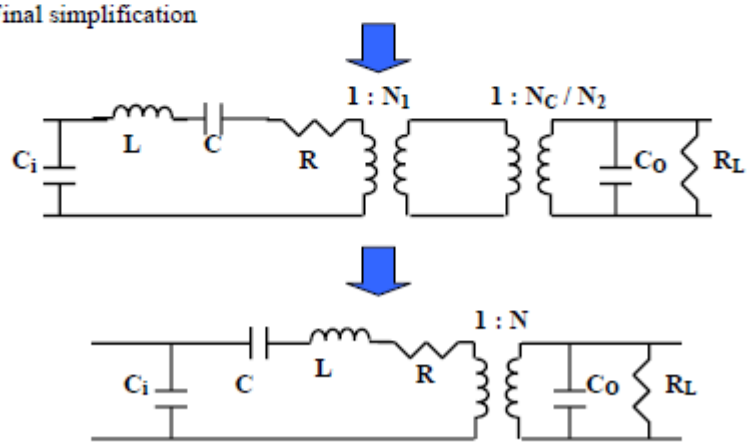


where

$$C = C' N_1^2 \quad \text{and} \quad L = L' / N_1^2$$

and, from before

$$N_1 = \frac{A\ W}{g_{33} d_1}$$

therefore

$$C = \frac{d1}{2WLY_{33}} \frac{A^2 W^2}{g_{33}^2 d_1^2} = \frac{A\ W}{2Y_{33} g_{33}^2 d_1}$$

$$L = 2\rho\ A\ W\ d_1 \frac{g_{33}^2 d_1^2}{A^2 W^2} = \frac{2\rho\ g_{33}^2 d_1^2}{AW}$$

$$N = \frac{N_1 N_C}{N_2} = \frac{A\ W}{g_{33} d_1} \frac{g_{33} d_2}{A\ W} = \frac{d_2}{d_1}$$

The last value we need to calculate is the motional resistance. This value is based upon the mechanical QM of the material and the acoustic resonant frequency.

Resonate Frequency

$$\omega_O = 1 / \sqrt{L\ C}$$

$$= \frac{1}{\sqrt{\frac{2\rho\ d_1\ g_{33}^2}{A\ W} \frac{A\ W}{2Y_{33} g_{33}^2 d1}}}$$

$$= \frac{1}{\sqrt{\frac{\rho\ d_1^2}{Y33}}} = \frac{1}{d_1 \sqrt{\frac{\rho}{Y_{33}}}}$$

$$c_{PZT} \equiv \text{speed of sound in PZT} = \sqrt{Y\ /\ \rho}$$

therefore

$$\omega_O = c_{PZT}\ /\ d_1$$

The equation shown above states that the resonant frequency is equal to the speed of sound in the material divided by the acoustic length of the device. This is the definition of acoustic resonance and acts as a good check of the model. The final derivation is the value of resistance.

$$Q_M \equiv 1/\ \omega_O R C$$

or

$$R = 1\ /\ \omega_O Q_M C$$

$$R = \frac{d_1 \sqrt{\rho / Y_{33}}}{Q_M} \quad \frac{2 Y_{33} g_{33}^2 d_1}{A W} = \frac{2 d_1^2 g_{33}^2 \sqrt{\rho Y_{33}}}{Q_M A W}$$

Note: $C_M$ and R are both functions of $Y_{33}$ and $Y_{33}$ is a function of $R_L$

It should be noted that the model is only valid for transformers driven at or near their fundamental resonate frequencies. This is because the initial mechanical model assumed a single vibration node located at the center of the stack. which is only true when the transformer is driven at fundamental resonance. There are more nodes when the transformer is driven at harmonic frequencies.

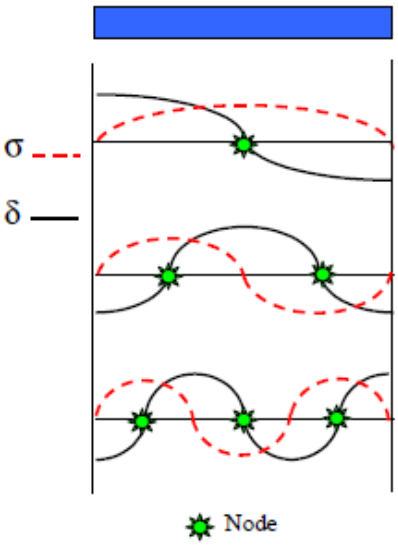


| Frequency | Wave Length |
|---|---|
| $\omega_O$ | $\lambda / 2$ |
| $2\omega_O$ | $\lambda$ |
| $3\omega_O$ | $3\lambda / 2$ |

Note: Stress is $90^o$ out of phase from displacement

There are no fixed nodes at frequencies other than resonance. This means that the transformer must be designed with the resonate mode in mind or phase cancellations will occur and there will be little or no voltage gain. It is often difficult to understand the concept of nodes and phase cancellation, so a simple analogy can be used. In this case, waves created in a waterbed will be used to explain the effect.

Pressing on the end of a waterbed creates a "wave" of displacement that travels down the length of the bed until it reaches the opposite end and bounces back. The water pressure (stress) is the lowest, or negative with respect to the water at rest, at a point just in front of the wave and highest at a point just behind the wave. The pressures at the crest and in the trough are at the same pressure as the bed at rest. The wave will reflect back and forth until resistance to flow causes it to dampen out. The average pressure over time at any point in the bed will be exactly the same as the pressure at rest. Similarly, the average stress in a transformer off resonance will approach zero and there will be no net output.

Pressing on the end of the same bed repeatedly just after the wave has traveled down the length, reflected off the end, returned and reflected off the "driven" end will result in a standing wave. This means that one half of the bed is getting thicker as the other half is getting thinner and the center of the bed will be stationary. The center is the node and the thickness plotted over time of either end will form a sine wave. There will be no net pressure difference in the center, but the ends will have a pressure wave which form a sine wave $90^{o}$ out of phase with the displacement. The transformer again works in the same manner with no voltage at the node and an AC voltage at the ends. It is fairly simple to expand this concept to harmonics and to other resonate shapes.

Conclusion:

The number of different applications for piezoelectric ceramic, and in particular PZT ceramic, is too great to address in a single paper. The basic principals that have been set forth in this primer can, however, be used to both understand and design piezoelectric structures and devices. The ability to create devices of varying applications and shapes is greatly enhanced by the used of multilayer PZT ceramics.

# Appendix C[9]

# Piezoelectric Constitutive

## A.1 Three-Dimensional Form of the Linear Piezoelectric Constitutive Equations

In general, poled piezoceramics (such as PZT-5A and PZT-5H) are transversely isotropic materials. To be in agreement with the IEEE Standard on Piezoelectricity [1], the plane of isotropy is defined here as the 12-plane (or the $xy$-plane). The piezoelectric material therefore exhibits symmetry about the 3-axis (or the $z$-axis), which is the poling axis of the material. The field variables are the stress components ($T_{ij}$), strain components ($S_{ij}$), electric field components ($E_k$), and the electric displacement components ($D_k$).

The standard form of the piezoelectric constitutive equations can be given in four different forms by taking either two of the four field variables as the independent variables. Consider the tensorial representation of the strain–electric displacement form [1] where the independent variables are the stress components and the electric field components (and the remaining terms are as defined in Section 1.4):

$$S_{ij} = s^E_{ijkl} T_{kl} + d_{kij} E_k \tag{A.1}$$

$$D_i = d_{ikl} T_{kl} + \varepsilon^T_{ik} E_k \tag{A.2}$$

which is the preferred form of the piezoelectric constitutive equations for bounded media (to eliminate some of the stress components depending on the geometry and some of the electric field components depending on the placement of the electrodes). Equations (A.1) and (A.2) can be given in matrix form as

$$\begin{bmatrix} \mathbf{S} \\ \mathbf{D} \end{bmatrix} = \begin{bmatrix} \mathbf{s}^E & \mathbf{d}^t \\ \mathbf{d} & \boldsymbol{\varepsilon}^T \end{bmatrix} \begin{bmatrix} \mathbf{T} \\ \mathbf{E} \end{bmatrix} \tag{A.3}$$

where the superscripts $E$ and $T$ denote that the respective constants are evaluated at constant electric field and constant stress, respectively, and the superscript $t$ stands for the transpose.

---

9 Piezoelectric Energy Harvesting, First Edition. Alper Erturk and Daniel J. Inman.

 ISBN: 978-0-470-68254

ound and Vibration, 261, 177–184.

The expanded form of Equation (A.3) is

$$\begin{bmatrix} S_1 \\ S_2 \\ S_3 \\ S_4 \\ S_5 \\ S_6 \\ D_1 \\ D_2 \\ D_3 \end{bmatrix} = \begin{bmatrix} s_{11}^E & s_{12}^E & s_{13}^E & 0 & 0 & 0 & 0 & 0 & d_{31} \\ s_{12}^E & s_{11}^E & s_{13}^E & 0 & 0 & 0 & 0 & 0 & d_{31} \\ s_{13}^E & s_{13}^E & s_{33}^E & 0 & 0 & 0 & 0 & 0 & d_{33} \\ 0 & 0 & 0 & s_{55}^E & 0 & 0 & 0 & d_{15} & 0 \\ 0 & 0 & 0 & 0 & s_{55}^E & 0 & d_{15} & 0 & 0 \\ 0 & 0 & 0 & 0 & 0 & s_{66}^E & 0 & 0 & 0 \\ 0 & 0 & 0 & 0 & d_{15} & 0 & \varepsilon_{11}^T & 0 & 0 \\ 0 & 0 & 0 & d_{15} & 0 & 0 & 0 & \varepsilon_{11}^T & 0 \\ d_{31} & d_{31} & d_{33} & 0 & 0 & 0 & 0 & 0 & \varepsilon_{33}^T \end{bmatrix} \begin{bmatrix} T_1 \\ T_2 \\ T_3 \\ T_4 \\ T_5 \\ T_6 \\ E_1 \\ E_2 \\ E_3 \end{bmatrix} \tag{A.4}$$

where the contracted notation (i.e., Voigt's notation: $11 \rightarrow 1$, $22 \rightarrow 2$, $33 \rightarrow 3$, $23 \rightarrow 4$, $13 \rightarrow 5$, $12 \rightarrow 6$) is used so that the vectors of strain and stress components are

$$\begin{bmatrix} S_1 \\ S_2 \\ S_3 \\ S_4 \\ S_5 \\ S_6 \end{bmatrix} = \begin{bmatrix} S_{11} \\ S_{22} \\ S_{33} \\ 2S_{23} \\ 2S_{13} \\ 2S_{12} \end{bmatrix}, \quad \begin{bmatrix} T_1 \\ T_2 \\ T_3 \\ T_4 \\ T_5 \\ T_6 \end{bmatrix} = \begin{bmatrix} T_{11} \\ T_{22} \\ T_{33} \\ T_{23} \\ T_{13} \\ T_{12} \end{bmatrix} \tag{A.5}$$

Therefore the shear strain components in the contracted notation are the engineering shear strains. It should be noted from the elastic, piezoelectric, and dielectric constants in Equation (A.4) that the symmetries of transversely isotropic material behavior ($s_{11}^E = s_{22}^E$, $d_{31} = d_{32}$, etc.) are directly applied.

## A.2 Reduced Equations for a Thin Beam

If the piezoelastic behavior of the thin structure is to be modeled as a thin beam based on the Euler–Bernoulli beam theory or Rayleigh beam theory, the stress components other than the one-dimensional bending stress $T_1$ are negligible so that

$$T_2 = T_3 = T_4 = T_5 = T_6 = 0 \tag{A.6}$$

Along with this simplification, if an electrode pair covers the faces perpendicular to the 3-direction, Equation (A.4) becomes

$$\begin{bmatrix} S_1 \\ D_3 \end{bmatrix} = \begin{bmatrix} s_{11}^E & d_{31} \\ d_{31} & \varepsilon_{33}^T \end{bmatrix} \begin{bmatrix} T_1 \\ E_3 \end{bmatrix} \tag{A.7}$$

which can be written as

$$\begin{bmatrix} s_{11}^E & 0 \\ -d_{31} & 1 \end{bmatrix} \begin{bmatrix} T_1 \\ D_3 \end{bmatrix} = \begin{bmatrix} 1 & -d_{31} \\ 0 & \varepsilon_{33}^T \end{bmatrix} \begin{bmatrix} S_1 \\ E_3 \end{bmatrix} \tag{A.8}$$

Therefore the stress–electric displacement form of the reduced constitutive equations for a thin beam is

$$\begin{bmatrix} T_1 \\ D_3 \end{bmatrix} = \begin{bmatrix} \bar{c}_{11}^E & -\bar{e}_{31} \\ \bar{e}_{31} & \bar{\varepsilon}_{33}^S \end{bmatrix} \begin{bmatrix} S_1 \\ E_3 \end{bmatrix} \tag{A.9}$$

where the reduced matrix of the elastic, piezoelectric, and dielectric constants is

$$\bar{\mathbf{C}} = \begin{bmatrix} \bar{c}_{11}^E & -\bar{e}_{31} \\ \bar{e}_{31} & \bar{\varepsilon}_{33}^S \end{bmatrix} = \begin{bmatrix} s_{11}^E & 0 \\ -d_{31} & 1 \end{bmatrix}^{-1} \begin{bmatrix} 1 & -d_{31} \\ 0 & \varepsilon_{33}^T \end{bmatrix} \tag{A.10}$$

Here and hereafter, an overbar denotes that the respective constant is reduced from the three-dimensional form to the plane-stress condition. In Equation (A.10),

$$\bar{c}_{11}^E = \frac{1}{s_{11}^E}, \quad \bar{e}_{31} = \frac{d_{31}}{s_{11}^E}, \quad \bar{\varepsilon}_{33}^S = \varepsilon_{33}^T - \frac{d_{31}^2}{s_{11}^E} \tag{A.11}$$

where the superscript $S$ denotes that the respective constant is evaluated at constant strain.

## A.3 Reduced Equations for a Moderately Thick Beam

If the piezoelasticity of the structure is to be modeled as a moderately thick beam based on the Timoshenko beam theory, the stress components other than $T_1$ (the stress component in the axial direction) and $T_5$ (the transverse shear stress) are negligible so that

$$T_2 = T_3 = T_4 = T_6 = 0 \tag{A.12}$$

is applied in Equation (A.4). Then,

$$\begin{bmatrix} S_1 \\ S_5 \\ D_3 \end{bmatrix} = \begin{bmatrix} s_{11}^E & 0 & d_{31} \\ 0 & s_{55}^E & 0 \\ d_{31} & 0 & \varepsilon_{33}^T \end{bmatrix} \begin{bmatrix} T_1 \\ T_5 \\ E_3 \end{bmatrix} \tag{A.13}$$

which can be written as

$$\begin{bmatrix} s_{11}^E & 0 & 0 \\ 0 & s_{55}^E & 0 \\ -d_{31} & 0 & 1 \end{bmatrix} \begin{bmatrix} T_1 \\ T_5 \\ D_3 \end{bmatrix} = \begin{bmatrix} 1 & 0 & -d_{31} \\ 0 & 1 & 0 \\ 0 & 0 & \varepsilon_{33}^T \end{bmatrix} \begin{bmatrix} S_1 \\ S_5 \\ E_3 \end{bmatrix} \tag{A.14}$$

Therefore the stress–electric displacement form of the reduced constitutive equations is

$$\begin{bmatrix} T_1 \\ T_5 \\ D_3 \end{bmatrix} = \begin{bmatrix} \bar{c}_{11}^E & 0 & -\bar{e}_{31} \\ 0 & \bar{c}_{55}^E & 0 \\ \bar{e}_{31} & 0 & \bar{\varepsilon}_{33}^S \end{bmatrix} \begin{bmatrix} S_1 \\ S_5 \\ E_3 \end{bmatrix} \tag{A.15}$$

Here, the reduced matrix of the elastic, piezoelectric, and permittivity constants is

$$\bar{\mathbf{C}} = \begin{bmatrix} \bar{c}_{11}^E & 0 & -\bar{e}_{31} \\ 0 & \bar{c}_{55}^E & 0 \\ \bar{e}_{31} & 0 & \bar{\varepsilon}_{33}^S \end{bmatrix} = \begin{bmatrix} s_{11}^E & 0 & 0 \\ 0 & s_{55}^E & 0 \\ -d_{31} & 0 & 1 \end{bmatrix}^{-1} \begin{bmatrix} 1 & 0 & -d_{31} \\ 0 & 1 & 0 \\ 0 & 0 & \varepsilon_{33}^T \end{bmatrix} \tag{A.16}$$

where

$$\bar{c}_{11}^E = \frac{1}{s_{11}^E}, \quad \bar{c}_{55}^E = \frac{1}{s_{55}^E}, \quad \bar{e}_{31} = \frac{d_{31}}{s_{11}^E}, \quad \bar{\varepsilon}_{33}^S = \varepsilon_{33}^T - \frac{d_{31}^2}{s_{11}^E} \tag{A.17}$$

Note that the transverse shear stress in Equation (A.15) is corrected due to Timoshenko [2,3]

$$T_5 = \kappa \bar{c}_{55}^E S_5 \tag{A.18}$$

where $\kappa$ is the shear correction factor [2–12].

## A.4 Reduced Equations for a Thin Plate

If the thin structure is to be modeled as a thin plate (i.e., Kirchhoff plate) due to two-dimensional strain fluctuations, the normal stress in the thickness direction of the piezoceramic and the respective transverse shear stress components are negligible:

$$T_3 = T_4 = T_5 = 0 \tag{A.19}$$

Equation (A.4) becomes

$$\begin{bmatrix} S_1 \\ S_2 \\ S_6 \\ D_3 \end{bmatrix} = \begin{bmatrix} s_{11}^E & s_{12}^E & 0 & d_{31} \\ s_{12}^E & s_{11}^E & 0 & d_{31} \\ 0 & 0 & s_{66}^E & 0 \\ d_{31} & d_{31} & 0 & \varepsilon_{33}^T \end{bmatrix} \begin{bmatrix} T_1 \\ T_2 \\ T_6 \\ E_3 \end{bmatrix} \tag{A.20}$$

which can be rearranged to give

$$\begin{bmatrix} s_{11}^E & s_{12}^E & 0 & 0 \\ s_{12}^E & s_{11}^E & 0 & 0 \\ 0 & 0 & s_{66}^E & 0 \\ -d_{31} & -d_{31} & 0 & 1 \end{bmatrix} \begin{bmatrix} T_1 \\ T_2 \\ T_6 \\ D_3 \end{bmatrix} = \begin{bmatrix} 1 & 0 & 0 & -d_{31} \\ 0 & 1 & 0 & -d_{31} \\ 0 & 0 & 1 & 0 \\ 0 & 0 & 0 & \varepsilon_{33}^T \end{bmatrix} \begin{bmatrix} S_1 \\ S_2 \\ S_6 \\ E_3 \end{bmatrix} \tag{A.21}$$

The stress–electric displacement form of the reduced constitutive equations becomes

$$\begin{bmatrix} T_1 \\ T_2 \\ T_6 \\ D_3 \end{bmatrix} = \begin{bmatrix} \bar{c}_{11}^E & \bar{c}_{12}^E & 0 & -\bar{e}_{31} \\ \bar{c}_{12}^E & \bar{c}_{11}^E & 0 & -\bar{e}_{31} \\ 0 & 0 & \bar{c}_{66}^E & 0 \\ \bar{e}_{31} & \bar{e}_{31} & 0 & \bar{\varepsilon}_{33}^S \end{bmatrix} \begin{bmatrix} S_1 \\ S_2 \\ S_6 \\ E_3 \end{bmatrix} \tag{A.22}$$

where

$$\bar{\mathbf{C}} = \begin{bmatrix} \bar{c}_{11}^E & \bar{c}_{12}^E & 0 & -\bar{e}_{31} \\ \bar{c}_{12}^E & \bar{c}_{11}^E & 0 & -\bar{e}_{31} \\ 0 & 0 & \bar{c}_{66}^E & 0 \\ \bar{e}_{31} & \bar{e}_{31} & 0 & \bar{\varepsilon}_{33}^S \end{bmatrix} = \begin{bmatrix} s_{11}^E & s_{12}^E & 0 & 0 \\ s_{12}^E & s_{11}^E & 0 & 0 \\ 0 & 0 & s_{66}^E & 0 \\ -d_{31} & -d_{31} & 0 & 1 \end{bmatrix}^{-1} \begin{bmatrix} 1 & 0 & 0 & -d_{31} \\ 0 & 1 & 0 & -d_{31} \\ 0 & 0 & 1 & 0 \\ 0 & 0 & 0 & \varepsilon_{33}^T \end{bmatrix} \tag{A.23}$$

Here, the reduced elastic, piezoelectric, and permittivity constants are

$$\bar{c}_{11}^E = \frac{s_{11}^E}{\left(s_{11}^E + s_{12}^E\right)\left(s_{11}^E - s_{12}^E\right)} \tag{A.24}$$

$$\bar{c}_{12}^E = \frac{-s_{12}^E}{\left(s_{11}^E + s_{12}^E\right)\left(s_{11}^E - s_{12}^E\right)} \tag{A.25}$$

$$\bar{c}_{66}^E = \frac{1}{s_{66}^E} \tag{A.26}$$

$$\bar{e}_{31} = \frac{d_{31}}{s_{11}^E + s_{12}^E} \tag{A.27}$$

$$\bar{\varepsilon}_{33}^S = \bar{\varepsilon}_{33}^T - \frac{2d_{31}^2}{s_{11}^E + s_{12}^E} \tag{A.28}$$

where the first term (Equation (A.24)) is the elastic constant that is related to the bending stiffness of a piezoelectric plate (accounting for the Poisson effect) in the absence of torsion.

## References


1. Standards Committee of the IEEE Ultrasonics, Ferroelectrics, and Frequency Control Society (1987) *IEEE Standard on Piezoelectricity*, IEEE, New York.
2. Timoshenko, S.P. (1921) On the correction for shear of the differential equation for transverse vibrations of prismatic bars. *Philosophical Magazine*, **41**, 744–746.
3. Timoshenko, S.P. (1922) On the transverse vibrations of bars of uniform cross-section. *Philosophical Magazine*, **43**, 125–131.
4. Mindlin, R.D. (1951) Thickness-shear and flexural vibrations of crystal plates. *Journal of Applied Physics*, **22**, 316–323.

5. Mindlin, R.D. (1952) Forced thickness-shear and flexural vibrations of piezoelectric crystal plates. *Journal of Applied Physics*, **23**, 83–88.
6. Cowper, G.R. (1966) The shear coefficient in Timoshenko beam theory. *ASME Journal of Applied Mechanics*, **33**, 335–340.
7. Kaneko, T. (1975) On Timoshenko's correction for shear in vibrating beams. *Journal of Physics D: Applied Physics*, **8**, 1927–1936.
8. Stephen, N.G. (1978) On the variation of Timoshenko's shear coefficient with frequency. *ASME Journal of Applied Mechanics*, **45**, 695–697.
9. Stephen, N.G. (1980) Timoshenko's shear coefficient from a beam subjected to gravity loading. *ASME Journal of Applied Mechanics*, **47**, 121–127.
10. Stephen, N.G. and Hutchinson, J.R. (2001) Discussion: shear coefficients for Timoshenko beam theory. *ASME Journal of Applied Mechanics*, **68**, 959–961.
11. Hutchinson, J.R. (2001) Shear coefficients for Timoshenko beam theory. *ASME Journal of Applied Mechanics*, **68**, 87–92.
12. Puchegger, S., Bauer, S., Loidl, D., Kromp, K., and Peterlik, H. (2003) Experimental validation of the shear correction factor. *Journal of Sound and Vibration*, **261**, 177–184.